

Energy dynamics, heat production and heat–work conversion with qubits: towards the development of quantum machines

Liliana Arrachea

Escuela de Ciencia y Tecnología and ICIFI, Universidad de San Martín, Av. 25 de Mayo y Francia (1650) Buenos Aires, Argentina

E-mail: larrachea@unsam.edu.ar

November 2022

Abstract. We present an overview of recent advances in the study of energy dynamics and mechanisms for energy conversion in qubit systems with special focus on realizations in superconducting quantum circuits. We briefly introduce the relevant theoretical framework to analyze heat generation, energy transport and energy conversion in these systems with and without time-dependent driving considering the effect of equilibrium and non-equilibrium environments. We analyze specific problems and mechanisms under current investigation in the context of qubit systems. These include the problem of energy dissipation and possible routes for its control, energy pumping between driving sources and heat pumping between reservoirs, implementation of thermal machines and mechanisms for energy storage. We highlight the underlying fundamental phenomena related to geometrical and topological properties, as well as many-body correlations. We also present an overview of recent experimental activity in this field.

<i>CONTENTS</i>	2
Contents	
1 Introduction	4
2 Energy dynamics: preliminary concepts	7
2.1 Quasi-static vs finite-time regimes	7
2.2 Adiabatic regime: slow dynamics	10
2.3 Adiabatic dynamics of a few-level quantum system weakly coupled to thermal baths	11
2.4 Floquet regime: fast periodic dynamics	12
2.5 Thermal bias: non-equilibrium stationary regime	13
2.6 Slow dynamics in combination with small thermal bias. Thermal geometric tensor and Onsager relations	15
2.7 From Lindblad equation to quantum trajectories	16
3 Models for a qubit and the environment of harmonic oscillators	17
4 Driving and energy dissipation	19
4.1 General considerations	19
4.2 Adiabatic regime and thermodynamic length	21
4.3 Shortcuts to adiabaticity	23
5 Power pumping	25
5.1 General considerations	25
5.2 Topological power pumping in the adiabatic regime	25
5.3 Topological pumping in the Floquet regime	28
6 Heat pumping	29
6.1 General considerations	29
6.2 Adiabatic heat pumping and geometric phase	29
6.3 Adiabatic heat pumping with a single qubit	30
7 Thermal machines	33
7.1 General considerations	33
7.2 Thermodynamic cycles	33
7.3 Finite-time Carnot heat engine	35
7.4 Adiabatic cycles and geometric properties	37
7.5 Optimal adiabatic heat engine in linear response	41
8 Batteries	42
9 Steady-state thermal transport	44
9.1 General considerations	44
9.2 The effect of strong correlations in linear response	44

9.3	The thermal-bias drop	46
9.4	Rectification	48
10	Superconducting qubits and cQED	49
10.1	Architectures	49
10.2	Circuit quantum electrodynamics	51
10.3	Implementing heat transport in quantum electromagnetic circuits	53
11	Experiments on quantum thermodynamics in cQED	54
11.1	Energy dynamics of measurements	54
11.2	Maxwell demon	56
11.3	Experimental measurement of a topological transition	59
11.4	Thermal machine and Otto cycle	61
11.5	Thermal transport	62
11.6	Steady-state heat engines and refrigerators	63
12	Final remarks	64
13	Acknowledgements	64
Appendix A	Details on the calculation of the $\Lambda_{\ell,\ell'}^S$ for a driven qubit coupled to a single bath	65
Appendix B	Master Equation for a driven qubit asymmetrically coupled to two reservoirs	65

1. Introduction

In the middle of the twentieth century an epochal revolution in technology took place after the development of semiconductors and electronic devices, accelerating, in the last decades, towards an impressive and constant miniaturization. Although quantum effects are crucial in the semiconductors, they operate as macroscopic bodies. The scenario has changed considerably with the emergence of the so called *quantum technologies* where the (quantum) devices operate at the level of single atoms, ions and spins, by fully exploiting the quantum-mechanical nature of these systems.

The building blocks of quantum computers are the qubits and several proposals have been formulated to realize this fundamental component [1]. These ongoing technological developments were triggered by several important scientific advances. In solid-state systems, nanofabrication techniques, enable the construction of nano-devices like quantum dots to confine a few electrons [2, 3], nanomechanical [4] and optomechanical [5] systems, electronic interferometers in topological insulators [6] as well as superconducting circuits [7, 8]. The field of atomic and molecular optical (AMO) physics devoted to study trapped atom/ions and photons has lead to unprecedented level of control from few qubits to complex quantum many-body states [9, 10]. Nitrogen vacancies (NV) centers in diamond [11], has turned into one of the most competitive implementations in many quantum information processing protocols. An overview of this continuously growing and successful adventure can be found in [12]. The diversity of operations in quantum devices include, quantum-state manipulation, measurements and the implementation of logic gates. Nowadays, prototypes of quantum computers are already used to implement machine-learning algorithms [13] as well as quantum simulations [14].

In quantum devices belonging to the new technological generation, the focus of the performance is naturally the precision and the computational possibilities. In order to benefit from the quantum properties of these devices it is necessary to overcome problems such as miniaturization, error correction, and scalability. There are also big expectations on the quantum advantage regarding the energetic optimization. However, it is acknowledged that this aspect is still unclear [15]. In this sense, there is an increasing consensus about the need of a special effort at the level of both fundamental and applied research to further understand this important side of the quantum technologies [16]. The understanding and control of the energy dynamics and entropy generation ubiquitous of all these systems is of paramount importance. In particular, the fact that most of their operations require the challenging conditions imposed by mK temperatures, motivates the search for efficient in-chip cooling and the possibility of converting the generated heat into useful work.

The introduction of thermal machines, like heat engines and refrigerators, has been at the heart of the industrial revolution that took place between mid-19th century and the beginning of the last century. Similarly, in the last 10 years, the efforts devoted to investigate heat manipulation/conversion in quantum devices grew enormously

[17, 18, 19, 20, 21, 22]. At the experimental level, one direction of research has been the implementation of the thermodynamic cycles and refrigeration mechanisms in few-level quantum systems, like atoms and ions [23, 24, 25], NV centers [26, 27]. Another direction is the study of thermoelectric effects, energy harvesting and refrigeration in a diversity of solid state devices, like quantum dots [28, 29, 30, 31, 32, 33, 34, 35, 36, 37, 38], superconducting nanostructures [39, 40, 41], nano electro-and optomechanical devices [42] and systems in the quantum Hall regime [43, 44, 45]. The third direction is the study of the energetics of superconducting qubits in quantum circuits, on which we focus in the present contribution. All these setups belong to the paradigm of *open quantum systems*, since they are based on a configuration where a few-level coherent quantum system is operated out of equilibrium in contact to macroscopic parts which play the role of reservoirs and/or the environment generated by their measurement and manipulation setup.

A qubit is the simplest system to generate a quantum-state superposition. So far, qubits realized in superconducting quantum circuits [46, 47, 48, 49, 50] are among the most advanced platforms regarding scalability and degree of concrete implementations. These qubits are akin the atomic realizations in quantum electrodynamic cavities, since the superconducting device is designed to behave as a two-level system while the embedding circuit behaves akin a photonic cavity. In addition, the quantum dynamics of the qubit-circuit system is formally similar to that induced by the atom-light interaction in the cavity [51]. The coupling between the qubit and the environment is a source of decoherence which is an undesirable but unavoidable effect in quantum information processing. In the investigation of many mechanisms related to the energy dynamics the qubit-environment coupling is a key ingredient, which is amenable to being controlled in hybrid circuit quantum electrodynamics (cQED) hosting superconducting qubits [52]. This possibility along with the high degree of control of the physical mechanisms (voltage gates and magnetic fluxes) to manipulate quantum states in these systems offer an ideal playground to investigate the fundamental mechanisms of quantum thermodynamics like heat transport, entropy production, energy storage and energy conversion.

Aim of this review is to focus on the body of work that dealt with heat/energy manipulation mechanisms which are proposed to take place or have been illustrated in qubit systems. Most of the selected topics are related to solid-state platforms like cQED. Nevertheless, many of the basic mechanisms and effects are ubiquitous in few-level quantum systems embedded in macroscopic or noisy environments and manipulated by time-dependent processes. There are several other very relevant reviews with focus on complementary topics. In particular, on quantum thermodynamics in connection with quantum information [17, 18], recent advances in the description of entropy production in non-equilibrium systems [21] and quantum thermodynamic devices [22]. On the specific topic of the realization of superconducting qubits there are also several reviews [46, 47, 48, 49, 50]. Of particular reference for the present work is the Colloquium by Karimi and Pekola [20], which focuses on quantum heat transport in condensed matter systems. We try to give some perspectives not covered there. In particular, we

address the topics of energy manipulation with time-dependent driving and mechanisms of energy conversion.

There is a rich variety of problems under the topics covered in this review, which are basically defined by the nature of the driving (slow, fast, single or multiple-source) and the characteristics of the environment (thermal bath, noisy, non-equilibrium, with feedback control). The number of physical situations range from the expected dissipation of energy to the realization of thermal machines to generate work or refrigerate. As in other branches of modern physics geometric and topological properties emerge in the route through these scenarios, and we devote some space to analyze them.

The presentation is organized as follows:

Section 2 is devoted to introduce basic concepts of quantum thermodynamics that will be useful to discuss the main mechanisms addressed in the forthcoming sections. In particular, we start presenting definitions of heat and work for quasi-static and finite-time non-equilibrium processes. We briefly introduce the different formalisms to describe of time-dependent quantum dynamics in the slow (adiabatic) and fast (Floquet) regimes. We also present the basic tools to describe the heat steady-state transport induced by thermal bias applied at the reservoirs. We finally discuss the description of the measurement processes as a noisy environment for the quantum system.

Section 3 is devoted to briefly present the simplest models to describe a qubit system coupled to an environment modeled by quantum harmonic oscillators.

Section 4 is devoted to the energy dynamics of a single qubit driven by time-dependent sources and coupled to a single thermal bath. This corresponds to the analysis of the entropy production and energy dissipation introduced by the driving process. A detailed description is possible within the adiabatic regime, where geometrical approaches and control procedures like shortcuts to adiabaticity have been proposed.

Section 5 is devoted to the mechanism of energy pumping for a qubit coupled to a single thermal bath or isolated. We analyze the adiabatic as well as the fast-driving regimes and discuss the geometrical and topological properties in a common framework.

Section 6 continues with the discussion of energy pumping, but in configurations with several thermal baths, in which case heat is pumped between the baths as a consequence of driving.

Section 7 introduces the effect of thermal biases between reservoirs along with time-dependent driving. The combination of these effects is the basis for the operation of thermal machines. We consider the case of thermodynamic cycles where the evolution takes place in steps, with the qubit evolving isolated or coupled to a single reservoir, as well as the adiabatic evolution taking place with the qubit coupled to two reservoirs with a thermal bias.

Section 8 is devoted to review setups to storage energy based on qubits.

Section 9 focuses on fundamental problems of many-body physics taking place in qubits coupled to the environment and their impact on the thermal response of this device. This includes, the effects of quantum phase transitions in the spin-boson problem as well as the problem of the thermal drop and non-linear effects leading to rectification

mechanisms. Related experimental works to some of these problems have been recently reviewed in Ref. [20].

Section 10 is devoted to briefly present the physical properties of superconducting devices hosting Josephson junctions, their coupling to the surrounding circuits and their representations in terms of effective two-level models in contact to harmonic oscillators. Full details have been presented in Refs. [46, 47, 48, 49, 50]

Section 11 is devoted to review experiments on quantum thermodynamics in qubits and quantum circuits. Finally, Section 12 is devoted to summary and conclusions.

2. Energy dynamics: preliminary concepts

Goal of this review is to analyze the energy dynamics in systems composed by one or a few interacting qubits coupled to an external environment, in non-equilibrium scenarios.

The system under consideration is generically described by the following Hamiltonian

$$H(t) = \sum_{\alpha} H_{\alpha} + H_S[\vec{X}(t)] + H_{\text{cont}}. \quad (1)$$

The first term describes the effect of the environment, which can be modeled by one or more Hamiltonian systems (labeled with α). The second term describes the few-level quantum system controlled by N time-dependent parameters. The label ℓ will be used to enumerate them and it is convenient for notation purposes to collect them as components of a vector, $\vec{X}(t) = (X_1(t), \dots, X_{\ell}(t), \dots, X_N(t))$. The last term describes the contact between the driven quantum system and the environment. Several mechanisms may take place that are associated to energy/entropy flow, like dissipation of energy, heat transport, pumping and heat-work conversion. We will address them in the forthcoming sections. The aim of this section is to introduce some formal concepts that will help us to analyze the associated dynamics.

2.1. Quasi-static vs finite-time regimes

The natural question that arises in the discussion of energy dynamics is how to identify heat and work in a time-dependent process. This is rather easy to answer in simple terms when the evolution is quasi-static with the system contacted to one or more reservoirs at the same temperature T . This situation has been discussed in textbooks [54] as well as in previous literature [17, 18, 21, 22]. The useful concept to this end is the *frozen* Hamiltonian H_t , which corresponds to taking a snapshot of the parameters $\vec{X}(t)$ at a given time t and define the Hamiltonian of Eq. (1) regarding the parameters as if they were not time-dependent. We can define a thermal density operator associated to this Hamiltonian, $\rho_t = e^{-H_t/(k_B T)} / \text{Tr} [e^{-H_t/(k_B T)}]$ and use this to calculate the change in the energy stored by the system, $U_t = \text{Tr} \left[\rho_t H_S \left(\vec{X}(t) \right) \right]$, as the system evolves from t to

$t + \delta t$. The result is

$$dU = \text{Tr} \left[d\rho_t H_S \left(\vec{X}(t) \right) \right] + \text{Tr} \left[\rho_t \frac{\partial H_S \left(\vec{X}(t) \right)}{\partial \vec{X}(t)} \right] \cdot d\vec{X}(t), \quad (2)$$

and we identify the first term as heat and the second one as work.

In time-dependent non-equilibrium processes and also in situations where the reservoirs may have different temperatures, it is more natural to define fluxes. In particular, we can formally define the power developed by the driving source characterized by $X_\ell(t)$ by first defining the force operator

$$\mathcal{F}_\ell = -\frac{\partial H}{\partial X_\ell}, \quad (3)$$

which results in the following expression for the power developed on the quantum system,

$$P(t) = \left\langle \frac{\partial H[\vec{X}(t)]}{\partial t} \right\rangle = \sum_\ell P_\ell(t),$$

$$P_\ell(t) = -\langle \mathcal{F}_\ell \rangle \dot{X}_\ell. \quad (4)$$

Similarly we can calculate the rate of change of the energy stored in each piece of the device, $\langle \dot{H}_j \rangle$ with $j \equiv \alpha, \text{sys}, \text{cont}$. A quantity of particular importance is the energy flux into the reservoirs,

$$J_\alpha(t) = \langle \dot{H}_\alpha \rangle = -\frac{i}{\hbar} \langle [H_\alpha, H] \rangle. \quad (5)$$

The expectation values in these expressions are taken with respect to non-equilibrium states. In general, Eqs. (4) and (5) cannot be calculated exactly and we must resort to a non-equilibrium quantum many-body approach in order to solve the problem within some degree of approximation. An exception corresponds to the case of bilinear Hamiltonians (Hamiltonians that can be expressed as combinations of products of one creation and one annihilation operator) for the reservoirs as well as the few-level quantum system and the contact term. Under such conditions, it is possible to exactly calculate these fluxes by recourse to scattering matrix or non-equilibrium Green's functions (Schwinger-Keldysh) formalisms [55, 56, 57, 58, 59, 60, 61]. This is the case of many problems of electron systems. However, this is not the case of few-level systems described by spin models in contact to reservoirs modeled by bosonic excitations. The latter is the relevant picture in many realizations of qubit systems.

In a process taking place between the times t_1 and t_2 we define the work developed by the time-dependent sources and the heat entering the reservoir α as follows,

$$W_{1 \rightarrow 2} = \int_{t_1}^{t_2} dt P(t),$$

$$Q_{\alpha, 1 \rightarrow 2} = \int_{t_1}^{t_2} dt J_\alpha(t), \quad (6)$$

with $P(t) = \sum_\ell P_\ell(t)$. While the definition of work is easily connected with the usual definition for a quasi-static process as in Eq.(2), the definition of heat in the time-domain

has been the subject of several discussions in the context of electron systems strongly coupled to fermionic reservoirs [62, 63, 64, 65, 66, 67, 68, 69, 70] and, more recently, also in the context of two-level systems [71]. In particular, there is no full consensus on how to properly account for the energy stored in the contact terms H_{cont} of Eq. (1).

We now recall that the expectation values for the power in Eq. (4) and of the energy flux in Eq. (5) are defined with respect to the non-equilibrium time-dependent state of the full many-body system, reservoirs and couplings. In order to make contact to the conventional thermodynamic description and Eq. (2), it is useful to split these non-equilibrium quantities into two components as follows,

$$\begin{aligned} P(t) &= P^{(\text{cons})}(t) + P^{(\text{non-cons})}(t), \\ J_\alpha(t) &= J_\alpha^{(\text{qs})}(t) + J_\alpha^{(\text{non-eq})}(t). \end{aligned} \quad (7)$$

The first components correspond to the expectation values for the power and the energy flux evaluated with the frozen state ρ_t instead of the full non-equilibrium state. They define the conservative power (cons) and quasi-static (qs) energy exchange between system and reservoirs, associated to a sequence of instantaneous equilibrium states described by ρ_t ,

$$\begin{aligned} P^{(\text{cons})}(t) &= - \sum_\ell \text{Tr} [\rho_t \mathcal{F}_\ell] \dot{X}_\ell(t), \\ J_\alpha^{(\text{qs})}(t) &= - \frac{i}{\hbar} \text{Tr} [\rho_t [H_\alpha, H_t]]. \end{aligned} \quad (8)$$

In finite-time processes there is an additional component of the power, $P^{(\text{non-cons})}(t)$, corresponding to non-conservative processes, including entropy production, which is accompanied by non-equilibrium energy exchange between the driven system and the reservoirs, $J_\alpha^{(\text{non-eq})}(t)$. These components are the most challenging to calculate but they describe the most interesting effects to be addressed in the present article.

Usually, the coupling between the system and the reservoirs is weak, in which case these quantities can be evaluated by means of solving master equations. These have the following general structure,

$$\frac{d\rho_S}{dt} = - \frac{i}{\hbar} [H_S, \rho_S] + \sum_\alpha \mathcal{L}_\alpha [\rho_S], \quad (9)$$

where ρ_S is the reduced density operator for the quantum system. The first term describes the unitary dynamics of the isolated system, while the "Lindbladian" \mathcal{L}_α depends on superoperators describing the effect of the coupling between system and the reservoirs [72]. The underlying assumptions in the derivation of this equation are (i) a weak coupling between system and reservoir, justifying the treatment of H_{cont} as a perturbation and (ii) reservoir with many degrees of freedom, which can be represented by a continuum density of states with short-memory (Markovian) dynamics. The terms entering \mathcal{L}_α depend on rates, which are functions of the couplings, the density of states and the temperature of the reservoir. In non-equilibrium situations with several thermal baths, this equation must be used with care. There are also discussions on the

appropriate basis to be chosen. The so called global version is based on eigenstates of H_S , while the local one is based on eigenstates of those operators entering H_S which also appear in H_{cont} [73, 74, 75, 76, 77, 78, 79]. The equation of motion of the matrix elements of ρ_S can be derived by means of non-equilibrium Green's function formalism [80, 81, 82, 91] in which case the natural basis is the set of eigenstates of H_S . A similar procedure can be followed to calculate the currents $J_\alpha(t)$.

2.2. Adiabatic regime: slow dynamics

In quantum mechanics the notion of adiabaticity is related to the slow evolution. In the context of closed systems, it refers to changes in the spectrum of a Hamiltonian as a function of time-dependent parameters without level crossings and slow evolution in time without transitions between states. This implies a typical time scale for the evolution that is much longer than the internal time scales associated to inter-level transitions. The scope of the latter definition can be extended to open quantum systems by taking into account that the level life-time related to the coupling between the system and the reservoirs defines an extra internal time scale. It is important to stress that in the context of open driven systems adiabatic is not a synonym of quasi-static evolution. Instead, it corresponds to the first non-equilibrium correction to the quasi-static evolution, which is proportional to the rate of change (velocity) of the time-dependent parameters or, equivalently, to the driving period in the case of cyclic protocols [61, 82, 83, 84].

In order to provide a more precise meaning of the adiabatic evolution, we summarize in what follows how to describe this regime in the general framework of the adiabatic linear-response formalism of Refs. [85, 86], assuming one or more reservoirs at the same temperature. This procedure is similar to Kubo formalism [87], but implementing the perturbation with respect to the frozen Hamiltonian. The adiabatic evolution in time of the expectation values of any observable \mathcal{O} is expressed as follows

$$O(t) = \langle \mathcal{O} \rangle_t + \sum_{\ell=1}^N \chi_t^{\text{ad}} [\mathcal{O}, \mathcal{F}_\ell] \dot{X}_\ell(t), \quad (10)$$

where $\langle \cdot \rangle_t$ indicates that the mean value is taken with respect to the thermal distribution ρ_t corresponding to the Hamiltonian frozen at the time t . This contribution is similar to the so-called Born-Oppenheimer approximation and it effectively describes a quasi-static evolution where the system is in equilibrium time by time. The other terms are the non-equilibrium adiabatic corrections, which depend on the adiabatic susceptibilities

$$\chi_t^{\text{ad}} [\mathcal{O}, \mathcal{F}_\ell] = -\frac{i}{\hbar} \int_{-\infty}^t dt' (t-t') \langle [\mathcal{O}(t), \mathcal{F}_\ell(t')] \rangle_t. \quad (11)$$

In the context of closed systems, an equivalent scheme was implemented with focus on the evolution of the quantum states [88, 89].

In this framework it is simple to identify the structure of Eqs. (7) when the energy fluxes in the reservoirs and the forces are evaluated following the previous procedure.

The first term of Eq. (10) leads to the quasi-static and conservative components defined in Eq. (8), while the non-equilibrium and non-conservative components read

$$\begin{aligned} P_\ell^{(\text{non-cons})}(t) &= \dot{X}_\ell(t) \sum_{\ell'} \Lambda_{\ell,\ell'}(\vec{X}) \dot{X}_{\ell'}(t), \\ J_\alpha^{(\text{non-eq})}(t) &= \sum_{\ell} \Lambda_{\alpha,\ell}(\vec{X}) \dot{X}_\ell(t), \end{aligned} \quad (12)$$

being $\Lambda_{\ell,\ell'} = -\chi_t^{\text{ad}}[\mathcal{F}_\ell, \mathcal{F}_{\ell'}]$ and $\Lambda_{\alpha,\ell} = -\chi_t^{\text{ad}}[\dot{H}_\alpha, \mathcal{F}_\ell]$.

2.3. Adiabatic dynamics of a few-level quantum system weakly coupled to thermal baths

To calculate explicitly quantities like those defined in Eq. (12) in the weak-coupling regime and for slow driving we can derive a quantum-master-equation following the procedure of Refs. [82, 90, 91]. This is based on expanding the matrix elements of $\rho_S(t)$ into a frozen and an adiabatic component. Symbolically, $\rho_S(t) = \rho^{(f)}(t) + \rho^{(a)}(t)$, where the superscript f indicates that we are considering the Hamiltonian frozen at a given time t_f , for which $\vec{X}(t_f) = \vec{X}$. The frozen component is the solution of the quantum master equation (9) corresponding to the frozen Hamiltonian.

The detailed structure of the Lindbladian depends on the system under study. In many cases it is proposed on phenomenological grounds. In Refs. [80, 81, 82, 91] a systematic derivation was proposed starting from a given Hamiltonian. This treatment is formulated in terms of Green's function (Schwinger-Keldysh), by implementing a perturbation expansion in the coupling strength. It focuses on stationary situations as well as on slow driving and applies to thermal baths at temperatures T_α . We summarize the outcome because this family of master equations is very useful to analyze the slow dynamics of qubits coupled to several baths [86, 91, 170]. The starting point is the Hamiltonian for the few-level system expressed in the *instantaneous basis of eigenstates*, $\{|s\rangle, j = 1, \dots, L\}$. The baths are represented by bosonic excitations described by $H = \sum_{k_\alpha} \varepsilon_{k_\alpha} a_{k_\alpha}^\dagger a_{k_\alpha}$. The couplings are expressed as follows

$$\begin{aligned} H_S(\vec{X}) &= \sum_{j=1}^L \varepsilon_j(\vec{X}) |j(\vec{X})\rangle \langle j(\vec{X})|, \\ H_{\text{cont},\alpha}(\vec{X}) &= \sum_{j,l=1}^L \sum_{k_\alpha} V_{k_\alpha} \xi_{\alpha,j,l}(\vec{X}) |j(\vec{X})\rangle \langle l(\vec{X})| \left(a_{k_\alpha}^\dagger + a_{k_\alpha} \right), \end{aligned} \quad (13)$$

being $\xi_{j,l}^\alpha(\vec{X})$ elements of the coupling matrix expressed in the instantaneous eigenbasis. The master equation for the frozen component, expressed in terms of the matrix elements, reads

$$\frac{d\rho_{lj}^{(f)}}{dt} = \frac{i\varepsilon_{lj}}{\hbar} \rho_{lj}^{(f)} + \sum_{m,n,\alpha} \left[(M_{ml,\alpha}^{jn} + M_{jn,\alpha}^{lm}) \rho_{mn}^{(f)} - M_{jm,\alpha}^{mn} \rho_{ln}^{(f)} - M_{ml,\alpha}^{mn} \rho_{nj}^{(f)} \right]. \quad (14)$$

We have introduced the definition $\epsilon_{lj} = \epsilon_l(\vec{X}) - \epsilon_j(\vec{X})$, and the rate functions

$$\Gamma_\alpha(\epsilon) = \gamma_\alpha n_\alpha(\epsilon), \quad \bar{\Gamma}_\alpha(\epsilon) = \gamma_\alpha [1 + n_\alpha(\epsilon)]. \quad (15)$$

$\gamma_\alpha(\epsilon) = \sum_{k_\alpha} V_{k_\alpha}/\hbar \delta(\epsilon - \epsilon_{k_\alpha})$ is the spectral function associated to the coupling to the bath and $n_\alpha(\epsilon) = 1/(e^{\epsilon/(k_B T_\alpha)} - 1)$ is the Bose-Einstein distribution function.

The adiabatic component can be calculated from

$$\frac{d\rho_{lj}^{(f)}}{d\vec{X}} \cdot \dot{\vec{X}}(t) = \frac{i\epsilon_{lj}}{\hbar} \rho_{lj}^{(a)} + \sum_{m,n,\alpha} \left[(M_{ml,\alpha}^{jn} + M_{jn,\alpha}^{lm}) \rho_{mn}^{(a)} - M_{jm,\alpha}^{mn} \rho_{ln}^{(a)} - M_{ml,\alpha}^{mn} \rho_{nj}^{(a)} \right]. \quad (16)$$

with

$$M_{ml,\alpha}^{jn} = \xi_{\alpha,ml}(\vec{X}) \xi_{\alpha,jn}(\vec{X}) \{ \Gamma_\alpha(\epsilon_{jn}) + \bar{\Gamma}_\alpha(\epsilon_{nj}) \}. \quad (17)$$

It is important to notice that there are two contributions to the derivative of the matrix elements of the frozen density matrix in Eq. (16) with respect to the parameters. One of the contributions is because of the change of the rates elements $M_{\alpha,j,l}$ as a consequence of the changes of the contacts $\xi_{\alpha,j,l}(\vec{X})$ and the energies $\epsilon_{jl}(\vec{X})$. The other contribution is because of the instantaneous states $|j(\vec{X})\rangle$. It is also interesting to highlight that the latter remain finite even when eliminating the effect of the coupling to the bath. In such case, Eq. (16) reduces to the adiabatic evolution for a driven closed system as described by "adiabatic perturbation theory" formulated in Refs. [88, 89].

Similarly, the frozen and adiabatic component of the energy current can be calculated from

$$J_\alpha^{f/a}(t) = \sum_{m,n,u} \epsilon_{un}(t) \text{Re} [M_{mn,\alpha}^{nu} \rho^{(f/a)}(t)]. \quad (18)$$

2.4. Floquet regime: fast periodic dynamics

The opposite limit to the quasi-static and adiabatic regimes, corresponds to very fast driving. In the regime of strong driving, the notion of a reservoir with a well defined temperature with which the few-level quantum system is contacted is not necessarily useful and the mechanism of thermalization is still under debate [92].

A common situation corresponds to periodic driving with one or more commensurate frequencies and the appropriate framework to describe these problems is Floquet theory [93] which is the time analog of Bloch theory for spatially periodic systems. This type of driving received significant attention recently for the potential to generate novel collective behavior in quantum systems, which may lead to novel states of the matter [92]. The realization of some of these exotic phases has been recently experimentally realized in a quantum processor of superconducting qubits [94].

In the case of a single frequency ω , the Hamiltonian satisfies $H(t + \tau) = H(t)$, with $\tau = 2\pi/\omega$. This operator can be expanded in Fourier series as

$$H(t) = \sum_k e^{ik\omega t} H_k. \quad (19)$$

The Floquet eigenstates have a structure consistent with this periodicity,

$$|\psi(t)\rangle = e^{i\varepsilon/\hbar t} \sum_{n=-\infty}^{+\infty} e^{-in\omega t} |\psi_n\rangle. \quad (20)$$

Hence, when substituted in the Schrödinger equation and using Eq. (19) we find

$$(\varepsilon + \hbar\omega n) |\psi_n\rangle = \sum_{m=-\infty}^{+\infty} H_m |\psi_{n+m}\rangle, \quad (21)$$

which defines a problem with a tight-binding structure in the synthetic Floquet lattice. The structure of this Eq. also reveals the exchange of "Floquet quanta" $\hbar\omega$ underlying this dynamics and effectively provides an environment for the driven system.

This formulation can be generalized for the case of M commensurate frequencies, in which case it is convenient to define $\vec{\omega} = (\omega_1, \dots, \omega_M)$ and also collect the corresponding Floquet indices in a vector \vec{n} . Eq. (21) is generalized to

$$(\varepsilon + \hbar\vec{\omega} \cdot \vec{n}) |\psi_{\vec{n}}\rangle = \sum_{\vec{m}} H_{\vec{m}} |\psi_{\vec{n}+\vec{m}}\rangle. \quad (22)$$

In this scenario, very interesting ideas have been formulated on the transport or exchange of power between the driving sources, some of them will be reviewed in Sec. 5.3. The relevant quantity to analyze is the power defined in Eq. (4). For the case where $\vec{X}(t) = \vec{\omega}t + \vec{\varphi}$, where $\vec{\varphi}$ encloses M independent phases, we get the following expression for the power developed by the ℓ -th force,

$$P_\ell(t) = \omega_\ell \langle \mathcal{F}_\ell \rangle. \quad (23)$$

The expectation value is calculated with respect to the non-equilibrium state $|\psi(t)\rangle$.

2.5. Thermal bias: non-equilibrium stationary regime

When the system is not driven (\vec{X} is constant in time) but it is contacted to several reservoirs at different temperatures, a heat current is established following the thermal bias through the device. Under these conditions the relevant quantity to analyze is the steady-state heat flux at each reservoir, J_α .

The simplest configuration to discuss the mechanism of thermal transport corresponds to a few-level system directly connected to two reservoirs at different temperatures, $T_h > T_c$. The natural process in this case is a stationary heat flux from the hot to the cold reservoir through the quantum system. On general grounds, we should expect that the energy fluxes into the two reservoirs are amenable to be expressed as power series of the thermal bias $\Delta T = T_h - T_c$,

$$J_\alpha = \sum_{n=1}^{\infty} \kappa_{\alpha,n} (\Delta T)^n, \quad \alpha = c, h. \quad (24)$$

The concomitant rate of entropy production at the reservoirs reads

$$\dot{S} = \sum_{\alpha=c,h} \frac{J_\alpha}{T_\alpha}, \quad (25)$$

and can be also expressed in terms of a Taylor series in ΔT . In the limit of small thermal bias, where only the linear component contributes, energy conservation is assumed. Hence $J_c = -J_h = J$, which implies $\kappa_{h,1} = -\kappa_{c,1} = G_{\text{th}}$. The latter parameter is the thermal conductance. When the linear-response contribution is substituted in Eq. (25) we get $\dot{S} = G_{\text{th}} (\Delta T)^2 / T_c$. This simple heuristic observation allows us to conclude that energy dissipation leading to entropy production is a non-linear process, which is consistent with the assumption that energy is conserved if we restrict ourselves to the linear-order contributions.

The linear regime is properly accounted for the Landauer-Büttiker formula, which can be derived exactly for bilinear Hamiltonians [55, 56, 57, 58, 59],

$$J_c = \int_{-\infty}^{+\infty} d\varepsilon \varepsilon \mathcal{T}(\varepsilon) [n_h(\varepsilon) - n_c(\varepsilon)] = -J_h = J, \quad \text{exact for bilinear hamiltonians,} \quad (26)$$

$\mathcal{T}(\varepsilon)$ is the so called transmission function which characterizes the transparency of the device to transmit an amount ε of energy across it, while $n_\alpha(\varepsilon) = 1/(e^{\beta_\alpha \varepsilon} - 1)$ is the Bose-Einstein distribution function (assuming that the bath is described as a gas of non-interacting bosonic excitations), depending on the temperature of the reservoir through $\beta_\alpha = 1/(k_B T_\alpha)$. The transmission function depends on the microscopic details of the setup, including the spectral properties of the reservoirs, the central system and the couplings. In some cases, the same structure of Eq. (26) is obtained for systems with many-body interactions within linear response, but with a temperature-dependent transmission function $\mathcal{T}(\varepsilon, T)$. We shall analyze some examples in Sec. 9.2.

Beyond linear response, and for non-bilinear Hamiltonians, it is necessary to resort to other non-equilibrium many-body techniques to independently calculate the currents at each reservoir. Notice that many-body interactions are expected to introduce inelastic scattering processes that generate dissipation. That type of effects are expected to generate dissipative components in the fluxes into the reservoirs. For weak coupling between system and reservoir, quantum master equations is the most popular framework. Following a similar derivation as that leading to Eq. (9), the current at each reservoir can be written as the frozen component of Eq. (18). The time dependence in this case is not introduced by the Hamiltonian, but by the fact that $\hat{\rho}^f(t)$ is the solution of the time-dependent equation (14). The relevant regime is the long-time solution

$$J_\alpha = \lim_{t \rightarrow \infty} J_\alpha(t). \quad (27)$$

The underlying assumption in this type of calculation is that the reservoirs have a well defined temperature. For situations where the temperature bias is large, many-body interactions may contribute to build-up an effective temperature profile along the quantum system if it has a spatial distribution. We shall discuss this aspect in Sec. 9.

2.6. *Slow dynamics in combination with small thermal bias. Thermal geometric tensor and Onsager relations*

The simultaneous effect of a thermal bias and driving is of great interest in the study of thermal machines operating in contact to thermal baths at different temperatures. In the case of slow dynamics and for a the case of two reservoirs with a small thermal bias ΔT – such that $\Delta T/T$ is a small parameter – the adiabatic formalism introduced in Sec. 2.2 can be adapted to include $\Delta T/T$ as an additional entry in an extended vector $\dot{\mathbf{X}} = (\dot{\vec{X}}, \Delta T/T)$. The extra entry associated to the temperature bias is labeled by $N + 1$. This procedure can be naturally implemented in a very general way starting from the Hamiltonian representation of the thermal bias introduced by Luttinger [95, 96] and following similar steps as in the adiabatic Kubo-like derivation presented in Sec. 2.2. Details can be found in Ref. [86]. Here, we outline the main result, according to which the expressions for the non-conservative power and the non-equilibrium heat fluxes presented in Eqs. (12) are extended to

$$\begin{aligned} P_\ell^{(\text{non-cons})}(t) &= \dot{X}_\ell(t) \sum_{\ell'} \Lambda_{\ell,\ell'}(\vec{X}) \dot{X}_{\ell'}(t) + \dot{X}_\ell(t) \Lambda_{\ell,N+1}(\vec{X}) \frac{\Delta T}{T}, \\ J_c^{(\text{non-eq})}(t) &= \sum_{\ell} \Lambda_{N+1,\ell}(\vec{X}) \dot{X}_\ell(t) + \Lambda_{N+1,N+1}(\vec{X}) \frac{\Delta T}{T}. \end{aligned} \quad (28)$$

The notation highlights the fact that the linear-response coefficients define a $(N + 1) \times (N + 1)$ matrix which is named the *thermal geometric tensor*. The geometrical nature is because of the dependence of all the entries on \vec{X} . The last term of the second equation is proportional to the thermal conductance of the system.

In the case of cycles, and focusing on quantities averaged over the period τ , the same argument of the previous section, regarding energy conservation of power-counting in $\dot{\mathbf{X}}$ leads us to conclude that

$$\int_0^\tau dt J_c^{(\text{non-eq})}(t) = - \int_0^\tau dt J_h^{(\text{non-eq})}(t) = Q_c. \quad (29)$$

Importantly, the linear response coefficients can be shown to satisfy Onsager relations [85, 86] so that

$$\Lambda_{N+1,\ell}(\vec{X}) = -s_\ell \Lambda_{\ell,N+1}(\vec{X}), \quad \Lambda_{\ell,\ell'}(\vec{X}) = s_\ell s_{\ell'} \Lambda_{\ell',\ell}(\vec{X}). \quad (30)$$

The sign $s_\ell = \pm$ depends on whether the operators \mathcal{F}_ℓ are even/odd under the transformation $t \rightarrow -t$.

Here, we see that the thermal geometric tensor has symmetric and antisymmetric components. The entropy generation is associated to the symmetric component. In fact, the entropy production is associated to the total dissipated work. This contains a component due to the work done by the non-conservative driving forces and another component which accounts for the thermal bias –the latter is the usual contribution

taken into account in thermoelectricity (see Ref. [19]) – and the result is

$$\begin{aligned} W^{(\text{diss})} &= \int_0^\tau dt \left\{ \sum_{\ell=1}^N P_\ell^{(\text{non-cons})}(t) + J_c^{(\text{non-eq})}(t) \frac{\Delta T}{T} \right\} \\ &= \int_0^\tau dt \dot{\vec{X}} \cdot \underline{\Lambda}^S(\vec{X}) \cdot \dot{\vec{X}} + \Lambda_{N+1, N+1} \left(\frac{\Delta T}{T} \right)^2, \end{aligned} \quad (31)$$

where we have introduced the notation $\underline{\Lambda}^S(\vec{X})$ for the matrix containing the symmetric component of $\Lambda_{\ell, \ell}(\vec{X})$.

All these results are valid for any system and for any type of coupling to the thermal baths. In the case of weak coupling, the explicit calculation of the coefficients defining the thermal geometric tensor can be accomplished by solving Eqs. (14), (16) and (18) with a small temperature difference ΔT and performing a linear expansion in this quantity.

2.7. From Lindblad equation to quantum trajectories

The description based on quantum master equations, briefly introduced in Sec. 2.1, resembles the classical Langevin dynamics of the Brownian particle embedded in the bath. Stochastic thermodynamics is the field where this theoretical description is elaborated in classical [97, 98, 100] and quantum-mechanical [101, 102, 103] contexts. Recently, there is a surge of interest in analyzing the effect of quantum measurements in the evolution of qubit systems. Measurements are key elements in quantum mechanics in general and are fundamental processes in the operation of quantum computing devices. In principle, a measurement protocol could be represented by a time-dependent term in the Hamiltonian of Eq. (1). However, if the consequent outcome is fast enough, it is appropriate to represent this effect as a stochastic perturbation. This point of view was adopted some time ago in the theory of continuous measurements and quantum trajectories [104, 105]. Nowadays, it motivates the study of phase transitions induced by the effect of measurements in arrays of qubit systems, which is an active avenue of research [106, 107, 108].

In the context of quantum thermodynamics, the stochastic effect of measurements formally plays an analogous role as the thermal bath but of a quantum nature [109, 110, 111, 112, 113, 114]. The description of the stochastic dynamics has been combined with Lindblad master equation for a single qubit weakly coupled to a single reservoir and we summarize below the main ideas. Lindblad equation is formally expressed as Eq. (9) with

$$\mathcal{L}[\rho_S] = \sum_{k=1}^{D^2-1} \Gamma_k \left(L_k \hat{\rho}_S L_k^\dagger - \frac{1}{2} \{ \rho_S, L_k^\dagger L_k \} \right), \quad (32)$$

being D the dimension of the Hilbert space of the system and $\{.,.\}$ denoting anticommutation. The quantities Γ_k are rates describing the coupling with the reservoir and L_k are "jump" operators, describing the changes between the different quantum

states of the system. The effect of the measurement is introduced by considering a stochastic unravelling of this equation. This can be implemented by taking the statistical average over a completely positive trace-preserving map that inverts Eq. (9). Such a procedure is achieved by introducing Kraus operators as follows [109]

$$\rho_S(t + dt) = \sum_{\mathcal{K}=\infty}^D M_{\mathcal{K}}(t) \rho_S(t) M_{\mathcal{K}}^\dagger(t), \quad (33)$$

where \mathcal{K} denotes the labeling of the eigenbasis defining the measuring apparatus, while

$$M_{\mathcal{K}}(t) = \left[1 - \frac{i}{\hbar} dt H_{\text{eff}}(t) + \sum_{k=1}^{D^2-1} \sqrt{\Gamma_k} dw_k^{\mathcal{K}}(t) L_k \right] \times \sqrt{\prod_k p(dw_k^{\mathcal{K}}(t))},$$

$$H_{\text{eff}}(t) = H_S(t) - \frac{i}{2} \sum_{k=1}^{D^2-1} \Gamma_k L_k^\dagger L_k. \quad (34)$$

Here $dw_k^{\mathcal{K}}(t)$ is an stochastic increment that satisfies

$$\langle dw_k^{\mathcal{K}}(t) \rangle_\gamma = 0, \quad \langle \langle dw_k^{\mathcal{K}}(t) dw_l^{\mathcal{K}}(t) \rangle \rangle_\gamma = dt \delta(t - t') \delta_{k,l}, \quad (35)$$

and $p(dw_k^{\mathcal{K}}(t))$ is the corresponding probability. Each realization of the stochastic increment defines a quantum trajectory. Hence, the notation $\langle \dots \rangle_\gamma$ indicates average over quantum trajectories.

Other procedures following similar ideas have been recently proposed for the analysis of measurements in non-equilibrium situations [126, 127]. Quantum fluctuations play a relevant role in this context [115, 116, 117, 118, 119, 120] and several works rely on the formalism based on quantum jumps and the trajectory description of the evolution of the system to analyze this effect [121, 122, 123, 124, 125]. We shall not address this topic in the present review and we defer the reader to other review articles where it has been covered [17, 18, 21, 22, 102, 114].

As we shall discuss in Section 2.7, in quasi-static processes it is usual to define heat and work following the same reasoning as in the case described in Eq. (2) upon calculating the traces with the operator $\rho_S(t)$ after solving Eq. (33) and taking the average over all the quantum trajectories.

3. Models for a qubit and the environment of harmonic oscillators

A qubit is a two-level system amenable to be operated in order to prepare quantum superpositions of the basis states. The paradigmatic Hamiltonian to describe such a system is,

$$H_{\text{qubit}} = -B_z \sigma^z - B_x \sigma^x, \quad (36)$$

where σ^x , σ^z are the Pauli matrices. We are considering the basis of eigenstates of the first term of Eq. (36), $\{|\uparrow\rangle, |\downarrow\rangle\}$. The effect of the second term is to generate the mixing of these two states. This Hamiltonian can be realized in a wide variety of

platforms, including atomic systems, semiconductors, NV centers, and superconductors [1]. In Sec. 10 we shall briefly explain its realization in superconducting devices.

We focus on environments which can be represented by sets of quantum harmonic oscillators. This model was introduced by Caldeira and Leggett in Refs. [128, 129, 130] and naturally describes a reservoir of photons or phonons. As we shall discuss in Sec. 10, microwave resonators and transmission lines in cQED are also represented by this type of model. The corresponding Hamiltonian reads

$$H_{\text{res}} = \sum_k \hbar\omega_k a_k^\dagger a_k, \quad (37)$$

where a_k^\dagger/a_k creates/destroys a bosonic mode with frequency ω_k . The number of relevant modes entering this Hamiltonian depends on the problem under study. We shall analyze in the forthcoming sections many situations where it contains an infinite number of modes, in which case this system behaves as a reservoir or a thermal bath.

A natural and simple coupling between the two systems is

$$H_{\text{qubit-res}} = \sum_k \vec{g}_k \cdot \vec{\sigma} \left(a_k^\dagger + a_k \right), \quad (38)$$

with $\vec{\sigma} = (\sigma^x, \sigma^y, \sigma^z)$. The coupling to the reservoir depends on the state of the qubit. For instance, in the case of $\vec{g}_k = (g_{k,x}, 0, 0, 0)$, the qubit and the bath are coupled when the state of the qubit has a projection along the x -direction in the Bloch sphere. In Sec. 10 we shall show that this type of coupling is naturally derived in common architectures of superconducting qubits coupled to transmission lines. In the theoretical description it is sometimes convenient to consider the coupling of Jaynes-Cummings model [131] of quantum optics, which reads

$$H_{\text{J-C}} = \sum_k g_k \left(\sigma^+ a_k + \sigma^- a_k^\dagger \right), \quad (39)$$

with $\sigma^\pm = \sigma^x \pm i\sigma^y$. This coupling is interpreted as a transition from the ground state to the excited state of the two-level system by absorbing a photon and the opposite process, where a photon is emitted as the state of the system changes from the excited to the ground state.

The Hamiltonian for the two-level system coupled to a bath of harmonic oscillators defines the celebrated spin-boson model [132, 130]. In the theoretical description it is useful to introduce an hybridization function characterizing the coupling of the two-level system with the environment,

$$\Gamma(\varepsilon) = 2\pi \sum_k |g_k|^2 \delta(\varepsilon - \hbar\omega_k). \quad (40)$$

For an environment with an infinite number of oscillator modes, this is a continuous function and it is usual to model it by a power-law $\Gamma(\varepsilon) \propto \varepsilon^s$. The case with $s = 1$ is named ohmic environment, while the cases with $s > 1, < 1$ are named, respectively,

super-ohmic and sub-ohmic. This model has a quantum phase transition at zero temperature depending on the strength of coupling between the system and the reservoir and the spectral properties of the latter (ohmic, subohmic or superohmic) [133, 134]. The phase transition from a state that is a combination of the two qubit states to one where the ground state is localized at one of them takes place above a critical coupling. The type of transition strongly depends on the nature of the bath. In the sub-ohmic case, the transition is of second-order [135, 136, 137, 138, 139, 140], while the ohmic case shows a Kosterlitz-Thouless transition [130, 141, 142]. The super-ohmic case does not have a phase transition but exhibits a crossover. Another interesting feature of the ohmic environment is the associated Kondo effect [143] at sufficiently low temperatures [144, 145]. In most of the real situations, mainly in cQED, the degree of coupling between the qubit and the environment is weak, which prevents the experimental analysis of this phase transition and justifies its theoretical study by means of Lindblad-type quantum master equations. Quite recently, however, strong-coupling configurations were realized between superconducting circuits and the electromagnetic environment [146, 147, 148, 149, 150], which enabled the realization of the strongly-coupled spin-boson model in this platform.

In the next sections we shall discuss different mechanisms of energy dynamics with focus on a single qubit. In spite of the simplicity of this system, when the effect of time-dependent driving is included and different settings with one or more reservoirs are considered, a rich variety of phenomena may take place. Our goal is to analyze several of them in detail. Concretely, we shall consider the case of the qubit coupled to a single reservoir at finite temperature under time-dependent driving, in which case we identify two interesting mechanism taking place: (i) energy dissipation because of the driving (ii) power exchange between driving sources. Then, we shall turn to analyze configurations where the qubit is coupled to two reservoirs at the same temperature and under time-dependent driving, where the interesting mechanism is the possibility of pumping energy between the two reservoirs as a consequence of the driving. Next, we shall analyze the configurations where the driven qubit is coupled to two reservoirs at different temperatures. This enables the realization of thermal machines: heat-engines and refrigerators. We shall also discuss the realization of batteries in configurations of qubits coupled to reservoirs and isolated. In the case of arrays with two reservoirs at different temperatures, we shall also analyze the thermal transport in the steady-state regime.

4. Driving and energy dissipation

4.1. General considerations

One of the simplest albeit non-trivial configurations is a single qubit under time-dependent driving coupled to a single bath with a well defined temperature T . In terms of the two-level Hamiltonian, these effects can be represented by the following

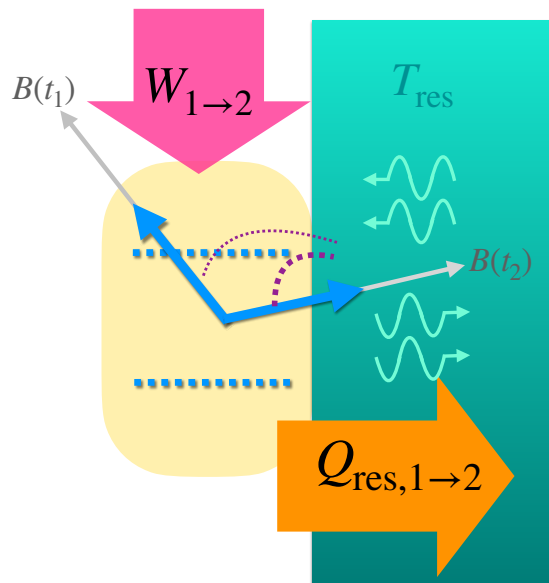


Figure 1. Illustration of the consequent energy dynamics of the qubit under a time-dependent operation in contact to a thermal bath. The qubit is represented by two-levels and the vector \vec{B} (grey arrow). The corresponding quantum state in Bloch coordinates is represented by the blue arrow. The energy dynamics consists in the exchange of work with the time-dependent sources and the exchange of heat between the qubit and the reservoir as described by Eqs. (6) and (7). The net effect in a finite-time process is the transformation of the work invested by the external sources into heat that is dissipated into the reservoir.

Hamiltonian

$$H_{\text{qubit}}(t) = -\vec{B}[\vec{X}(t)] \cdot \vec{\sigma}, \quad (41)$$

with $\vec{B}[\vec{X}(t)] = (B_x[\vec{X}(t)], B_y[\vec{X}(t)], B_z[\vec{X}(t)])$ depending on time through the protocols $\vec{X}(t)$, while $\vec{\sigma} = (\sigma^x, \sigma^y, \sigma^z)$ is composed by the three Pauli matrices operating in the qubit Hilbert space. It is natural to assume the coupling between the driven qubit and the bosonic reservoir described by Eq. (38).

The full system is described by the Hamiltonian

$$H(t) = H_{\text{qubit}}(t) + H_{\text{qubit-res}} + H_{\text{res}}, \quad (42)$$

where $H_{\text{res}} = \sum_k \hbar\omega_k a_k^\dagger a_k$ is the Hamiltonian of the Caldeira-Leggett bath of harmonic-oscillator modes as in Eq. (133).

The device and represented by the Hamiltonian of Eq. (42) is illustrated in Fig. 1. As a consequence of the driving represented by $\vec{B}(t)$ the qubit state changes in time. In general, this also affects the degree of coupling between the qubit and the reservoir. In this process, energy is exchanged between the driving sources and the qubit-reservoir system. If it takes place at a finite-time this corresponds to a non-equilibrium evolution of the combined qubit-reservoir system and the net result is the

dissipation of the supplied energy in the form of heat into the reservoir. The rest of this section is devoted to analyze this mechanism.

4.2. Adiabatic regime and thermodynamic length

We analyze here the mechanism of dissipation introduced by the time-dependent driving in the adiabatic regime. We recall that the main general ideas of this approach were presented in Sec. 2.2.

The dissipation is accounted for the non-conservative component of the developed power, Eq. (12), $P^{(\text{diss})} \equiv P^{(\text{non-cons})}$. We conclude that the net entropy production as the system is driven between the times t_1 and t_2 can be expressed as

$$T\Sigma = W^{(\text{diss})} = \sum_{\ell, \ell'} \int_{t_1}^{t_2} dt \dot{X}_\ell(t) \Lambda_{\ell, \ell'}^S(\vec{X}) \dot{X}_{\ell'}(t), \quad (43)$$

being T the temperature of the reservoir, Σ the total entropy production and $W^{(\text{diss})}$ the net dissipated work.

At this point we can introduce the ideas associated to the geometric description of the energy dissipation and entropy production of slowly driven systems, which recently became a topic of interest in finite-time thermodynamics. A fundamental concept behind this description is the *thermodynamic length* introduced in Refs. [152, 153] and further elaborated in Refs. [154, 155, 156, 157, 158, 159, 160, 161, 162, 163].

The key property is the fact that $\Lambda_{\ell, \ell'}^S(\vec{X}(t))$ is positive definite because of Eq. (43) and the fact that the second law of the thermodynamics implies $\Sigma \geq 0$. Consequently, this tensor has the necessary properties to be the metric of a Riemannian space. In a Riemannian metric it is possible to define the distance along curves connecting different points. The length of a curve parameterized by t , from t_1 to t_2 is

$$\mathcal{L} = \int_{t_1}^{t_2} dt \sqrt{\dot{\vec{X}}(t) \cdot \underline{\Lambda}^S(\vec{X}) \cdot \dot{\vec{X}}(t)}, \quad (44)$$

where we denoted by $\underline{\Lambda}(\vec{X})$ the matrix with elements $\Lambda_{\ell, \ell'}(\vec{X})$. The curves of minimal distance are called geodesics. Using Cauchy-Schwartz inequality, $\int_{t_0}^{t_1} dt f^2 \int_{t_1}^{t_2} dt g^2 \geq \left[\int_{t_1}^{t_2} dt f g dt \right]^2$, with $g = 1$ and f being the argument of the integral of Eq. (44) leads to the following relation

$$T\Sigma \geq \frac{\mathcal{L}^2}{\delta t}, \quad (45)$$

with $\delta t = t_2 - t_1$. The dissipated power $T\Sigma$ is a non-geometric quantity because it depends on the way in which the path in the parameter space is circulated. Nevertheless Eq. (45) tells us that it is lower-bounded by a purely geometric quantity which depends on the path, the *thermodynamic length* \mathcal{L} . The lower bound of Eq. (45) is saturated when the integrand is constant along the path. This corresponds to circulating at a velocity that satisfies a constant dissipation rate at each point of the trajectory. Among all the possible protocols, there exist one path –the geodesic– for which \mathcal{L} and therefore

the dissipation is minimal [154, 155, 159]. This is a remarkable property, which is very useful in the design of optimal finite-time protocols.

In the limit of weak coupling to the reservoir, this description can be combined with a Lindblad master equation and the adiabatic expansion explained in Sec. 2.2. Here we summarize the main steps. The starting point is the density matrix expressed in the instantaneous frame of eigenstates of the qubit Hamiltonian. This is achieved by transforming the Hamiltonian of Eq. (41) with a unitary transformation $U(\vec{X})$ as follows

$$H_{\text{qubit}}(\vec{X}) = |\vec{B}(\vec{X})\rangle U(\vec{X}) \sigma^z U^{-1}(\vec{X}). \quad (46)$$

In the case of a qubit, a very convenient representation relies on introducing vectors with the matrix elements $\rho^{(f/a)}$ in Eqs. (14) and (16), which are defined from the decomposition of the frozen density operator in Pauli matrices as follows

$$\rho^{(f)} = \frac{(\sigma^0 + \vec{\rho}^{(f)} \cdot \vec{\sigma})}{2}, \quad \rho^{(a)} = \frac{\vec{\rho}^{(a)} \cdot \vec{\sigma}}{2} \quad (47)$$

with $\vec{\rho}^{(f/a)} = \left(\rho_x^{(f/a)}, \rho_y^{(f/a)}, \rho_z^{(f/a)} \right)$, and

$$\rho_x^{(f/a)} = \rho_{12}^{(f/a)} + \rho_{21}^{(f/a)}, \quad \rho_y^{(f/a)} = i(\rho_{12}^{(f/a)} - \rho_{21}^{(f/a)}), \quad \rho_z^{(f/a)} = \rho_{11}^{(f/a)} - \rho_{22}^{(f/a)}. \quad (48)$$

In this notation, the action of the Lindbladian operator in the master equation for ρ define a matrix $\mathcal{M}(\vec{X})$ and a vector $\vec{\gamma}$ in terms of which the stationary solution of Eq. (14) and Eq. (16) can be written as follows

$$\mathcal{M}(\vec{X}) \vec{\rho}^{(f)}(\vec{X}) = \vec{\gamma}^{(f)}(\vec{X}), \quad \sum_{\ell} \frac{\partial \vec{\rho}^{(f)}(\vec{X})}{\partial X_{\ell}} \dot{X}_{\ell} = \mathcal{M}(\vec{X}) \vec{\rho}^{(a)}(\vec{X}). \quad (49)$$

The solution is

$$\vec{\rho}^{(a)}(\vec{X}) = \sum_{\ell} \mathcal{M}^{-1}(\vec{X}) \frac{d\vec{\rho}^{(f)}(\vec{X})}{dX_{\ell}} \dot{X}_{\ell}. \quad (50)$$

As mentioned in Sec. 2.2, it is important to consider in $d\vec{\rho}^{(f)}(\vec{X})/dX_{\ell}$, not only the changes because of $\mathcal{M}(\vec{X})$, but also the change of basis introduced by $U(\vec{X})$ in Eq. (46). The dissipated energy because of the driving mechanism in a time interval between t_1 and t_2 reads

$$W^{(\text{diss})} = \sum_{\ell} \int_{t_1}^{t_2} dt \text{Tr} \left[\rho^{(a)} \sum_{\ell} \frac{\partial H_{\text{qubit}}(\vec{X})}{\partial X_{\ell}} \right] \dot{X}_{\ell} \equiv \sum_{\ell} \int_{t_1}^{t_2} dt \text{Tr} \left[\rho^{(a)} \sum_{\ell} \mathcal{F}_{\ell}(\vec{X}) \right] \dot{X}_{\ell}. \quad (51)$$

where $H_{\text{qubit}}(\vec{X})$ denotes the frozen Hamiltonian of the driven qubit. Introducing the representation

$$\mathcal{F}_{\ell}(\vec{X}) = \vec{f}_{\ell}(\vec{X}) \cdot \vec{\sigma}, \quad (52)$$

and substituting Eq. (50) in Eq. (51) leads to the expression of Eq. (43) with

$$\Lambda_{\ell', \ell}^S(\vec{X}) = \mathcal{M}^{-1}(\vec{X}) \frac{d\vec{\rho}^{(f)}(\vec{X})}{dX_{\ell}} \cdot \vec{f}_{\ell'}(\vec{X}). \quad (53)$$

These ideas became recently very useful in the study of the slow evolution of driven qubits. They were the guide in the search for optimal protocols to minimize the dissipation in a single driven qubit weakly contacted to a reservoir modeled by the Hamiltonian of Eq. (137) and also for a set of coupled qubits [164, 165]. Notice that while the bound of Eq. (45) is known to exist, the explicit form of the geodesic implies solving a non-trivial differential equation. In Ref. [164] the derivation leading to Eq. (50) was formulated in the language of Lindbladian operators and the Drazin inverse. Analytical expressions were derived for a single qubit a bath of harmonic oscillators modeled by Eq. (42) with $\vec{X}(t) = (B(t), \theta(t), \varphi(t))$ and

$$\vec{B}(\vec{X}) = B\vec{n}, \quad \vec{n} = (\cos \varphi \sin \theta, \sin \varphi \sin \theta, \cos \theta), \quad (54)$$

for which the unitary transformation entering Eq. (46) reads

$$U(\vec{X}) = \begin{pmatrix} \cos(\theta/2) & -e^{-i\varphi} \sin(\theta/2) \\ e^{i\varphi} \sin(\theta/2) & \cos(\theta/2) \end{pmatrix} \quad (55)$$

Details of the calculation are presented in Appendix A.

The result for the symmetric component of the thermal geometric tensor defining the metric in Eq. (44) is [164]

$$\Lambda_{\ell, \ell'}^S = \text{Diag}(\beta\lambda_B, B\lambda_q, B\lambda_q \sin^2 \theta), \quad (56)$$

with

$$\lambda_B = \frac{1}{\Gamma(B)} \frac{\sinh(\beta B)}{\cosh^3(\beta B)}, \quad \lambda_q = \frac{1}{\Gamma(B)} \tanh^2(\beta B). \quad (57)$$

The function $\Gamma(B) = \gamma_0 B^s$ with $s = 1, > 1, < 1$ defines the spectral properties of the bosonic bath (Ohmic, super-Ohmic and sub-Ohmic, respectively).

This behavior is intriguing, since we can see that radial protocols are less dissipative than those evolving tangentially over a solid angle in the low temperature regime where $\beta B > 1$. This reveals the different nature of these two protocols. The radial one affects an exponentially small fraction of the populations and has a small impact at low enough temperatures. Instead, the tangential one directly affects the off-diagonal elements of the density matrix (coherences). This remarkable different behavior exhibits the relevance of optimizing the protocols in order to reduce the dissipation.

These ideas were also used to minimize the dissipation in finite-time Otto and Carnot cycles implemented in qubits [166, 167], to analyze the work fluctuations in these systems [168, 169], and more recently, to minimize the dissipation in cycles implemented in qubits simultaneously coupled to several reservoirs [170, 171].

4.3. Shortcuts to adiabaticity

The first ideas behind the concept of shortcuts to adiabaticity were proposed by Berry [172] in the context of closed quantum systems and are formulated in simple terms in the abstract of that paper:

For a general quantum system driven by a slowly time-dependent Hamiltonian, transitions between instantaneous eigenstates are exponentially weak. But a nearby Hamiltonian exists for which the transition amplitudes between any eigenstates of the original Hamiltonian are exactly zero for all values of slowness.

Such nearby Hamiltonian is constructed by adding "counter-diabatic" terms to the original time-dependent one. In practice, this implies considering the evolution defined by the following effective Hamiltonian

$$H_{\text{eff}}(t) = H(t) + i\hbar \sum_n (|\partial_t n\rangle\langle n| - \langle n|\partial_t n\rangle|n\rangle\langle n|), \quad (58)$$

where $\{|n\rangle\}$ are the instantaneous eigenstates of the original Hamiltonian $H(t)$.

For some years now, this is a topic of great interest with many applications and the recent developments are covered in Ref. [173]. Taking into account the analysis of the dissipation in finite-time protocols discussed in Sec. 4.2, it is expected that this type of mechanism could be useful to minimize dissipation without requiring slow driving. The explicit calculation of the counter-diabatic terms in Eq. (58) is a non-trivial problem since they depend on the states of the full Hamiltonian. While that calculation is in principle possible for closed systems, this is a difficult task in the case of quantum systems coupled to reservoirs [174, 175]. Furthermore, the additional counter-diabatic terms are expected to generate additional dissipation.

An interesting and different approach amenable to be used in open quantum systems was proposed in Refs. [165, 176]. The strategy is similar to the adiabatic linear response formalism reviewed in Sec. 2.2. However, instead of considering a slow evolution, an arbitrary fast evolution with a small amplitude is considered. This is basically the scenario of usual linear response theory and Kubo formalism [87]. Concretely, small changes in the amplitudes of the parameters but arbitrary speed as the system evolves from t_0 to $t_1 = t_0 + \delta t$ are assumed such that

$$\vec{X}(t) = \vec{X}(t_0) + g(t)\delta\vec{X}, \quad (59)$$

with $g(t_0) = 0$ and $g(t_1) = 1$. In this approach the Hamiltonian of the system is expanded as

$$H(t) = H(\vec{X}_0) - g(t) \sum_{\ell} \mathcal{F}_{\ell}(\vec{X}_0) \delta X_{\ell}. \quad (60)$$

Expressing the definition of the work given in Eq. (6) as

$$W_{0 \rightarrow 1} = - \sum_{\ell} \int_{t_0}^{t_1} \langle \mathcal{F}_{\ell}(\vec{X}) \rangle \dot{X}_{\ell}(t) dt = W^{(\text{cons})} + W^{(\text{diss})}, \quad (61)$$

and calculating $\langle \mathcal{F}_{\ell} \rangle$ in linear response, it is found

$$W^{(\text{diss})} = \sum_{\ell, \ell'} \delta X_{\ell} \delta X_{\ell'} \int_{t_0}^{t_1} dt \int_{-\infty}^t dt' \dot{g}(t) \Psi_{\ell, \ell'}(t - t') \dot{g}(t'), \quad (62)$$

with

$$-\frac{d\Psi_{\ell,\ell'}(t-t')}{dt'} = \chi_{\ell,\ell'}(t-t') = -\frac{i}{\hbar}\Theta(t-t')\langle[\mathcal{F}_\ell(t), \mathcal{F}_{\ell'}(t')]\rangle_0, \quad (63)$$

being $\chi_{\ell,\ell'}(t-t')$ the retarded susceptibility, $\Theta(t)$ is the Heaviside function and $\langle.\rangle_0$ indicates that the statistical averages are calculated with respect the Hamiltonian $H(\vec{X}_0)$. In Ref. [165] it is argued that there exist special protocols satisfying the small amplitude condition in a qubit system where the coupling with reservoir is vanishing small and having $W^{(\text{diss})} = 0$. For finite coupling, we should expect $W^{(\text{diss})} \neq 0$, even in the limit where the coupling is weak. In such cases, Eq. (62) could be used to minimize $W^{(\text{diss})}$ in fast processes. The comparison of this approach with the optimization in the adiabatic regime analyzed in Section (4.2) is an interesting open problem.

5. Power pumping

5.1. General considerations

The mechanism of power pumping consists in the exchange of power between driving sources of different nature in quantum systems under cyclic driving. It may take place in open as well as in closed quantum systems and has been been studied in qubits in Refs. [177, 178, 179].

The net power pumping between two sources ℓ , ℓ' is quantified by the time-average of

$$P_{\ell,\ell'}^{(\text{pump})}(t) = \frac{P_\ell(t) - P_{\ell'}(t)}{2}, \quad (64)$$

where $P_\ell(t)$ is defined in Eq. (4).

In the adiabatic regime discussed in Sec. 2.2 substituting the expansion of Eq. (12) in Eq. (64) leads to

$$P_{\ell,\ell'}^{(\text{pump})}(t) = \frac{P_\ell(t) - P_{\ell'}(t)}{2} = \dot{X}_\ell(t) \Lambda_{\ell,\ell'}^A(\vec{X}) \dot{X}_{\ell'}(t), \quad \text{adiabatic}, \quad (65)$$

where we have dropped the conservative component because its average over a cycle vanishes. This equation stresses that only the antisymmetric component of $\Lambda_{\ell,\ell'}(\vec{X})$ contributes. Recalling that in Sec. 4 it was shown that only the symmetric component of this tensor contributes to dissipation, we see that power pumping can be viewed as the complementary process to dissipation. In fact, driving forces with an associated antisymmetric adiabatic susceptibility do not contribute to dissipation but behave similarly to a Lorentz force. This has been discussed in driven electron systems Ref. [180, 181, 182] and in models of coupled harmonic oscillators [160]. This mechanism is likely to be related to other work-work conversion proposals studied in the literature[183, 184].

5.2. Topological power pumping in the adiabatic regime

One of the most paradigmatic effects associated to the adiabatic evolution is the generation of a geometric phase that accumulates in a cyclic protocol. This phase

contributes independently to the dynamical time-dependent one and provides signatures of the properties of a quantum system. In quantum mechanics this concept has been put forward by Berry [185, 186, 187], but such a phase is not exclusive of this field and also appears in the slow evolution of classical systems [188]. Importantly, this is a fundamental concept in the characterization of topological phases of matter [189, 190, 191, 192, 193, 194]. In fact, Chern insulators, which are one of the best well-known topological states of matter and include the quantum Hall state, are characterized by a quantized Berry phase normalized by 2π : the Chern number. The Berry phase can be alternatively evaluated as an area integral of the Berry curvature.

Remarkably, these geometrical properties can be found in the adiabatic dynamics of single qubit system. Here, the relevant regime corresponds to low enough temperatures where the system evolves close to the instantaneous ground state. This was shown in Ref. [195] and it was experimentally verified in Ref. [196], which will be reviewed in Sec. 11.3. Here, we start by briefly reviewing the main ideas of Ref. [195] expressing them in the same notation of previous sections. In that work, the adiabatic dynamics of the Hamiltonian of Eq. (41) is analyzed and it is shown that some protocols are characterized by a Berry phase. In particular, spherical coordinates as defined in Eq. (54) are considered and a protocol with B constant and constant velocity $\dot{\theta}$ is implemented. The adiabatic dynamics of the expectation value of $\mathcal{F}_\phi = -\partial H_{\text{qubit}}/\partial\phi$ (see Sec. 2.2) is

$$\langle \mathcal{F}_\phi \rangle(t) = \langle \mathcal{F}_\phi \rangle_t + \Lambda_{\phi,\theta}(\theta, \phi)\dot{\theta}(t). \quad (66)$$

For the system in the ground state, $|g\rangle$, the calculation of the adiabatic susceptibility leads to

$$\Lambda_{\phi,\theta} = \Omega_g = i\hbar [\langle \partial_\phi g | \partial_\theta g \rangle - \langle \partial_\theta g | \partial_\phi g \rangle], \quad (67)$$

where we see that it is purely antisymmetric and coincides with the definition of the Berry curvature. The explicit calculation gives $\Lambda_{\phi,\theta} = \hbar/2 \sin \theta$, and the integration over the spherical surface leads to the definition of the Chern number, which is found to be quantized,

$$C_g = \frac{1}{2\pi} \int_0^\pi d\theta \int_0^{2\pi} d\phi \Omega_g = 1. \quad (68)$$

This result indicates that $\langle \mathcal{F}_\phi \rangle$ can be characterized by the Chern number and that it can be quantized for some protocols. As we highlighted in Eq. (67), the Berry curvature is related to the antisymmetric component of $\Lambda_{\ell,\ell'}$ and this property has also been noticed in open quantum systems connected to reservoirs at finite temperature [86].

The fact that $\Lambda_{\ell,\ell'}^A$ defines forces characterized by topological numbers in a qubit and recalling Eq. (65) suggests the possibility of topological power pumping in the adiabatic regime of these systems. This is precisely confirmed by analyzing the results reported in Ref. [179]. In that paper, and also in Refs. [177, 178], the Hamiltonian of Eq. (41) is considered with

$$\vec{B}(\vec{X}) = \frac{B_0}{2} (\sin X_1, \sin X_2, 2 + \delta - \cos X_1 - \cos X_2). \quad (69)$$

This model is formally identical to the reciprocal-lattice representation of a model for a Chern insulator [197, 198]. In the present case, there are two driving parameters, $\vec{X} = (X_1(t), X_2(t))$, and the corresponding adiabatic reaction forces are

$$\begin{aligned}\mathcal{F}_1 &= -\frac{\partial H}{\partial X_1} = \frac{B_0}{2} [\sigma_x \cos X_1 + \sigma_z \sin X_1], \\ \mathcal{F}_2 &= -\frac{\partial H}{\partial X_2} = \frac{B_0}{2} [\sigma_y \cos X_2 + \sigma_z \sin X_2].\end{aligned}\quad (70)$$

The implemented driving protocol is

$$X_\ell(t) = \omega_\ell t + \varphi_\ell, \quad (71)$$

with frequencies ω_ℓ , $\omega_{\ell'}$ such that they are small enough to justify the adiabatic description. The explicit calculation of the pumped power considering the system in the ground state leads to

$$P_{1,2}^{(\text{pump})}(\vec{X}) = \frac{P_1 - P_2}{2} = \omega_1 \omega_2 \Lambda_{1,2}^A(\vec{X}), \quad (72)$$

with $\Lambda_{1,2}^A(\vec{X}) = \Omega_g$, given by Eq. (67) upon substituting ϕ, θ by 1, 2. Therefore, the pumped power is expressed as a Berry curvature. The Hamiltonian of Eq. (69) is periodic in the parameters \vec{X} . Hence it is natural to focus on the two-dimensional region where $-\pi \leq X_\ell < \pi$, $\ell = 1, 2$, which behaves as the synthetic Brillouin zone (sBz) of the Hamiltonian of Eq. (69) defined in the synthetic reciprocal space of coordinates \vec{X} . Averaging over all possible initial conditions φ_1, φ_2 is regarded as a way to quantify the mean pumped power for irrational frequencies, corresponding to the case where ω_1/ω_2 is an irrational number. Such an average can be written as

$$\overline{P}^{(\text{pump})}(1, 2) = \omega_1 \omega_2 \int_{\text{sBz}} \frac{d^2 X}{(2\pi)^2} \Omega_g(\vec{X}) \equiv \hbar \omega_1 \omega_2 C_g, \quad (73)$$

where C_g is the Chern number. From the formal point of view, this number is the same as the one characterizing the Chern insulator calculated for the ground state of the Hamiltonian of Eq. (69) formulated in the reciprocal space of a square lattice [197, 198]. The explicit result is

$$C_g = \begin{cases} 0, & \delta > 0, & \text{trivial,} \\ 1/2, & \delta = 0, & \text{Dirac,} \\ 1, & \delta < 0, & \text{topological,} \end{cases}$$

corresponding, respectively, to a trivial phase with a gap between the ground and excited states for all values of \vec{X} , a system with a Dirac point for $\vec{X} = 0$ and a topological gapped phase. Consequently, in the first case the mean pumped power is zero, while in the other cases it is defined by an universal quantity proportional to the Chern number.

5.3. Topological pumping in the Floquet regime

Topological quantized pumping of energy between two driven sources was originally proposed to take place under non-adiabatic conditions far-from-equilibrium conditions in Refs. [177, 178]. These papers focus on the time-dependent Hamiltonian defined in Eqs. (41) and (69) with the protocol of Eq. (71) in the Floquet regime. For arbitrary large commensurate frequencies it is possible to solve the driven Hamiltonian by recourse to the Floquet theory summarized in Sec. 2.4.

Introducing the Floquet representation in the Schrödinger equation leads to the structure of Eq. (22) with $\vec{n} = (n_1, n_2)$, associated to the Floquet modes of $\vec{\omega} = (\omega_1, \omega_2)$. In the present problem these coupled equations can be Fourier-transformed to the "momentum" representation $\vec{q} = (q_1, q_2)$ to obtain the effective Hamiltonian

$$H = \sum_{\vec{q}} H_{\vec{q}} + \sum_{\vec{n}} H_{\vec{n}}, \quad (74)$$

with $H_{\vec{n}} = -\hbar\vec{n}\cdot\vec{\omega}$ while $H_{\vec{q}}$ is the Hamiltonian of Eq. (41) with \vec{B} defined in Eq (69) and $\vec{X} \equiv \vec{q}$, independent of t . In this way, an effective dynamics ruled by a time-independent Hamiltonian defined in a two-dimensional lattice is generated. Using the analogy with the lattice model and relying on semiclassical equations of motion for crystals perturbed by slow electromagnetic fields [200] an expression for the pumped power is derived. It reads

$$P_{1,2}^{(\text{pump})}(t) = \omega_1\omega_2|\Omega_{\vec{q}}|, \quad (75)$$

where $\Omega_{\vec{q}}$ is the Berry curvature of a given band \vec{q} . The structure of this equation is very similar to the corresponding one in the adiabatic regime expressed in Eq. (72). Extending this expression to the case of incommensurate frequencies is interpreted as an average over the Brillouin zone of \vec{q} , which leads to the definition of the Chern number as in Eq. (73). The difference between the adiabatic and the Floquet cases is that in the adiabatic one this quantity was calculated over the ground state of the frozen qubit Hamiltonian. Instead, in the present case it is calculated in the Floquet space. These ideas were further explored and implemented in an electronic spin embedded in an NV center in a diamond [199]. In Ref. [178] this mechanism was analyzed for a qubit coupled to reservoirs.

The usefulness of the topological power exchange to control the spin dynamics in the system coupled to a circuit or cavity QED was analyzed in Ref. [201] and its realization in platforms containing arrays of qubits was discussed in Refs.[202, 203, 204]. A unique feature that make topological phenomena so appealing is their robustness against perturbations and it is very promising to find such properties in the context of energy exchange in qubit systems.

6. Heat pumping

6.1. General considerations

Quantum pumping, in particular particle pumping, has been a subject of great interest in the context of electron systems for some time now [83, 90, 205, 206, 207, 209]. Basically, it consists in inducing a net particle transport between two reservoirs with neither electrical nor thermal bias but by means of a periodic asymmetric modulation the embedded quantum system. A widely investigated example is a quantum dot consistent of a double-barrier structure confining a few quantum levels in contact to electron reservoirs. Without applying any electrical or thermal bias, gate voltages are locally applied at the walls following an asynchronous cyclic protocol. A simple version of such protocols consists in deforming one of the confining walls enabling electrons to flow from the neighboring reservoir into the quantum dot levels while keeping the other wall fixed. After the electrons fill-in the quantum-dot levels, the wall is restored to its initial situation while the opposite wall is deformed to facilitate the flow of the electrons from the quantum dot towards its neighboring reservoir. After the electrons leave the quantum dot, the wall is restored. Hence, the initial configuration is recovered with a net transfer of electrons from one reservoir to the other as a consequence of the deformation of the confining walls.

This mechanism has a counterpart in the heat [61, 210, 211], phononic [212, 213, 214, 215], and spin [216, 217, 218] transport.

6.2. Adiabatic heat pumping and geometric phase

We discuss below a concrete and intuitive mechanism for heat pumping operating in a single qubit. Here, we introduce the main ideas to describe this phenomenon in the adiabatic regime. We focus on the slowly driven system performing a cycle of period τ , so that the parameters satisfy $\vec{X}(t + \tau) = \vec{X}(t)$ while connected to two reservoirs (l, r) at the same temperature T . It is important to notice that, in order to discern the two reservoirs, there should be some asymmetry in the couplings. In the case of the qubit, this can be achieved with couplings to the reservoirs as in Eq. (38) that are defined by different and non co-linear vectors $\vec{g}_{k,l}$ and $\vec{g}_{k,r}$ for the two reservoirs.

The starting point is to considering the heat current defined in Eq. (7). It is possible to introduce the adiabatic expansion given by Eq. (12) to calculate the heat flowing into each reservoir in a cycle

$$Q_\alpha = \int_0^\tau dt J_\alpha(t) = \sum_\ell \int_0^\tau \Lambda_{\alpha,\ell}(\vec{X}) \dot{X}_\ell. \quad \alpha = l, r \quad (76)$$

where this term represents the non-equilibrium heat induced by the driving processes. Since the processes associated to entropy production are described by Eq. (43) and are second-order in $\dot{\vec{X}}$, we conclude that this first-order component satisfies

$$Q_l = -Q_r = Q^{(\text{pump})}, \quad (77)$$

which defines the *pumped heat* in the slow-driving regime. Here we notice that this definition is similar to the concept of power pumping previously defined in Eq. (64). In that case the exchange of energy takes place between two driving forces, while in the present case, it takes place as heat exchange between the two baths. In fact, in analogy to Eq. (64) we can define from Eq. (77), $P^{\text{(heat-pump)}} = (Q_l - Q_r)/2\tau$. Furthermore, as in the case of power pump, geometrical concepts similar to the Berry phase are useful to describe this mechanism. In fact, for the sake of making the geometrical nature more explicit, it is useful to introduce the vector $\vec{\Lambda}(\vec{X}) = (\Lambda_{1,1}(\vec{X}), \dots, \Lambda_{1,N}(\vec{X}))$, according to which the pumped heat per cycle reads

$$Q^{\text{(pump)}} = \oint \vec{\Lambda}(\vec{X}) \cdot d\vec{X}. \quad (78)$$

The closed integral corresponds to the trajectory in the parameter space defining the cyclic protocol of the driving parameters. This structure is similar to the case of charge pumping, [83, 209]. The heat pumping takes place along with energy dissipation. The description of these processes is identical as in Sec. 4, taking into account the coupling to several thermal baths.

6.3. Adiabatic heat pumping with a single qubit

We now discuss the mechanism of adiabatic pumping in the context of single-qubit setups. We focus on the case studied in Refs. [86, 170]. The model is similar to the one considered in Sec. 4.1, in a configuration where the qubit is coupled to left (l) and right (r) reservoirs at the same temperature T . The driven qubit is modeled by the Hamiltonian of Eq. (41) with $\vec{B}(t) = \vec{X}(t) = (B_x(t), 0, B_z(t))$. Importantly, the couplings to the two reservoirs must be implemented with two non-commuting operators. Otherwise, it would be possible to define an effective single bath with a linear combination of modes of the different reservoirs. We consider the coupling Hamiltonian of Eq. (38) with $\vec{g}_l = (0, 0, g^z)$ for the left bath and $\vec{g}_r = (g^x, 0, 0)$ for the right one. Hence

$$H_{\text{cont},l} = g^z \sum_{k_l} (a_{k_l}^\dagger + a_{k_l}) \sigma^z, \quad H_{\text{cont},r} = g^x \sum_{k_r} (a_{k_r}^\dagger + a_{k_r}) \sigma^x. \quad (79)$$

In the weak coupling regime, this problem can be solved with the procedure explained in Sec. 2.3. Details are presented in Appendix B. With those elements, following Ref. [170] it is possible to obtain analytical results for the vector $\vec{\Lambda}$ defining the pumped heat in Eq. (78),

$$\vec{\Lambda}(\vec{B}) = \frac{\beta B \sin^2 2\theta}{\cosh^2(2\beta B)} \vec{n}, \quad (80)$$

where \vec{n} is the unit vector along the radial direction in the $(B_x, B_z) \equiv B(\sin \theta, \cos \theta)$ plane. In terms of it, the pumped heat reads

$$Q^{\text{(pump)}} = \oint \vec{\Lambda}(\vec{B}) \cdot d\vec{B} = \int \int (\nabla_{\vec{B}} \times \vec{\Lambda}(\vec{B})) \cdot d^2\vec{B}, \quad (81)$$

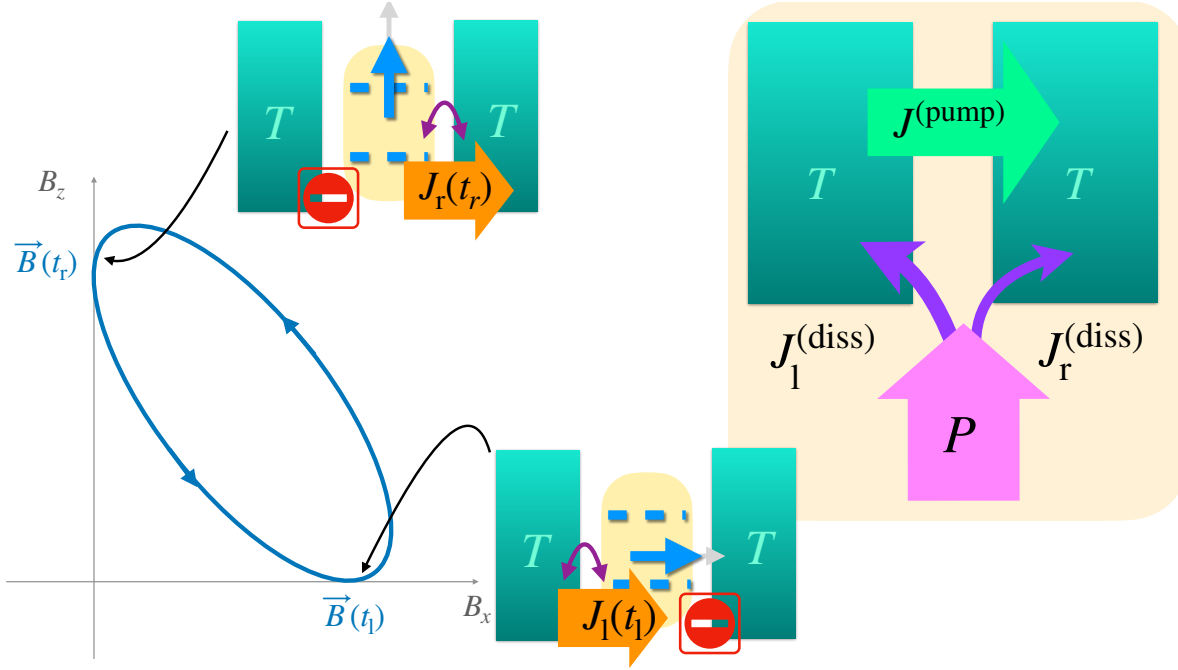


Figure 2. Example of a protocol leading to quantum pumping in the configuration of a driven qubit asymmetrically coupled to reservoirs at the same temperature (see text). The sketches illustrate the instantaneous Hamiltonian and the heat fluxes at the instants t_1 and t_r . The net result over the cycle is highlighted in the colored box.

In the last step we have introduced Stokes' theorem to express the line integral over the protocol in the form of a flux integral through the area enclosed by the protocol. This result is interesting because it makes explicit the fact that, in order to have heat pumping in a cyclic protocol with this device, it is necessary to follow a trajectory in the parameter space where $|\vec{B}| = B$ changes. The analysis of $\left(\nabla_{\vec{B}} \times \vec{\Lambda}(\vec{B})\right)_y$ is extremely helpful to visualize the optimal protocols.

An example of the pumping cycle is sketched in Fig. 2. The two components of $\vec{B}(t)$ evolve cyclically but with a phase lag. At a given instant t_1 the vector $\vec{B}(t_1)$ points along the x direction and the state is polarized in the x direction of the Bloch sphere. Such a state forbids the energy exchange with the right reservoir. This can be explicitly seen by noticing that Eqs. (B.4) and (B.5) with $B_z = 0$ reduces to the master equation of the qubit coupled only to the left bath. There is a heat flux $J_1(t_1) = \langle \dot{H}_1 \rangle$ between the qubit and the left bath. Assume $k_B T > B(t_1)$, so that heat flows from the left reservoir into the qubit at this time. At another instant $t_r > t_1$, $\vec{B}(t_r)$ the state is rotated so that it points along z and let us assume that the protocol is such that $B(t_r) > B(t_1)$ with $B(t_r) > k_B T$. At this time there is not energy exchange with the left reservoir. In fact, for $B_x = 0$, Eqs. (B.4) and (B.5) correspond to the qubit coupled only to the right bath. An energy flow $J_r(t_r) = \langle \dot{H}_r \rangle$ takes place between the qubit and the right bath. Since we assumed $B(t_r) > k_B T$, the heat now flows from the qubit to the right bath. If the cycle is completed by decreasing B to the value $B(t_1)$, the result is a net

transfer of heat from the left to the right as a consequence of the qubit driving. This type of cycles realize the mechanism of heat pumping and the direction of the pumped heat flux can be inverted by reversing the protocol. As in the case of the configuration analyzed in Sec. 4 the driving generates heat that is dissipated into the reservoirs, as indicated in the right sketch of Fig. 2. The distribution of this dissipated heat among the two reservoirs depends on details like their density of states and their coupling with the qubit.

The total dissipated energy for this problem can be calculated following the steps explained in Sec. 4. In Ref. [170], analytical expressions are derived for the present example. The result is

$$W^{(\text{diss})} = \int_0^\tau dt \dot{\vec{B}} \cdot \underline{\Lambda} \cdot \dot{\vec{B}} = \int_0^\tau dt \left[\lambda_B \dot{B}^2(t) + \lambda_\theta B^2(t) \dot{\theta}^2(t) \right], \quad (82)$$

with

$$\lambda_B = \frac{\beta \sinh(\beta B)}{2\gamma B \cosh^3(\beta B)}, \quad \lambda_\theta = \frac{\gamma}{2B^2}, \quad (83)$$

where $\gamma = \gamma_l = \gamma_r$ is the coupling strength, which is assumed to be the same for the two baths. We can identify a behavior akin to the example of the driven qubit coupled to a single reservoir discussed in Ref. [164] and in Sec. 4. In fact, radial protocols, weighted with λ_B , dissipate differently from protocols involving rotations of the qubit states without changing the spectrum. The latter are weighted with λ_θ . The regime where one is dominant with respect to the other depends on the ratio $B/k_B T$. As already observed in Sec. 4, radial protocols are associated to changes in the populations and have a small weight at low temperatures compared to B/k_B .

In Ref. [86] the following protocol is implemented in this device,

$$B_x(t) = B_{x,0} + B_{x,1} \cos(\Omega t + \phi), \quad (84)$$

$$B_z(t) = B_{z,0} + B_{z,1} \cos(\Omega t), \quad (85)$$

with $B(t) = \sqrt{B_x^2(t) + B_z^2(t)}$. The solution in the weak coupling regime leads to the conclusion $Q^{(\text{pump})} \propto \sin(\phi)$. In Ref. [170] it was shown that the optimal protocol regarding the maximum heat pumping corresponds to a trajectory in the (B_x, B_z) plane that encloses a full quadrant. The result is

$$Q_{\text{Max}}^{(\text{pump})} = \pm k_B T \log(2). \quad (86)$$

Interestingly, this quantity is known as *Landauer limit* and corresponds to the maximum possible entropy change in a two-level system [219, 220]. It defines a fundamental limit for the thermodynamic cost of erasing information. The original proposal constitutes a breakthrough in relating thermodynamics and statistical mechanics with information theory. It has been covered in detail in review articles, like Ref. [17, 18] and it is the motivation of many recent experiments [221, 222, 223, 224, 225, 226, 227, 228, 229, 230, 231]. In the present context, this limit is achieved in a protocol that consists of an infinite-long trajectory. Such a protocol would take infinite time to be accomplished.

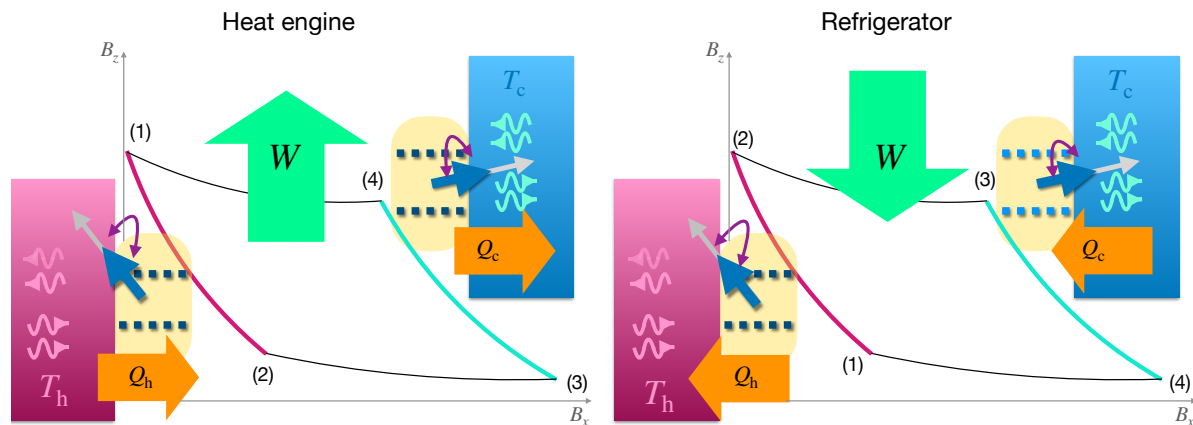


Figure 3. Illustration of a Carnot cycle in a qubit for the heat engine and refrigerator operations.

Hence, it corresponds to a quasistatic limit which defines the bound for any other finite-time protocol. The two signs of this equation correspond to the different ways of circulating the path. More discussion will be presented in Sec. 7.4 in relation to the role of pumping in the operation of thermal machines.

Interestingly, pumping can be also induced in this setup under periodic variations of the temperatures of the two reservoirs, $\delta T_1(t)$ and $\delta T_r(t)$ with respect to the reference temperature T [232, 233]. The possibility of realizing topological charge pumping with qubits in cQED was suggested in Ref. [234] in a quite different setup based on two qubits, and experimental results on charge pumping in a superconducting circuit has been reported in Ref. [235]. No experimental studies of heat pumping in qubits have been reported yet.

7. Thermal machines

7.1. General considerations

So far we have analyzed effects that are generated purely by time-dependent driving. Thermal machines operate with the cyclically driven working substance – represented by the qubit in our case of interest – contacted with reservoirs with a temperature bias. In this scenario heat-work conversion is the key mechanism.

7.2. Thermodynamic cycles

The implementation of quasi-static cycles similar to the classical thermodynamical ones in a single qubit has been considered in the qubit Hamiltonian defined in Eq. (41). In particular, the well known Carnot, Otto, Stirling and other cycles have been recently studied in Refs. [166, 167, 236, 237, 238, 239, 240, 241, 242, 243, 244, 245]. Some of the related discussion has been covered in the review articles of Refs. [17, 22, 246, 247]. We

briefly summarize some important aspects.

The relevant mechanisms can be easily understood by expressing the qubit Hamiltonian as follows,

$$H_{\text{qubit}}(t) = -B(t) \bar{\sigma}^z, \quad (87)$$

with $\bar{\sigma}^z$ operating in the instantaneous eigenbasis of Eq. (41). The *Carnot* cycle is sketched in Fig. 3 for the qubit operating between a cold and a hot thermal baths at temperatures T_c and T_h , respectively. It consists of four steps: (1) The qubit evolves coupled to the hot reservoir as the parameters change leading to a change of $B(t)$ from $B_1 = B(t_1)$ to $B_2 = B(t_2)$. In general, this process takes place in a finite time. In the ideal quasi-static cycle this is assumed to be long enough to justify considering the system in equilibrium with the bath at every instant during the evolution. In this step of the cycle there is exchange of heat, Q_h and work $W_{1 \rightarrow 2}$ with the reservoir. If the evolution is such that the heat flows from the qubit towards the reservoir, the device operates as a refrigerator, otherwise it operates as a heat engine. (2) The qubit evolves isolated from the two reservoirs between $B_2 = B(t_2)$ and $B_3 = B(t_3)$. In this process, only work ($W_{2 \rightarrow 3}$) is exchanged between the system and the driving sources. (3) The qubit evolves coupled to the cold reservoir from B_3 to $B_4 = B(t_4)$. In this step there is again exchange of both heat Q_c and work ($W_{3 \rightarrow 4}$) with the reservoir. (4) The last step is an evolution isolated from the reservoir from B_4 to $B_5 = B(t_5) = B(t_1)$ and takes place without exchange of heat with any of the reservoirs but exchanging work ($W_{4 \rightarrow 1}$) between the qubit and the external driving sources. The steps (2) and (4) are usually named "adiabatic" as in classical cycles, where this concept applies to processes in which no heat is exchanged. The practical way to implement this type of evolution in classical systems is by means of a fast change of the parameters of the working substance. We recall, however (see Sec. 2.2), that in quantum mechanics the concept of "adiabaticity" is instead associated to a very slow evolution and is not necessarily associated to a process where there is no heat exchange in the case of an open quantum system.

An important concept to qualify the operation of the cycle is the efficiency (in the case of the heat engine) and the coefficient of performance (in the refrigerator). They are, respectively, defined as

$$\eta = \frac{W}{Q_h}, \quad COP = \frac{-Q_c}{W}, \quad (88)$$

where the $W = W_{1 \rightarrow 2} + W_{2 \rightarrow 3} + W_{3 \rightarrow 4} + W_{4 \rightarrow 1}$ is the total work done in all the cycle. These definitions follow the convention that $Q_\alpha > 0$ when it enters the reservoir α and $W > 0$ when work is delivered by the driving sources into the system. In each step $W_{i \rightarrow j}$ may have any sign, depending on the protocol.

The heat and the work in the different steps of the cycle are defined in Eqs. (6). The conservation of the energy in the cycle implies

$$W = Q_h + Q_c. \quad (89)$$

For a quasi-static evolution we can use the definitions of Eqs. (8) to explicitly verify that this relation holds for the conservative work $W^{(\text{cons})}$, and the quasistatic

heat exchanges $Q_h^{(\text{qs})}$, $Q_c^{(\text{qs})}$. In addition, since for the quasi-static processes there is no entropy production, and the total change of the entropy in these reversible processes reads

$$\sum_{\alpha} \Delta S_{\alpha} = \sum_{\alpha} \frac{Q_{\alpha}^{(\text{qs})}}{T_{\alpha}} = 0. \quad (90)$$

Therefore, Eq. (89) can be expressed as

$$W^{(\text{cons})} = Q_h^{(\text{qs})} \frac{(T_h - T_c)}{T_h}, \quad \text{Carnot}, \quad (91)$$

which when substituted in Eqs. (88) leads to the well-known Carnot results for the efficiency and the coefficient of performance,

$$\eta_C = \frac{T_h - T_c}{T_h}, \quad \text{COP} = \frac{1}{\eta_C}, \quad \text{Carnot}. \quad (92)$$

For non-equilibrium finite-time protocols, the components $W^{(\text{non-cons})}$ and $Q_{\alpha}^{(\text{non-eq})}$ contribute **as will be discussed below**. Furthermore, a precise description should also take into account the time-dependent processes of switching on and off the contacts to the reservoirs. The latter are usually neglected in the literature although, recently, the effect of smooth changes in the system-reservoir coupling were found to speed-up the isothermal evolutions of Carnot cycles [248].

The Otto cycle is also based on a four-stroke protocol. The main difference with respect to the Carnot one is in the steps (1) and (3) where the evolution in contact with the reservoirs takes place at constant B , hence only heat is exchanged in these processes. This cycle is very convenient from the computational point of view, since only heat is exchanged in the strokes (1) and (3) while only work is exchanged in the strokes (2) and (4), which implies important simplifications in the calculations. The implementation of Otto cycles has been the focus of many theoretical and experimental works [17, 22, 246, 247] with recent focus on many-body effects [249] and speed up protocols [249, 250, 251, 252, 253, 254, 255] to enhance the performance. This cycle has been widely analyzed in the literature and we defer the reader to Refs. [17, 22, 246, 247].

7.3. Finite-time Carnot heat engine

A good part of the literature on cycles in qubits focuses on a Carnot cycles with a quasi-static evolution in the steps where the system is in contact to reservoirs, and a fast evolution in the steps where it is decoupled [236, 237, 238, 239, 240, 242, 243, 244, 245]. Recently, finite-time effects in the evolution in contact to the reservoirs were addressed [166, 167, 241]. At finite time, besides the efficiency, the other quantities qualifying the performance of the machine are the output power, in the case of the heat engine, and the cooling power, in the case of the refrigerator. For a machine operating in a period τ these quantities read

$$P^{(\text{he})} = -\frac{W}{\tau}, \quad P^{(\text{cool})} = -\frac{Q_c}{\tau}. \quad (93)$$

The drawback of the finite-time operation is the energy dissipation and entropy production. The effect of the dissipation in Carnot cycles where the evolution in contact with the reservoirs takes place at finite times was analyzed in the literature in Refs. [256, 257]. The main step is to include the contribution of the dissipated energy due to the finite-time evolution during the strokes where the system evolves coupled to the reservoirs. The corresponding heat exchanges with the cold and hot baths read

$$Q_\alpha = Q_\alpha^{(\text{rev})} + W_\alpha^{\text{diss}} = T_\alpha \Delta S_\alpha + T_\alpha \Sigma_\alpha, \quad \alpha = \text{c, h}, \quad (94)$$

where ΔS_α is the reversible change in the entropy, while the dissipative contribution associated to the entropy production is denoted by Σ_α . The latter accounts for the finite-time processes and vanishes in the limit of an ideal cycle. According to the sign convention adopted here, the irreversible contributions are always positive, indicating that the dissipated energy flows into the reservoirs. Instead, the sign of the reversible component $Q_\alpha^{(\text{rev})}$ depends on direction of the heat flux.

In Ref. [166] the conditions to obtain a maximum power in a finite-time Carnot heat engine is studied considering one and several coupled qubits as the working substance and slow evolutions in the evolutions in contact with the reservoirs. A useful step is to introduce a change in the notation in order to get an explicit dependence of the entropy production with the duration of the strokes, τ_α , $\alpha = \text{c, h}$. This is achieved by changing of the integration variable in Eq. (43) to $s = t/\tau_\alpha$, which leads to the following expression for the entropy production,

$$W_\alpha^{\text{diss}} = \frac{1}{\tau_\alpha} \sum_{\ell, \ell'} \int_0^1 ds \dot{X}_\ell \Lambda_{\ell, \ell'}^{(S)}(\vec{X}) \dot{X}_{\ell'} = T_\alpha \frac{\bar{\Sigma}_\alpha}{\tau_\alpha}, \quad (95)$$

where now $\dot{X}_\ell = dX_\ell/ds$. Introducing the same change of variables, the reversible part can be expressed following Eq. (12),

$$Q_\alpha^{(\text{rev})} = T_\alpha \Delta S_\alpha = \sum_\ell \int_0^1 ds \Lambda_{\alpha, \ell}(\vec{X}) \dot{X}_\ell, \quad (96)$$

with $\Delta S_c = -\Delta S_h = \Delta S$. Eq. (89) remains valid, even in the case of non-conservative processes. Hence, the power of the heat engine defined in Eq. (4) as well as the efficiency defined in Eq. (88) read

$$P^{(\text{he})} = -\frac{Q_c + Q_h}{\tau}, \quad \eta^{(\text{he})} = \frac{Q_c + Q_h}{Q_h}, \quad (97)$$

being $\tau = \tau_c + \tau_h$. The optimization of the durations leading to the maximum power of the heat engine was previously discussed in Ref. [256, 257]. The result is obtained after substituting Eqs. (94) and (95) into Eq. (97)

$$P^{(\text{he})} = -\frac{1}{\tau} \left(-\Delta S \Delta T + T_c \frac{\bar{\Sigma}_c}{\tau_c} + T_h \frac{\bar{\Sigma}_h}{\tau_h} \right). \quad (98)$$

Maximizing with respect to the durations leads to

$$\tau_c = \tau_h \sqrt{\frac{T_c \bar{\Sigma}_c}{T_h \bar{\Sigma}_h}}, \quad \tau_h = \frac{2T_h \bar{\Sigma}_h}{\Delta S \Delta T} \left(1 + \sqrt{\frac{T_c \bar{\Sigma}_c}{T_h \bar{\Sigma}_h}} \right), \quad (99)$$

being $\Delta T = T_h - T_c$. Substituting these optimal durations in Eq. (97), the expression for the maximum power is obtained,

$$P^{\max} = \frac{(\Delta S)^2}{4} \frac{(T_h - T_c)^2}{\left(\sqrt{T_h \bar{\Sigma}_h} + \sqrt{T_c \bar{\Sigma}_c} \right)^2}. \quad (100)$$

We see that the power optimized with respect to the durations of the cycle still depends on the coefficients $\bar{\Sigma}_\alpha$ characterizing the energy dissipation into the bath. These quantities depend on the microscopic details of the driven system, the baths, the couplings to the baths and the evolution protocols. For adiabatic driving, the description in terms of the thermodynamic length described in Sec. 4.2 can be used to design the optimal protocols. This was precisely the goal of Ref. [166] with focus on weak coupling between system and reservoirs.

In these conditions it is shown that the bound for P^{\max} is proportional to the heat capacity of the working substance. Since the heat capacity can scale supraextensively with the number of constituents of the engine, this result is useful in the design of optimal many-body Carnot engines including the effect of many-body interactions and phase transitions [258].

In the case of Otto cycles the finite-time optimization focuses on the steps where the system evolves decoupled from the reservoirs by means of shortcuts-to-adiabaticity. This implies including counter-diabatic terms in the protocols as in Eq. (58). These suppress inter-state transitions in the free evolution, which improves the performance in these type of cycles [22].

As mentioned in Sec. 2.7, the identification of the energy exchanges of quantum measurements as heat and work is non-trivial. Irrespective of this identification, the measurement mechanism can be regarded as an exchange of energy which can be used to fuel thermodynamical-like cycles of quantum working substances. There are several implementations in qubit systems [127, 113, 259, 260, 261, 262] and similar ideas were also followed in other quantum systems [263, 264, 265]. In Sec. 11.2 we will discuss an experimental implementation.

7.4. Adiabatic cycles and geometric properties

This type of cycles are closely related to the pumping mechanism discussed in Sec. 6 and it can be implemented basically in the same setup as the one considered there. The crucial difference is the addition of a thermal bias between the two reservoirs, so that one of them is hot (say the right one) and the other one is cold, having temperatures $T_h = T_c + \Delta T$ and T_c , respectively. We can now formulate the question of whether

it is possible to implement the same pumping mechanism as before to overcome the thermal bias, in order to make a refrigerator out of this device. The answer is yes and the machine can be compared with the Archimedes' screw, which has been used since the time of the ancient Greeks to pump water against gravity by rotating a screw inside a pipe (see sketch of Fig. 4). Notice that this also illustrates the pure pumping mechanism discussed in Sec. 6 if the pipe is placed horizontally. In the case of a thermal bias, the device relies on the pumping mechanism induced by the driving to overcome the heat leak from the hot to the cold reservoir induced by the temperature bias, in the same way that the Archimedes' pump relies on the rotation of the screw to pump the water upwards. If the pumping mechanism operates in reverse, so that it transfers heat from the right to the left in the sketch of Fig. 4, part of the energy transported because of the thermal bias can be used to drive the machine, which operates as a heat engine in this case. This should be compared with the Archimedes machine operating in reverse, realizing a generator, in which case the water flowing down through the pipe contributes to rotate the screw. The realization of these machines in the quantum realm has been widely investigated in the context of electron systems under the operation with slow cyclic driving and electrical bias and the denomination "motor" has been coined for them [266, 267, 268, 269, 270, 271, 272, 273]. In Ref. [85] a unified framework analogous to the theory of thermoelectricity in linear response was presented to describe motors and thermal machines operating in the adiabatic regime under small electrical and thermal biases. These ideas were further elaborated in Ref. [86] with focus on the thermal machines and their geometric properties.

Adiabatic thermal machines usually operate in permanent contact to the reservoirs. The driving generates a heat pumping mechanism in addition to dissipation into the reservoirs. In order to have pumping, we typically need to break spacial symmetries as in the case of the rotating screw of Archimedes' machine. In the example of the qubit discussed in Sec. 6 this is achieved by implementing different kind of couplings with the two reservoirs and an asymmetric driving protocol.

As in the case of the thermodynamical cycles, the possible operations are heat engine and refrigerator. The relevant energy fluxes are sketched in Fig. 5. In Ref. [86, 170] these two operations are analyzed for the machine based on the setup of Fig. 4 with $\vec{X}(t) \equiv \vec{B}(t)$ in the qubit Hamiltonian and asymmetric coupling to the hot and cold reservoirs as in Sec. 6. In what follows we discuss the characterization of this machine in the regime where the driving is slow and in addition the temperature difference $\Delta T = T_h - T_c$ is small to justify a linear-response treatment in $\Delta T/T$, being T the reference temperature. From the formal point of view this implies combining the linear response description of the thermal bias with the adiabatic description as presented in Sec. 2.6. One of the quantities of interest in the operation of these machines is the heat transported between the reservoirs, given by Eq. (29)

$$Q^{(\text{tr})} = \int_0^\tau dt \left\{ \sum_\ell \Lambda_{N+1,\ell}(\vec{X}) \dot{X}_\ell + \Lambda_{N+1,N+1}(\vec{X}) \frac{\Delta T}{T} \right\}, \quad (101)$$

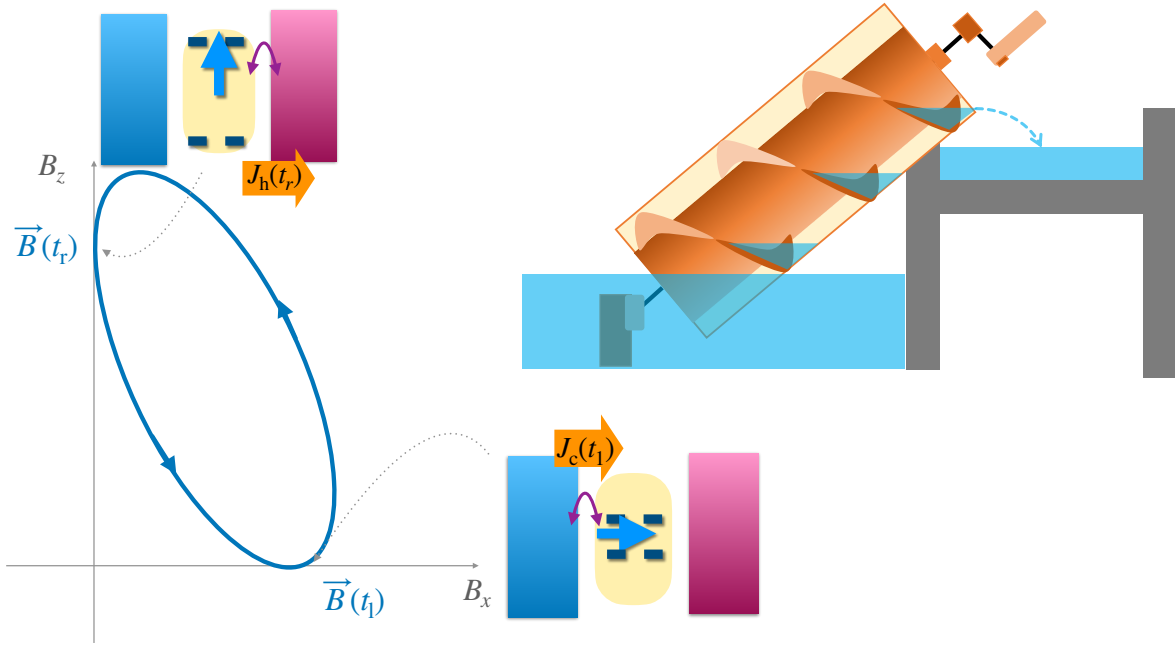


Figure 4. When the protocol of Fig. 2 is implemented on the qubit between reservoirs at different temperatures, the pumping mechanism can be used against the thermal bias. The device operates as a refrigerator and the mechanism bears resemblance with Archimedes' screw (see sketch).

where the label (tr) highlights that this component of the heat is transported between the two reservoirs, in the sense that $Q^{(\text{tr})} = Q_c = -Q_h$. We can distinguish the process of pumping in the first term and the response to the thermal bias in the second one. The other quantity of interest is the work performed by the driving forces. Following Eq. (7) we can identify a conservative and a non-conservative component, $W = W^{(\text{cons})} + W^{(\text{non-cons})}$. The first component corresponds to calculating Eq. (8) over the cycle, which explicitly leads to $W^{(\text{cons})} = 0$. The non-conservative component is obtained from Eq. (28) and reads

$$W = \int_0^\tau dt \left\{ \dot{\vec{X}} \cdot \underline{\Lambda}(\vec{X}) \cdot \dot{\vec{X}} + \sum_\ell \dot{X}_\ell \Lambda_{\ell, N+1}(\vec{X}) \frac{\Delta T}{T} \right\}, \quad (102)$$

For the case of a qubit driven by the protocol sketched in Fig. 4, we have $\vec{X}(t) \equiv \vec{B}(t) = (B_x(t), B_z(t))$ and the Onsager relations of Eq. (30) for this particular protocol can be shown to satisfy $\Lambda_{3,\ell}(\vec{B}) = -\Lambda_{\ell,3}(\vec{B})$, for $\ell = 1, 2$. Hence, introducing the notation $\vec{\Lambda}(\vec{B}) = (\Lambda_{3,1}(\vec{B}), \Lambda_{3,2}(\vec{B}))$, Eqs. (101) and (102) lead to

$$\begin{aligned} Q^{(\text{tr})} &= \oint d\vec{B} \cdot \vec{\Lambda}(\vec{B}) + \kappa \frac{\Delta T}{T}, \\ W &= \int dt \dot{\vec{B}} \cdot \underline{\Lambda}(\vec{B}) \cdot \dot{\vec{B}} - \frac{\Delta T}{T} \oint d\vec{B} \cdot \vec{\Lambda}(\vec{B}). \end{aligned} \quad (103)$$

As already mentioned, the first term of $Q^{(\text{tr})}$ is purely due to pumping $Q^{(\text{pump})} = \oint d\vec{B} \cdot \vec{\Lambda}$

– compare with Eqs. (78) and (81) – while the second term is the thermal leak induced by the temperature difference ($\kappa \equiv \int_0^\tau dt \Lambda_{3,3}$ is proportional the thermal conductance). In the expression of the work we can identify in the first component the dissipative contribution when comparing with Eq. (43) and (82). The second term describes the mechanism of heat-work conversion and it is the fundamental piece for the device to operate as a thermal machine. It reads

$$-W^{(\text{heat-work})} = \frac{\Delta T}{T} Q^{(\text{pump})}. \quad (104)$$

This relation is a generalization of Eq. (91) to the case of a finite-time cycle. This term is the dominant contribution to W in the case of very slow cycles. In fact, notice that the second term of W in Eq. (103) is first-order in $\dot{\vec{B}}$ while the first one is second-order. This is in accordance with the idea that dissipation decreases as the evolution becomes closer to the quasi-static limit.

The two operational modes depend on the sign of the pumped heat $Q^{(\text{pump})}$. When the pumped heat flows upstream with respect to the temperature bias $Q^{(\text{pump})} < 0$ it can compensate the effect of the heat leak represented by the second one, resulting in $Q^{(\text{tr})} < 0$ (heat exits the cold reservoir). The machine works as a refrigerator and the pumping generates an extra amount of work through the mechanism of heat-work conversion, $W^{(\text{heat-work})} > 0$. This situation is sketched in the left panel of Fig. 5. The reversed operation corresponds to the heat engine, in which case, $Q^{(\text{pump})} > 0$ and the pumped heat flows downstream with respect to the temperature bias. In this case, the heat-work conversion offers a mechanism where the second term of W in Eq. (103) compensates the dissipative one, enabling the possibility of extracting useful work from the machine. This is sketched in the right panel of Fig. 5.

We can now proceed as in Ref. [170] to express Eqs. (103) in terms of geometric quantities. To this end it is convenient to introduce the change of variables $s = t/\tau$ and to define

$$A = \int_0^1 ds \vec{\Lambda} \cdot \dot{\vec{B}}, \quad L^2 = \int_0^1 ds \dot{\vec{B}} \cdot \underline{\Lambda} \cdot \dot{\vec{B}}, \quad \langle \kappa \rangle = \int_0^1 ds \kappa, \quad (105)$$

where the names A and L^2 are related to the geometrical meaning of these quantities. In fact L^2 is related to the thermodynamic length introduced in Sec. 4.2, while A can be expressed in terms of an area by recourse to Stokes' theorem, as discussed in Sec. 6,

$$A = \oint \vec{\Lambda} \cdot d\vec{B} = \int \int (\nabla_{\vec{B}} \times \vec{\Lambda}) \cdot d^2\vec{B}, \quad (106)$$

where the surface in the space of parameters is enclosed by the boundary defined by the protocol. Hence, this quantity can be interpreted as an area in the parameter space weighted by a Berry-type curvature $(\nabla_{\vec{B}} \times \vec{\Lambda})$. Therefore, Eqs. (103) reduce to

$$Q^{(\text{tr})} = A + \tau \langle \kappa \rangle \frac{\Delta T}{T}, \quad W = \frac{L^2}{\tau} - \frac{\Delta T}{T} A. \quad (107)$$

7.5. Optimal adiabatic heat engine in linear response

The two components of the net work per cycle presented in Eq. (107) can be expressed as geometrical properties in the parameter space. In fact, the dissipative one depends on the metric and can be related to the thermodynamic length as discussed in Sec. 4.2, while the heat-work term depends on the "Berry-curvature" as shown in Eqs. (106). In Ref. [170] these properties are used to optimize the performance of a qubit following the protocol of Fig. 4. We now summarize the procedure for the case of the heat engine operation. The starting point is the definition of the power and the efficiency in terms of the geometric quantities introduced before. This reads

$$\begin{aligned} P^{(\text{he})} &= -\frac{W}{\tau} = \frac{\Delta T}{T} \frac{A}{\tau} [1 - (\tau_D/\tau)], \\ \eta &= -\frac{W}{Q^{\text{tr}}} = \eta_C \frac{1 - (\tau_D/\tau)}{1 + (\tau_D/\tau_\kappa)} \end{aligned} \quad (108)$$

with the definitions

$$\tau_D = \frac{T}{\Delta T} \frac{L^2}{A}, \quad \tau_\kappa = \frac{T}{\Delta T} \frac{A}{\langle \kappa \rangle}. \quad (109)$$

It is easy to calculate the optimal duration of the cycle in order to maximize the power and the efficiency. The results are, respectively,

$$\tau_P = 2\tau_D, \quad \tau_\eta = \tau_D + \sqrt{\tau_D(\tau_D + \tau_\kappa)}, \quad (110)$$

which upon substituting in Eq. (108) lead to the expressions for the optimal expressions for the power and the efficiency. Particularly interesting is the expression for the maximum power, which reads

$$P_{\text{max}}^{(\text{he})} = \frac{1}{4} \frac{\Delta T^2}{T^2} \frac{A^2}{L^2}. \quad (111)$$

We see that the problem of optimizing the protocol in the parameter space in order to maximize the power developed by the heat engine reduces to the optimization of the ratio between an area and a length in a space with a non-trivial metric. In the case of the Euclidean metric the solution is a circle, as is well-known since the time of the ancient Greeks. Remarkably, for an arbitrary metric this is still an open problem in geometry, which known as the *isoperimetric* or *Cheeger* problem [274, 275, 276].

The geometrical properties introduced before are very useful to the design of optimal protocols in qubit thermal machines. In Ref. [170] the problem of the driven qubit asymmetrically coupled to the two thermal baths illustrated in Fig. 5 is analyzed in detail. Some results regarding the operation without thermal bias are covered in Sec. 6.3, including the calculation the pumped heat, $Q^{(\text{pump})}$, and the dissipated energy because of the driving, $W^{(\text{diss})}$. In the linear response regime with respect to ΔT , these quantities define A and L^2 , respectively, through Eqs. (105). Recalling Eq. (86), we notice that the optimal protocol regarding the maximum A corresponds to a path evolving from the origin along the axis $B_x > 0$, followed by a quarter of circumference of infinite radius and closing along the axis B_z circulating from infinite to the origin. Those

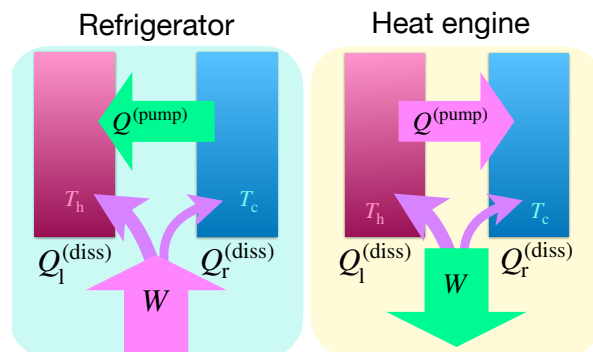


Figure 5. Sketch of the operational modes of the thermal machine

protocols are, however, not optimal regarding dissipation. The numerical analysis of the optimal solution of this isoperimetric problem was found to be ellipses in the (B_x, B_z) plane, circulated at a \vec{B} dependent speed $\dot{\vec{B}}(\vec{B})$. The latter is defined in order to get a constant dissipation rate at every point of the trajectory, which is the condition leading to a minimum thermodynamic length for a given path, Eq. (44), as discussed in Sec. 4.

8. Batteries

Quantum batteries is another subject of active investigation [277, 278, 279, 280, 281, 282, 283, 284]. These are quantum systems with a discrete-level spectrum manipulated by time-dependent processes in a way that they can store or deliver energy. The study of quantum batteries was triggered by Ref. [277] and has a significant development in the context of qubit systems. The goal of that paper is the calculation of the amount of work that can be extracted from a small quantum mechanical system which temporarily stores energy: the battery. Previously, the concept of "ergotropy" had been introduced as the maximum work that can be unitarily extracted from a given quantum state given a reference Hamiltonian [285]. Refs. [277, 286] focus on the calculation of the maximum extractable work in the framework of several subsystems and conclude that, in general, entangled unitary operations extract more work than independent ones. Refs. [278, 287, 288] focus on the complementary problem of charging the battery. In all these studies the models are purely closed systems, while more complex setups including the baths and dissipation processes are considered in Refs. [280, 282, 283, 289, 290, 291].

A proposal of quantum battery with high charging power in platforms of cQED systems was presented in Ref. [279] and further elaborated in Ref. [292]. The goal is to extend the comparison of the operation of N qubits in parallel vs the operation of the N entangled qubits as in previous works. In this study each unit is defined by a single qubit coupled to a resonator mode, while the entangled system corresponds to the N qubits coupled to a common resonator mode. The considered model for the collective configuration is described by Dicke Hamiltonian [293]

$$H_\lambda(t) = \hbar\omega_c a^\dagger a + \omega_0 S_z + 2\lambda(t)\omega_c S_x (a^\dagger + a), \quad (112)$$

with $S_j = \hbar/2 \sum_{\ell=1}^N \sigma_{\ell}^j$, which describes the N qubits coupled to the resonant mode of frequency ω_c when $\lambda(t) \neq 0$. The parallel configurations consist of N copies of this Hamiltonian for a single qubit. The battery is operated in a cycle, that is ruled by the time-dependent protocol followed by the coupling term $\lambda(t)$. The latter is defined by charging, storage and discharging times (respectively τ_c , τ_s , τ_d), as follows,

$$\lambda(t) = \begin{cases} \bar{\lambda} & , \quad 0 < t < \tau_c, \\ 0 & , \quad \tau_c \leq t \leq \tau_c + \tau_s, \\ \bar{\lambda} & , \quad \tau_c + \tau_s < t < \tau_c + \tau_s + \tau_d. \end{cases} \quad (113)$$

The steps are: (1) The initial state is $|\psi^N(0)\rangle = |N\rangle \otimes |g, \dots, g\rangle$, which corresponds to the N excitations in the resonator and the ground state of the N decoupled qubits. The coupling to the resonator is switched on during an interval of duration τ_c . (2) The resonator decouples for a time-interval of duration τ_s . (3) The resonator is coupled again for the discharging step of duration τ_d . The conclusion of these studies is that the charged energy as well as the charging power is enhanced in the correlated array in comparison to the parallel one. The fraction of energy stored in the battery that can be extracted in order to perform thermodynamic work, however is reduced and depends on the details of the preparation of the initial state.

Another type of quantum battery in the context of cQED was proposed in Ref. [284]. The setup consists in a single qubit coupled through a time-dependent protocol similar to Eq. (113) with a many-modes waveguide. In this setting, a resonant mode in the waveguide acts as a battery while the qubit is the auxiliary system. A photon beam with a frequency resonant with the qubit (ω_0) is injected into the waveguide with an input power $P_{\text{in}} = \hbar\omega_0 \dot{N}_{\text{in}}$, being \dot{N}_{in} the incoming flux of photons. Because of the coupling with the qubit, there is a reflected pulse with power $P_{\text{out}} = \hbar\omega_0 \dot{N}_{\text{out}}$, being \dot{N}_{out} the outgoing flux of photons. The considered Hamiltonian to describe the qubit and its coupling to the beam reads

$$H(t) = -\frac{\hbar\omega_0}{2}\sigma_z + i\hbar\sqrt{\gamma(t)\dot{N}(t)}(\sigma_-e^{i\omega_0 t} - \sigma_+e^{-i\omega_0 t}), \quad (114)$$

where the coupling protocol is determined by $\gamma(t)$. The output power is calculated by solving the master equation for the qubit coupled to the resonator and the dynamical equation for the reflected outgoing field,

$$b_{\text{out}}(t) = b_{\text{in}}(t) + \sqrt{\gamma}\sigma_-(t), \quad (115)$$

from where it is possible to evaluate $E = \text{Tr}[\rho(t)H(t)]$ and

$$P_{\text{out}}(t) = P_{\text{in}}(t) - \dot{E}(t). \quad (116)$$

The charging process corresponds to take advantage of the spontaneous emission of the qubit ($\dot{E}(t) < 0$) injecting extra photons into the waveguide, hence charging the battery. This device was experimentally realized in an implementation of a Maxwell demon [294], which will be discussed in Sec. 11.2.

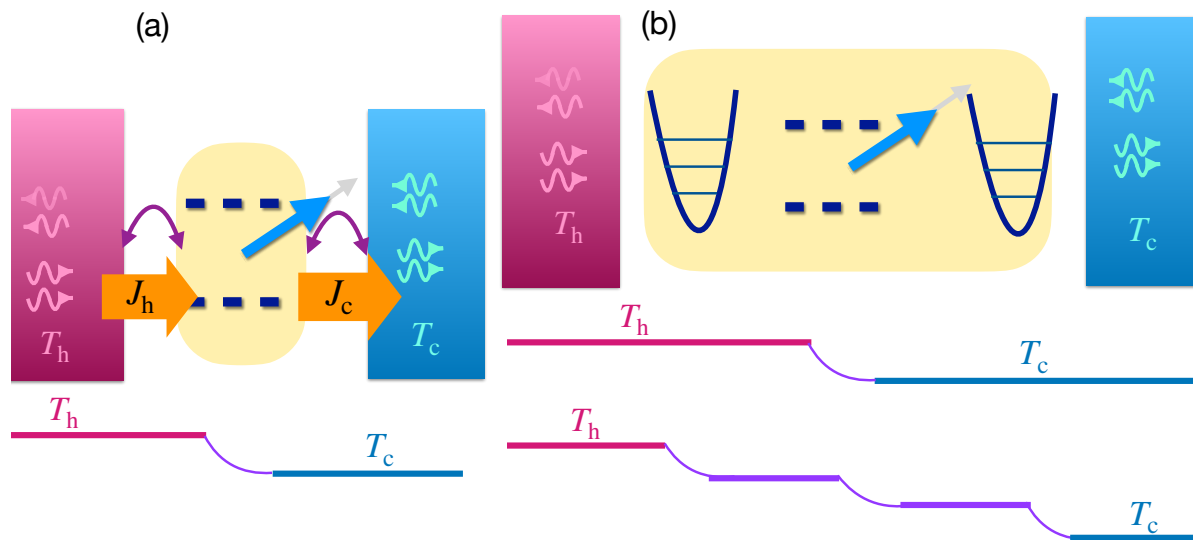


Figure 6. Illustration of the thermal transport process when: (a) the qubit is contacted to reservoirs at different temperatures at fixed \vec{B} and (b) the qubit is contacted to reservoirs at different temperatures through resonators. Below each configuration, possible temperature profiles are indicated.

9. Steady-state thermal transport

9.1. General considerations

When the qubit is placed in contact to two reservoirs with different temperatures without any driving mechanism, heat flows through it from the reservoir at high temperature T_h to the cold one with temperature T_c . A sketch is presented in Fig. 6. In this section we review two aspects of the heat transport through this device. The first one is related to the degree of coupling between the qubit and the reservoir. The second one is related to the structure of the reservoir and non-linear effects in the thermal transport.

9.2. The effect of strong correlations in linear response

As mentioned before, the Hamiltonian for the two-level system coupled to a bath of harmonic oscillators is equivalent to the spin-boson model [132, 130], whose equilibrium properties received a significant attention some time ago. This model has a quantum phase transition at zero temperature depending on the degree of coupling between the system and the reservoir and the spectral properties of the latter (ohmic, subohmic or superohmic) [133, 134]. This quantum phase transition is a consequence of the many-body correlations in this system.

In the context of electron transport, strong correlations are crucial to generate the mechanisms of Coulomb blockade and Kondo, which have a significant impact in the transport properties at low temperatures [295, 296]. It is, therefore, interesting to investigate similar features in qubit systems. Many-body effects in the thermal transport

of the spin-boson model have been investigated in several works [297, 298, 299, 300, 301, 302, 303]. Refs. [304, 305] present a systematic study of the low-temperature behavior of the thermal conductance beyond weak coupling between qubit and reservoir, on the basis of several many-body methods and a numerical quantum Monte-Carlo technique. The derived equation for the heat current for the qubit model with $\vec{B} = (B_x, 0, 0)$ in Eq. (41) and couplings $\vec{g}_k = (0, 0, g_k^z)$ from Schwinger-Keldysh non-equilibrium Green's-function technique [307, 308] reads

$$J_c = -J_h = \frac{\alpha\gamma}{8} \int d\varepsilon \varepsilon \text{Im} [\chi(\varepsilon)] I(\varepsilon) [n_h(\varepsilon) - n_c(\varepsilon)]. \quad (117)$$

It is assumed

$$\Gamma_\nu(\varepsilon) = \alpha_\nu I(\varepsilon), \quad \nu = h, c, \quad I(\varepsilon) = 2 \frac{\varepsilon}{\hbar} \left(\frac{\varepsilon}{\varepsilon_c} \right)^{s-1} e^{-\varepsilon/\varepsilon_c}, \quad (118)$$

being ω_c an energy cutoff, $\alpha = \alpha_c + \alpha_h$, and $\gamma = 4\alpha_c\alpha_h/\alpha^2$. The function

$$\chi(\varepsilon) = -\frac{i}{\hbar} \int_0^t \langle dt [\sigma_z(t), \sigma_z(0)] \rangle e^{i\frac{\varepsilon}{\hbar}t}, \quad (119)$$

is the spin susceptibility. In the linear response regime, the expectation values are calculated with respect to the many-body equilibrium states with the reservoirs at the mean temperature $T = (T_c + T_h)/2$. Hence, $\chi(\varepsilon)$ is a function of T . We see that Eq. (117) has the structure of Eq. (26), in spite of the fact that this Hamiltonian is non-bilinear but has many-body interactions. It is possible to define a transmission function $\mathcal{T}(\varepsilon, T) = \alpha\gamma \text{Im} [\chi(\varepsilon)] I(\varepsilon)/8$. Given this function, it is easy to derive in this regime the following expression for the thermal conductance, $G_{\text{th}} \sim \mathcal{T}(0, T)G_Q$, such that $J_c = G_{\text{th}}\Delta T$ with $G_Q = T_c(\pi k_B)^2/(3h)$ being the quantum of thermal conductance, which defines the limit for the quantum thermal transport through a single-channel bosonic or fermionic system [309, 310, 311].

Ref. [304] focuses on the Kondo signatures at low temperature in this regime, while in Ref. [305] a more detailed analysis including the comparison of the different methods to evaluate the susceptibility defined in Eq. (119) is presented. A crucial effect of the coupling to the bath is the renormalization of the parameter B_x of the Hamiltonian to an effective value Δ_{eff} which depends on α and on the bare value of B_x . This parameter represents the effective superposition of the two basis states of the qubit in the presence of the environment and defines the relevant energy scale of the problem. The approximations considered in Ref. [305] are the "sequential tunneling", which corresponds to calculating $\chi(\varepsilon)$ with the reduced density matrix calculated with the Lindblad master equation (9). The other one considered is the so called "co-tunneling" approximation, which corresponds to including in the master equation higher order processes in the contact term by recourse to perturbation theory. The third method is the so called "NIBA" (non-interacting-blip approximation), which is described by a rate equation derived after integrating out the bosonic bath with the Feynman-Vernon

functional technique and dropping some terms [306]. The latter is a non-perturbative technique, and the approximation is based on neglecting some family of high-order processes. The results are compared with numerically exact calculations with continuum time quantum Monte Carlo. A summary of the main results is presented below:

- *Ohmic bath*, $s = 1$. The thermal conductance below the critical value $\alpha_c = 1$ changes the behavior as a function of T . At low temperatures ($k_B T \ll \Delta_{\text{eff}}$), the numerical results agree well with those of the co-tunneling calculation. In this regime, the thermal conductance is always proportional to T^3 . This universal behavior is typical of the Kondo effect. At moderate ($k_B T \sim \Delta_{\text{eff}}$) and high temperatures ($k_B T \gg \Delta_{\text{eff}}$), the numerical results deviate from the co-tunneling formula and agree well with NIBA. The thermal conductance obtained by this method is proportional to $T^{3-2\alpha}$ at low temperatures. Sequential tunneling fails to predict the low-temperature behavior and for high temperature it is valid only in the limit $\alpha \ll \alpha_c$. For $\alpha > \alpha_c$, the renormalized parameter Δ_{eff} tends to zero and the system is localized in one of the states at low temperatures. The behavior of the thermal conductance in this regime is well described by NIBA.
- *Sub-Ohmic bath*, $s < 1$. In this case, the critical value for the localized-to-delocalized transition, α_c , is a function of s . Below α_c , at moderate and high temperatures, the numerical results agree well with the NIBA. At low temperatures ($k_B T \ll \Delta_{\text{eff}}$), the numerical results agree well with the co-tunneling formula, showing T^{2s+1} -dependence. The sequential-tunneling formula cannot be applied to the sub-ohmic case.
- *Super-Ohmic bath* $s > 1$. At low temperatures ($k_B T \ll \Delta_{\text{eff}}$), the numerical results agree with the co-tunneling description and show T^{2s+1} -dependence, regardless of the strength of the system-reservoir coupling, while the agreement is better with NIBA at higher temperatures.

9.3. The thermal-bias drop

One of the fundamental issues in quantum electron transport induced by a voltage bias applied at the reservoirs is which is the behavior of the voltage drop along the quantum system placed between the two reservoirs at different chemical potentials and to what an extent such details affect the transport [312]. These aspects are mainly relevant beyond linear response in the bias and similar questions can be posed regarding the temperature bias. Deep inside each of the macroscopic reservoirs the temperature has a well defined value. When the small-size quantum system is composed of several subsystems which independently intervene in the contact with the reservoirs at different temperatures it may happen that some of them tend to thermalize with the neighbouring reservoir. This would cause the temperature drop to concentrate inside the quantum system. Another possibility is an abrupt drop at the contact (Fig. 6.b). These questions are fundamental and very timely after recent experimental results [314, 315], where thermal transport is investigated in a qubit system coupled with resonators which are in turn coupled with

reservoirs. The experiments and the interpretations will be discussed in Sec. 11.5. The Hamiltonian for the considered setup reads

$$\begin{aligned}
 H = & H_{\text{qubit}} + \sigma_z \sum_{\nu=c,h} [g_\nu (b_\nu^\dagger + b_\nu) + \hbar\Omega_\nu b_\nu^\dagger b_\nu] \\
 & + \sum_{\nu=c,h,k} \left[g_{\nu,k} (b_\nu^\dagger + b_\nu) (a_{\nu,k}^\dagger + a_{\nu,k}) + \hbar\omega_{\nu,k} a_{\nu,k}^\dagger a_{\nu,k} \right], \quad (120)
 \end{aligned}$$

where the first line describes the qubit coupled to the resonators, while the second one describes the resonators coupled to the cold and hot reservoirs.

By analogy with electron transport [312], we expect the behavior of the thermal drop to be strongly dependent on the details of the system, like the degree of coupling between the different subsystems in comparison with the coupling with the reservoirs and the presence of many-body interactions, which may generate a mechanism of local or global thermalization. The transmission properties of a qubit coupled to resonators which are coupled to reservoirs of many-harmonic oscillators like the experimental configuration of Refs. [314, 315] is very special from the theoretical point of view. This is because it is technically simple to include the resonators into the description of the reservoirs by defining a spectral function $\Gamma(\varepsilon)$ for that combined system in order to substitute Eq. (118). This is precisely the procedure followed in Refs. [316, 317]. The result is Eq. (118) with

$$I_\nu(\varepsilon) = 2\alpha_\nu \varepsilon \frac{(\hbar\Omega_\nu)^2}{(\hbar\Omega_\nu^2 - \varepsilon^2)^2 + (2\gamma_\nu \varepsilon)^2}, \quad (121)$$

where α_ν depends on the couplings $g_\nu, g_{\nu,k}$ while γ_ν depends on the coupling $g_{\nu,k}$. We see that the functional dependence is a Lorentzian in contrast with the power-law behavior of Eq. (118). In these references, the heat current through the qubit coupled to the effective reservoirs described by Eq. (121) is calculated within the NIBA approximation. Notice that this description is equivalent to assume that the temperature drop takes place at the qubit, while the resonators are perfectly thermalized with the neighboring reservoirs. In Ref. [317] the thermal current is analyzed in linear response in the temperature bias. As expected after the discussion of Sec. 9.2 the structure of Eq. (121) introduces non-trivial and non-universal features in the behavior of the thermal conductance as a function of the mean temperature. Similar studies in more complex configurations were presented in Refs. [318, 319]. The behavior for large temperature bias remains an open problem.

In configurations where the couplings of the resonators with the reservoirs are weak, this problem may be related to the discussion of the validity of the local master equation vs the global one, which has been the subject of many studies [73, 75, 79, 76, 77, 78, 313]. The question in most of this literature is the appropriateness of using a local basis to express the reduced density matrix within the framework of master equations of Lindbladian nature, which are derived in perturbation theory with respect to the couplings with the reservoirs. Local master equations are valid when also the coupling

between the different subsystems is perturbative, while in the global case, the density matrix is expressed in the eigenbasis of the system composed of several connected parts.

9.4. Rectification

For some time now thermal rectification in nano-scale systems is a subject of great interest theoretically and experimentally in phononic structures [320, 321, 322, 323, 324, 325, 326, 327, 328], spin chains [329, 330, 331], quantum dots [332, 333, 334] and superconductors [335, 336]. Thermal rectification or thermal-diode effect means that the thermal transport depends, not only on the magnitude of the temperature bias, but also on its direction. Typically, the origin of such an effect is the existence of nonlinearities and asymmetries in the setup and the regime where it takes place is beyond linear response.

In the context of qubits coupled to photonic baths thermal rectification was predicted in Ref. [337] and this effect was recently experimentally confirmed in Ref. [315] in the configuration where the qubit is coupled to resonators, which are in turn coupled to thermal baths at different temperatures. This experiment is briefly discussed in Sec. 11.5 and already motivated several theoretical works [338, 339, 340, 341]. This a difficult theoretical problem which requires the proper treatment of many-body physics along with far from equilibrium conditions, which must be solved approximately. Unlike the case of the thermal conductance, this problem cannot be solved exactly numerically because of its far-from-equilibrium nature.

In Ref. [340] rectification is studied in an anharmonic quantum oscillator coupled to two bosonic thermal baths with Ohmic density of states at different temperatures. In the limit of very strong anharmonicity the system reduces to a qubit. The problem is solved with different techniques: master equation taking cotunneling into account, nonequilibrium Green's functions using the Majorana representation for the spin, and exact calculations based on Feynman-Vernon path-integral approach. The calculation based on non-equilibrium Green's functions [307, 308] similar to the one leading to Eq. (117) and considering the hybridization functions of the two reservoirs, defined in Eq. (118), proportional one another leads to the following expression for the heat current in the left reservoir

$$J(\Delta T) = \int d\varepsilon \varepsilon \mathcal{T}(\varepsilon, T, \Delta T) [n_l(\varepsilon) - n_r(\varepsilon)], \quad (122)$$

with $T_{l/r} = T \pm \Delta T/2$. The convention is such that for $\Delta T >, < 0$ the heat flow exits/enters this reservoir. Importantly, although Eq. (122) has a structure which resembles Eq. (26), the dependence of the transmission function on ΔT breaks the symmetry with respect to the exchange of the hot and cold reservoirs. The explicit expression of this function depends on the regime and the method of calculation. The rectification coefficient is defined as

$$R = \frac{J(\Delta T) + J(-\Delta T)}{J(\Delta T) - J(-\Delta T)}, \quad (123)$$

where no (perfect) rectification corresponds to $R = 0, (1)$, respectively. For weak coupling this parameter is found to be upper bounded by $\lambda(T_h - T_c)/(T_h + T_c)$, where $\lambda = (\Gamma_l - \Gamma_r)/(\Gamma_l + \Gamma_r)$ is the asymmetry parameter of the bath spectral functions. For strong coupling and low temperatures there is a strong dependence on the type or coupling to the reservoirs (\vec{g}_l, \vec{g}_r) . Interestingly, all the methods agree in the limit where the energy gap between the two levels is larger than the temperature. However, this is the regime of lower rectification. For low temperatures, large values of R are found in this setup.

In Ref. [341] an array of two qubits coupled each of them to two LCR circuits with different temperatures was considered. The Hamiltonian describing this system is

$$H_{\text{qubits}} = \sum_{\nu=c,h} \left[H_\nu + \sum_{j=1,2} \left(\vec{B}_j \cdot \vec{\sigma}_j + H_{\nu,j} \right) \right] + \gamma \sigma_1^z \sigma_2^z, \quad (124)$$

where H_ν are the Hamiltonians of the baths and the terms $H_{\nu,j}$ represent the coupling of each qubit to the two baths. The problem is solved by master equations with transition rates that depend on the temperature through the Johnson-Nyquist noise spectral function of the LCR circuits [342]. A high rectification ratio is found in this configuration for asymmetric couplings to the hot and cold reservoirs.

10. Superconducting qubits and cQED

Superconducting devices with Josephson junctions and capacitances may be designed to realize qubits. This is a very well established platform which has been proposed some time ago. Several architectures have been implemented and improved, which allow for the control and manipulation of the quantum states by recourse to magnetic fluxes and gate voltages. The working principles and details on the operation of these devices have been covered in at least four review articles [46, 47, 48, 50]. Here, we briefly review the Cooper pair box and the transmon architectures. Besides variations of these configurations like the charge and flux qubits, there are recent developments towards the realization of qubits in superconducting Josephson junctions by using the Andreev bound states in the junction [343, 344]. Another intensively explored platform based on superconductors is the topological one, in which case the qubits are realized in the Majorana zero modes localized at the ends of superconducting wires with spin-orbit coupling and with an applied magnetic field [345, 346].

10.1. Architectures

The simplest configuration to realize a superconducting qubit is the *Cooper pair box* (CPB) which is sketched in Fig. 7 (see left top panel). It consists in a Josephson junction between two superconductors with a low capacitance C_J and a phase bias φ . The knobs to manipulate the device are provided by the magnetic flux and a gate voltage V_g , contacted to one of the superconductors by means of a capacitance C_g .

The superconducting gap Δ is sufficiently large to prevent the quasiparticle tunneling through the junction and the charge transport takes place only by the tunneling of Cooper pairs. The Hamiltonian describing this system reads

$$H_{\text{Junction}} = H_{\text{ch}} + H_{\text{J}} = 4E_{\text{C}} \left(\hat{N} - N_{\text{g}} \right)^2 - E_{\text{J}} \cos(\hat{\varphi}), \quad (125)$$

where the first term describes the capacitive effects while the second one is associated to the Josephson effect. \hat{N} is the operator describing the difference in the number of Cooper pairs contained by each superconductor, $N = N_1 - N_2$ (where N_l is the number of Cooper pairs in the superconductor l) and $N_{\text{g}} = C_{\text{g}}V_{\text{g}}/2e$ is the excess charge controlled by the gate voltage. The corresponding charging energy is $E_{\text{C}} = e^2/2(C_{\text{g}} + C_{\text{J}})$. In this representation, N is the quantum mechanical conjugate of the operator $\hat{\varphi}$, $\hat{N} = -i\hbar\partial/(\partial\varphi)$. This Hamiltonian can be written in the basis of eigenstates of \hat{N} as follows

$$H_{\text{CPB}} = \sum_N \left\{ 4E_{\text{C}} (N - N_{\text{g}})^2 |N\rangle\langle N| - \frac{E_{\text{J}}}{2} (|N\rangle\langle N+1| + |N+1\rangle\langle N|) \right\}, \quad (126)$$

where the first term describes the charging energy, while the second one described the tunneling of Cooper pairs through the junction. The lowest eigenenergies of this Hamiltonian as functions of N_{g} are shown in Fig. 7 (a)-(d). For $E_{\text{C}} \gg E_{\text{J}}$, the spectrum is dominated by the first term of the Hamiltonian. The eigenstates have a large component with fixed N , except for N_{g} close to half-integer values, corresponding to the degeneracy points of the charging energy. At these points the second term of the Hamiltonian generates an avoided crossing between two adjacent states. The qubit state is realized when focusing, for instance, at gate voltages leading to $N_{\text{g}} \simeq 1/2$ which correspond to values close to the degeneracy point of $N = 0, 1$ of the charging term. Close to this point, the previous Hamiltonian can be expressed in the form of Eq. (36) as follows,

$$H_{\text{qubit}} = -B_z\sigma^z - B_x\sigma^x = -B[\cos(\theta)\sigma^z + \sin(\theta)\sigma^x], \quad (127)$$

with the definitions

$$B_z = 2E_{\text{C}}(1 - 2N_{\text{g}}), \quad B_x = E_{\text{J}}/2, \quad B = \sqrt{B_x^2 + B_z^2}, \quad \theta = \tan^{-1}(B_x/B_z), \quad (128)$$

while σ^z , σ^x are Pauli matrices expressed in the basis $|\uparrow\rangle \equiv (1, 0)^T$ and $|\downarrow\rangle \equiv (0, 1)^T$ where 0, 1 are the corresponding values of N and T denotes the transpose operation.

This Hamiltonian has a tunable parameter B_z , which can be controlled by the gate voltage that sets N_{g} . This qubit configuration can be improved by connecting the two superconductors in a loop. In this way, the effective Josephson coupling in Eq. (125) is given by [46]

$$H_{\text{J}} = (E_{\text{J}_1} + E_{\text{J}_2}) \cos(\pi\Phi/\Phi_0) \sqrt{1 + d^2 \tan^2(\pi\Phi/\Phi_0)} \cos(\hat{\varphi} - \varphi_0), \quad (129)$$

where $E_{\text{J}_1} = \alpha E_{\text{J}_2}$ and E_{J_2} are the tunneling amplitudes for the Cooper pairs at the junctions, $d = (1 - \alpha)/(1 + \alpha)$ and $\varphi_0 = d \tan(\pi\Phi/\Phi_0)$. The effective Hamiltonian for

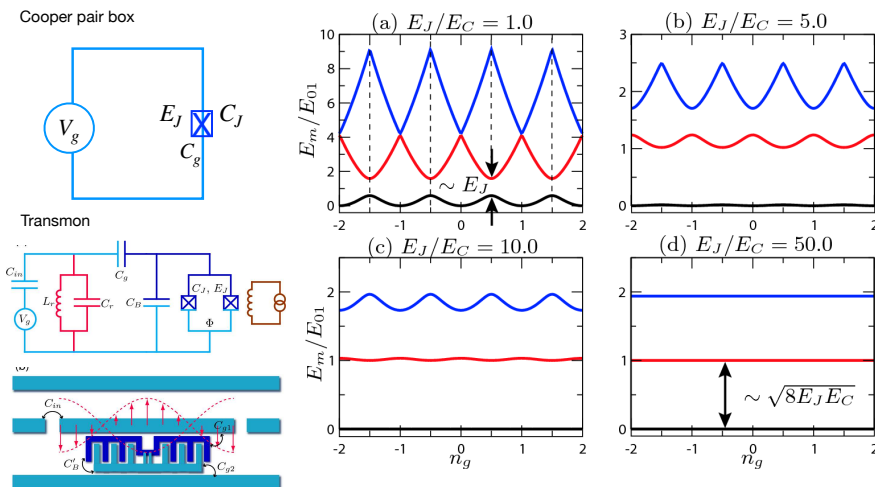


Figure 7. Sketch of the Cooper pair box (top left) and transmon (bottom left) circuits. The spectrum for different ratios of E_J/E_C is shown in the right panels. (Adapted from Ref. [348]).

the qubit is given by Eq. (125) with the Josephson term modulated by the magnetic flux Φ through the loop in units of the flux quantum $\Phi_0 = hc/2e$ as defined in Eq. (129). In this way, not only the gate voltage but also the magnetic flux can be used as control parameters to manipulate the effective qubit Hamiltonian of Eq. (127).

Another popular architecture is *the transmon*. This circuit has been proposed in Ref. [348] and has the advantage with respect to the CPB of being less sensitive to charge noise. It is sketched in Fig. 7 (see bottom left). One of the main differences with respect to the CPB is that this circuit hosts two Josephson junctions shunted by an additional capacitance C_B . The Hamiltonian for this circuit is also given by Eq. (125), with $E_C = e^2/2(C_g + C_J + C_B)$, while $\hat{\varphi}$ denotes the total phase difference between the two superconductors, which is set by the magnetic flux Φ . The transmon operates in the opposite limit of the CPB, namely $E_C \ll E_J$, in which case the low-energy spectrum of the Hamiltonian of Eq. (125) consists in approximately constant energy levels as functions of the offset charge N_g , as shown in Fig. 7 (d).

10.2. Circuit quantum electrodynamics

We have previously presented some architectures for superconducting circuits, and shown that it can effectively behave as a two-level quantum system. As mentioned before, when we also consider the surrounding circuit we have the scenario of a qubit embedded in an electrodynamic cavity. The role of the cavity is played by the combination of capacitive and inductive circuit elements (resonators). In fact, the dynamics of a transmission line (TL) of length L with a cross section of dimensions

much smaller than L can be effectively described by the following 1D Lagrangian,

$$\mathcal{L} = \int_{-L/2}^{L/2} dx \left(\frac{l}{2} j^2 - \frac{1}{2c} q^2 \right) = \int_{-L/2}^{L/2} dx \left[\frac{l}{2} \dot{\theta}^2 - \frac{1}{2c} (\nabla\theta)^2 \right], \quad (130)$$

being l and c , respectively, the inductance and capacitance per unit length, while $j(x, t)$ and $q(x, t)$ are, respectively, the local current and charge densities. In last identity of the previous equation the following representation was introduced,

$$\theta(x, t) = \int_{-L/2}^x dx' q(x', t). \quad (131)$$

The equation of motion for this Lagrangian is the wave equation with velocity $v = 1/\sqrt{lc}$. The solution for open boundary conditions with $\theta(-L/2, t) = \theta(L/2, t) = 0$ can be expanded in normal modes as follows

$$\theta(x, t) = \sqrt{\frac{2}{L}} \sum_k \cos\left(\frac{k\pi x}{L} + \alpha_k\right) \theta_k(t), \quad (132)$$

where $\alpha_k = 0, (\pi/2)$, for k odd (even) integers, respectively. The quantum-mechanical Hamiltonian for this cavity can be formulated by identifying the coordinates θ_k along with the conjugated momenta $\pi_k = l\dot{\theta}_k$ and defining the operators

$$\hat{\theta}_k = \sqrt{\frac{\hbar\omega_k c}{2}} \frac{L}{k\pi} \left(a_k(t) + a_k^\dagger(t) \right), \quad \hat{\pi}_k = -i\sqrt{\frac{\hbar\omega_k l}{2}} \left(a_k(t) - a_k^\dagger(t) \right), \quad (133)$$

with $\omega_k = k\pi v/L$ and $[a_k, a_{k'}^\dagger] = \delta_{k,k'}$. Therefore, the voltage on the transmission line can be expressed as

$$V(x, t) = \frac{1}{c} \frac{\partial\theta(x, t)}{\partial x} = - \sum_k \sqrt{\frac{\hbar\omega_k}{Lc}} \sin\left(\frac{k\pi x}{L} + \alpha_k\right) \left(a_k(t) + a_k^\dagger(t) \right). \quad (134)$$

To treat the coupling between a qubit realized in the CPB architecture and the circuit we must add to the voltage V_g in Eq. (126) the voltage at the connecting point of the TL. Assuming that the qubit is coupled at the coordinate $x = 0$ of the TL, we substitute $N_g \rightarrow N_g^{\text{dc}} + C_g V(0, t)/2e$ in Eq. (126). Focusing as before on the two lowest-energy states with $N = 0, 1$ close to the degeneracy point we get for the qubit coupled to the LC circuit the following effective Hamiltonian

$$H_{\text{CPB-TL}} = -[B_z \sigma^z + B_x \sigma^x] + \sum_k g_k \left(a_k^\dagger + a_k \right) (1 - 2N_g - \sigma^z). \quad (135)$$

We have defined in the previous equation $g_k = -eC_g V_k / (C_g + C_J)$ with $V_k = \sqrt{\hbar\omega_k/cL}$ while B_x, B_z are given by Eq. (128) with N_g given by the dc component N_g^{dc} . Changing to the basis that diagonalizes the Hamiltonian for the isolated qubit, it reads

$$H_{\text{CPB-TL}} = \frac{\Omega}{2} \bar{\sigma}^z + \sum_k g_k \left(a_k^\dagger + a_k \right) [1 - 2N_g - \cos(\theta) \bar{\sigma}^z + \sin(\theta) \bar{\sigma}^x], \quad (136)$$

with $\Omega = \sqrt{E_J^2 + [4E_C(1 - 2N_g^{\text{dc}})]^2}$ and θ defined in Eq. (128).

Similarly, for the case of the transmon, the coupling between the qubit and the transmission line reads [348],

$$H_{\text{trans-TL}} = \frac{\Omega}{2} \bar{\sigma}^z + \sum_k \bar{g}_k (a_k^\dagger + a_k) \bar{\sigma}^x, \quad (137)$$

with $\bar{g}_k \simeq g_k \{E_J/(8E_C)\}^{1/4}$. The qubit coupled to the electromagnetic environment represented as a set of many quantum-oscillator modes effectively defines a spin system coupled to a Caldeira-Legget type of bath [128], as mentioned in Sec. 3. Notice that Eqs. (136) and (137) have the structure of Eq. (38). In the literature the rotating wave approximation is sometimes introduced in the calculations, which leads to a coupling of the form $g_k \sigma^+ a_k + H.c.$, corresponding to the James-Cummings Hamiltonian given by Eq. (39) [348].

The coupling of a qubit to a single resonator corresponds to considering a single resonant k in Eqs. (136) and (137) instead of many modes. Such circuits are used to introduce operations in the qubit, to perform the readout and to implement couplings between several qubits. In particular, couplings, containing $\bar{\sigma}^z$ instead of $\bar{\sigma}^x$ in Eq. (137) have been implemented in designed architectures of transmons [350, 351, 352, 353]. Ref. [50] presents a complete overview of the degree of development of this technology. The transmon qubit is one the most used one nowadays because of its stability.

10.3. Implementing heat transport in quantum electromagnetic circuits

Real circuits typically contain resistive elements (LRC circuits). The resistors produce thermal noise and behave as thermal photon sources. This mechanism is discussed in detail in Ref. [20, 349] and is the concrete way to implement a temperature reservoir and to induce thermal transport in these devices. The spectral function describing the noise correlations of the voltage defined in Eq. (134), is given by

$$S_V(\omega) = \int_{-\infty}^{+\infty} dt e^{i\omega t} \langle V(0, t) V(0, 0) \rangle = 2R \frac{\hbar\omega}{1 - e^{-\beta\hbar\omega}}, \quad (138)$$

being R the resistance of the circuit and $\beta = 1/(k_B T)$. In the limit of $k_B T \gg \hbar\omega$ this expression tends to the classical fluctuation-dissipation result $S_V(\omega) \rightarrow 2k_B T R$. In typical devices, the temperature corresponding to the level separation in the superconducting loop is 0.5K, which implies that the operational temperatures for these devices should be lower than this.

Following Ref. [20, 349] we summarize the description of the heat transport through a qubit or an array of qubits and resonators embedded into two circuits with resistors R_h and R_c at different temperatures T_h (hot) and T_c (cold). Given a spectral function $S_{V_h}(\omega)$ defined as in Eq. (138) for the hot resistor, the incident power spectral density at the cold resistor is given by

$$S_{P_c}(\omega) = \frac{\mathcal{T}_{c-h}(\omega)}{4R_h} S_{V_h}(\omega), \quad (139)$$

where the (dimensionless) function $\mathcal{T}_{c-h}(\omega)$ describes the transmission probability between the two resistive circuits through the array of qubits connecting them. Therefore, the power entering the cold reservoir from the hot one reads

$$P_c = \int_{-\infty}^{+\infty} d\omega S_{P_c}(\omega) = \int_{-\infty}^{+\infty} d\omega \hbar\omega \mathcal{T}_{c-h}(\omega) [n_h(\omega) + 1/2], \quad (140)$$

being $n_h(\omega) = 1/[1 - e^{\hbar\omega/(k_B T_h)}]$ the Bose-Einstein distribution function corresponding to the temperature of the hot bath. Following the same reasoning for the power entering the hot reservoir from the cold one and assuming reciprocity such that $\mathcal{T}_{c-h}(\omega) = \mathcal{T}_{h-c}(\omega)$, the net heat flux between the two reservoirs is determined from

$$P_{\text{net}} = P_c - P_h = \int_{-\infty}^{+\infty} d\omega \hbar\omega \mathcal{T}_{c-h}(\omega) [n_h(\omega) - n_c(\omega)], \quad (141)$$

which has the same structure as the Landauer-Büttiker description of Eq. (26).

11. Experiments on quantum thermodynamics in cQED

The possibility of coupling a superconducting qubit to resonators acting as harmonic-oscillators environments motivated the study of a rich variety of thermodynamic concepts in this setup. The relevant mechanisms have been discussed in the previous sections. In the present section we review some reported experiments in this direction as well as some theoretical proposals of experiments.

11.1. Energy dynamics of measurements

Unlike the ideal picture usually presented in textbooks, the process of measuring a quantum state is not instantaneous but it takes place in a finite time and it depends on the details of the interaction between the quantum system and the measurement apparatus.

In *quantum non-demolition* measurements the goal is the continuous monitoring of the quantum system. The measurement process implies the coupling of the quantum system to a classical measuring device. In principle, such devices have much more noise than any one dictated by the quantum uncertainty principle. An effective method to reduce these effects is to isolate the quantum system from the measuring device to perform an *indirect measurement*. This process takes place for the quantum system coupled to a quantum probe and proceeds in two steps: (i) The system undergoes a unitary interaction with the probe, which is initially pre-prepared in a known quantum state. (ii) The probe interacts with a classical measurement device. In experiments, all physical processes occur over some finite timescale. Assuming the knowledge of the Hamiltonian describing the coupling between these two systems, this two-step procedure can be used to describe a *continuous measurement* if it occurs over an infinitesimally short time step and is repeated continuously. In this case, information is continuously extracted from the probe as it interacts with the measured system.

The analysis introduced in Ref. [354] defines the basis for a set of experiments where the trajectory of a cQED qubit is recorded [355, 356, 357, 358, 359]. The probe system is a single resonator mode of frequency f_{res} and couples to the qubit as described in Sec. 3 under the conditions where second-order processes in the coupling dominates. This defines a dispersive coupling and is modeled by the following Hamiltonian

$$H_{\text{disp-coup}} = \vec{B} \cdot \vec{\sigma} + h \left(f_{\text{res}} - \frac{\chi}{2} \sigma^z \right) \left(a^\dagger a + \frac{1}{2} \right) \quad (142)$$

This system has a dispersive coupling in z and can be easily diagonalized for $\vec{B} = (0, 0, B_z)$ in the basis $|\sigma, n\rangle$, where the first entry denotes the state of the qubit and the second one labels the state of the resonator. We see that with this type of dispersive coupling the frequency of the resonator mode is shifted by an amount that depends on the state of the qubit. Hence, by measuring any physical property that depends on this frequency it is possible to infer the state of the qubit. In practice, this is achieved by sending a signal of a given frequency to the cavity and measure the transmitted or reflected signal. The phase of the transmission signal, in particular, depends on the difference between the frequency of the injected wave and the one of the cavity, which provides the information of the state of the qubit. This measurement procedure is named homodyne detection [360] and it basically provides information on $\langle \sigma^z \rangle$. It can be complemented with another optical technique (heterodyne detection) that records the spontaneous fluorescent emission of the qubit, which provides information of the components $\langle \sigma^x \rangle$ and $\langle \sigma^y \rangle$. The analysis of these measurements enables the reconstruction of the *quantum trajectory* and offers the possibility of keeping track on the evolution of the quantum state. In order to theoretically describe the evolution of the quantum state in contact to the noisy environment including the backaction introduced by the measurement, a useful technique is the stochastic master equation introduced in Sec. 2.7. This is a generalization of the one that describes the dynamics of the quantum state coupled to the reservoirs, with an additional stochastic term to describe the effect of the measurement.

Motivated by these experiments, Refs. [361, 362, 363] address the description of the concomitant energy dynamics and these ideas were more recently experimentally tested in Ref. [359]. In this work it is analyzed how quantum heat and work can be consistently identified in systems whose environment consists of a continuously coupled quantum detector.

The Hamiltonian describing the qubit corresponds to Eq. (36) with $B_z = 0$ and a coupling to the electromagnetic environment is given by the Jaynes-Cummings Hamiltonian Eq. (39). Hence, the dispersive coupling is along x, y and the information of $\langle \sigma_x \rangle$ obtained by homodyne detection is recorded. The sketch of the experimental device is shown in Fig. 8 (a). The evolution of the density matrix is described by an stochastic master equation like the one discussed in Section 2.7 with an stochastic term describing the effect of the measurement. Each trajectory corresponds to a particular realization of the experiment. As a result, for an infinitesimal time interval, the change in

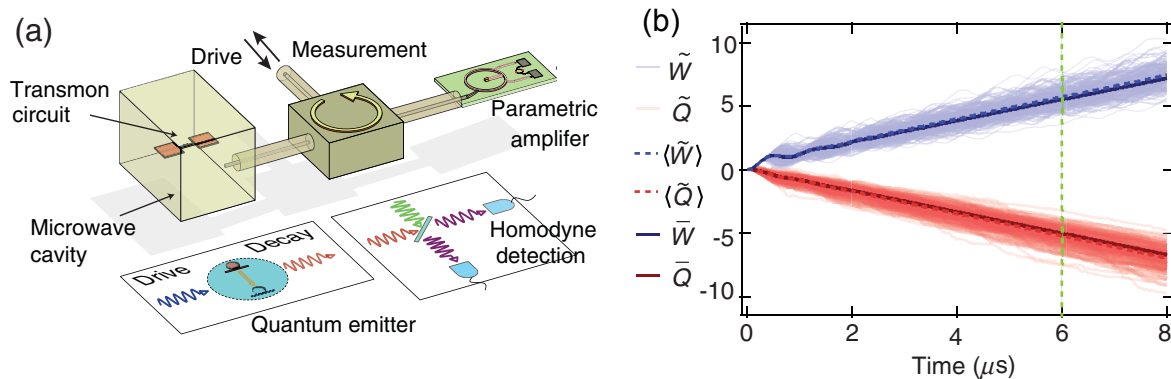


Figure 8. (a) Experimental setup to drive the qubit and record the quantum trajectories to analyze the work and heat (Adapted from Ref. [359]). (b) Recorded quantities. \tilde{W} and \tilde{Q} correspond to work and heat calculated for individual trajectories, while $\langle \tilde{W} \rangle$ and $\langle \tilde{Q} \rangle$ are the corresponding averages over trajectories. The values \bar{W} and \bar{Q} correspond to the calculations based on the Lindbladian dynamics.

the density operator of a quantum trajectory is written as $d\tilde{\rho}_t = \delta\mathcal{W}[\tilde{\rho}_t] dt + \delta\mathcal{Q}[\tilde{\rho}_t] dt$, where $\delta\mathcal{W}$ and $\delta\mathcal{Q}$ are superoperators associated to the respective unitary and non-unitary dynamics. As indicated by the notation, and by analogy to Eqs. (8), the first term can be used to calculate the conservative component of the work and the second one to calculate the quasi-static heat. In this way, heat and work for individual trajectories can be recorded. Results are shown in Fig. 8(b), where we can also see that the averages over quantum trajectories and the calculations based on a pure Lindbladian evolution without any stochastic component show a very good agreement.

11.2. Maxwell demon

The Maxwell demon is an imaginary character introduced by Maxwell to discuss a *gedanken* experiment devoted to illustrate the second law of thermodynamics [365]. The main idea is the implementation of processes forbidden to spontaneously occur because of the second law, thanks to the help of an intelligent creature. An example is the split of a mixture of gasses so that those with larger kinetic energy are collected in a compartment separated by a wall from those with lower kinetic energy. This is accomplished with the help of the demon, who classifies the particles according to their velocities and separates them into the compartments by conveniently opening or closing a door in the wall. The solution to the seeming paradox is solved by properly accounting for the information processed by the demon. This results in an entropy and energy balance which is in full agreement with the laws of thermodynamics.

A realization of the Maxwell demon in a transmon qubit coupled to a resonator was reported in Ref. [294]. Here we summarize the main idea. Assume that the qubit is first coupled to a thermal bath that prepares it in a thermal state and it is afterwards coupled to a "battery". The latter is of the type proposed in Ref. [284] and consists of

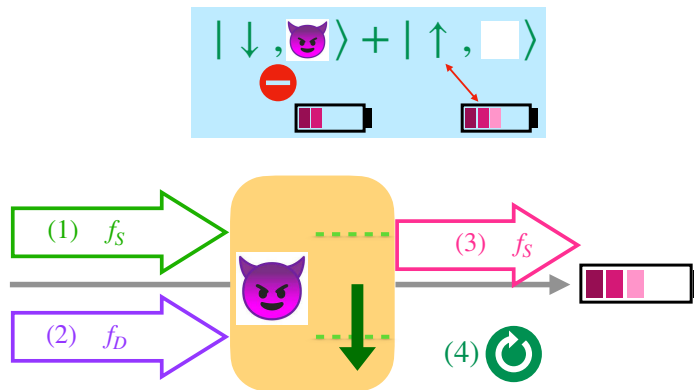


Figure 9. Sketch of the cycle studied in Ref. [294]. (1) Preparation of the state. (2) The demon is driven and prepared with n_D photons. (3) The battery is connected. Without the demon, it should supply photons to the qubit. Because of the demon, it receives photons from the qubit and it is charged. (4) Reset step. The colored box indicates the superposition state of the qubit and the action of the demon. The latter forbids the absorption of photons from the battery and only allows the emission.

a π -pulse with a resonant frequency that switches the populations between the excited state and the ground state by absorbing or emitting photons, as discussed in Section 8 [see Eqs. (114) - (116)]. For a thermal state at a low temperature, the ground state is more populated than the excited one. Therefore, the rate of absorption is larger than that of emission, resulting in a net power transferred from the battery to the qubit. This process decreases as the temperature of the thermal state increases and the population of the ground state and the excited one become similar. In the setup studied in Ref. [294] a resonator is coupled to the qubit in a way that it plays the role of a demon which favors the process of emission of photons when the system is coupled to the battery by preventing the absorption. This results in a net transfer of power from the system to the battery.

We now briefly discuss the concrete experiment. The combined qubit-demon system is described by the Hamiltonian of Eq. (142) with $\vec{B} \equiv (0, 0, hf_S/2)$ and the resonator playing the role of the demon with $f_{\text{res}} \equiv f_D$. A cycle is implemented as follows: (1) The state of the qubit is prepared in a thermal state at a temperature T_h or in a superposition quantum state. (2) The resonator (demon) is driven with a frequency f_D with a pulse of duration longer than χ^{-1} and shorter than the coherence times of the qubit and cavity. The process is designed to create $n_D = \langle a^\dagger a \rangle$ photons in the resonator only if the qubit is in the ground state ($|\downarrow\rangle$). The corresponding eigenstates of the Hamiltonian of Eq. (142) are $|\downarrow\rangle \otimes |n_D\rangle$ with energy $E_{\downarrow, n_D} = -hf_S/2 + h(f_D + \chi/2)n_D$ and $|\uparrow\rangle \otimes |0\rangle$ with energy $E_{\uparrow} = hf_S/2$. (3) A π -pulse, playing the role of a battery, is sent at a frequency f_S . The action of such a pulse with the demon in the $n_D = 0$ state is the same as without demon and consists in switching the populations of the two qubit states. Instead, any other state of the qubit-demon system with $n_D \neq 0$ is off-resonance with the pulse by an energy $-\chi n_D$ and the absorption of a photon accompanied by a switch of the qubit

state is not allowed. The only allowed process for the qubit is the emission of a photon by changing the state from $|\uparrow\rangle$ to $|\downarrow\rangle$. (4) The last step consists in resetting the demon by coupling it to a bath at temperature $T_c < T_h$. This completes the cycle. See sketch of Fig. 9.

In the experiment of Ref. [294] the power at the battery is recorded in step (3). It is verified that with the demon with $n_D = 0$ the battery releases power to the system, while with $\langle n_D \rangle = 0.9$ the battery receives power. In a thermal state, the photon emission from the system into the battery when the demon intervenes ($\langle n_D \rangle \neq 0$) becomes more important as the temperature increases, and this behavior is verified in this experiment. On the other hand, when the state is prepared in a quantum superposition, the outcome is expected to be similar to a high-temperature initial state and this is also observed in the experiment. The results are interpreted by modeling the coupling of the system to the baths and battery in the framework of Lindblad master equation Eq. (9).

A similar setup was theoretically considered in Ref. [366], where the thermal baths of step (1) is substituted by a measurement. The idea is very similar, except for the fact that the role of the demon is to perform projective measurements in order to select the excited state of the qubit. These type of non-demolition measurements can be accomplished by a system that is well described by the Hamiltonian of Eq. (142), where the coupling term commutes with the Hamiltonian of the qubit. The demon resonator is excited with microwave pulses, the response depends on the state of the qubit and it is calibrated as a readout element.

The qubit-demon device described by the Hamiltonian of Eq. (142) with the demon used to perform measurements was also considered in Ref. [367] to experimentally verify a fluctuation theorem. Fluctuation theorems [368, 369, 370, 371, 372, 373] are regarded as generalizations of the second law of thermodynamics and are valid away from equilibrium. The experiment by Masuyama and coworkers analyzes a fluctuation theorem formulated in Ref. [374], which reads

$$\langle e^{-\sigma - I_{\text{Sh}}} \rangle_{\text{PM}} = 1 - \lambda_{\text{fb}}, \quad (143)$$

where $\langle \dots \rangle_{\text{PM}}$ denotes the statistical average over the projective-measurement (PM) protocols, I_{Sh} is the stochastic Shannon entropy the demon acquires in the PM and $\sigma = -(W + \Delta F)/k_B T$ is the entropy change in the qubit, being W the work extracted from the qubit and ΔF the change in the free energy (in the experiment $\Delta F = 0$). The constant λ_{fb} in the previous equation is associated to irreversible processes. The implemented protocol consists in two projective measurements with feedback control. The sequence is: (1) The qubit state is prepared in a thermal state (2) A measurement by the demon is performed with outcome $x = \uparrow$ or \downarrow . The demon gains stochastic entropy $I_{\text{Sh}} = -p(x)$ in this process. (3) A feedback operation is performed. This consists in leaving the state of the qubit unmodified if it is in the ground state or applying a π -pulse if it is in the excited state. In the latter case work is extracted from the qubit-demon, as discussed before. (4) The amount of extracted work is measured by a second projective measurement $z = \uparrow$ or \downarrow . The result is $W(x, z) = E(x) - E(z)$,

where $E(x)$, $E(z)$ are the energies of the states x and z of the qubit. In this way, the quantity $\langle e^{W/k_B T - I_{\text{Sh}}} \rangle_{\text{PM}} = \sum_{x,z} p(x,z) e^{W(x,z)/k_B T - I_{\text{Sh}}(x)}$ is experimentally recorded and compared with the theoretical estimate of the right hand side of Eq. (143). The latter is calculated by recourse to a quantum master that takes into account the qubit relaxation during the pulse sequence. The agreement between experimental and theoretical results is excellent.

A similar device and description was used in Ref. [359] to track the quantum trajectories of a driven qubit. The aim of this experiment is to analyze the decomposition of changes in the internal energy of the qubit into heat and work, as discussed in Section 2.7. In the experiment, the results of two-point measurements similar to those in Ref. [367] are compared with the predictions of quantum master equations based on the Hamiltonian of Eq. (142). A more complex configuration involving two transmon qubits was considered in Ref. [375], where a mixed-state target qubit is purified by a pure-state demon qubit connected via an off-resonant transmission line. A nice overview and comparison among these experiments has been presented in Ref. [376].

In Ref. [377] a different experimental setting to implement a Maxwell demon in cQED was proposed, which bares a closer resemblance to the original idea formulated by Maxwell. The gas chambers are substituted by LRC resonators with a tunable frequency at different temperatures and the compartment separating these two reservoirs is realized by a qubit. This system is basically the one discussed in Sec. 9 (see Fig. 6) and the spontaneous process dictated by the thermodynamics laws is the heat transport from the hot to the cold reservoir through the qubit. The action of the demon is implemented by monitoring the quantum state of the qubit and manipulating the strength of its contact to the reservoirs. This manipulation can be realized by selecting the frequency of the resonator. When it coincides with the one associated to the qubit level spacing the contact is switched on while when these two frequencies are detuned the contact is switched off. Hence, if the qubit is detected to be in the ground state, it is put in contact with the cold reservoir, in order to favor the absorption of photons from this bath. Instead, when it is detected to be in the excited state it is put in contact with the hot one, in order to favor the emission of photons into this bath. The net effect is a transfer of heat from the cold to the hot reservoir.

11.3. Experimental measurement of a topological transition

In Sec. 5.2 we have briefly reviewed Ref. [195] where the fact that the Berry curvature could be measured in the adiabatic dynamics of a qubit was pointed out. Refs. [196, 378] present the experimental verification of these ideas.

In Ref. [202] a transmon qubit is evolved in the adiabatic regime following the proposal of Ref. [195]. Concretely, the Hamiltonian of Eq. (41) was considered with

$$\vec{B}(\theta, \phi) = \frac{\hbar}{2} (\Delta_1 \cos \theta + \Delta_2, \Omega_1 \sin \theta \cos \phi, \Omega_1 \sin \theta \sin \phi). \quad (144)$$

This model has a topological transition as a function of Δ_2/Δ_1 , where the Chern number

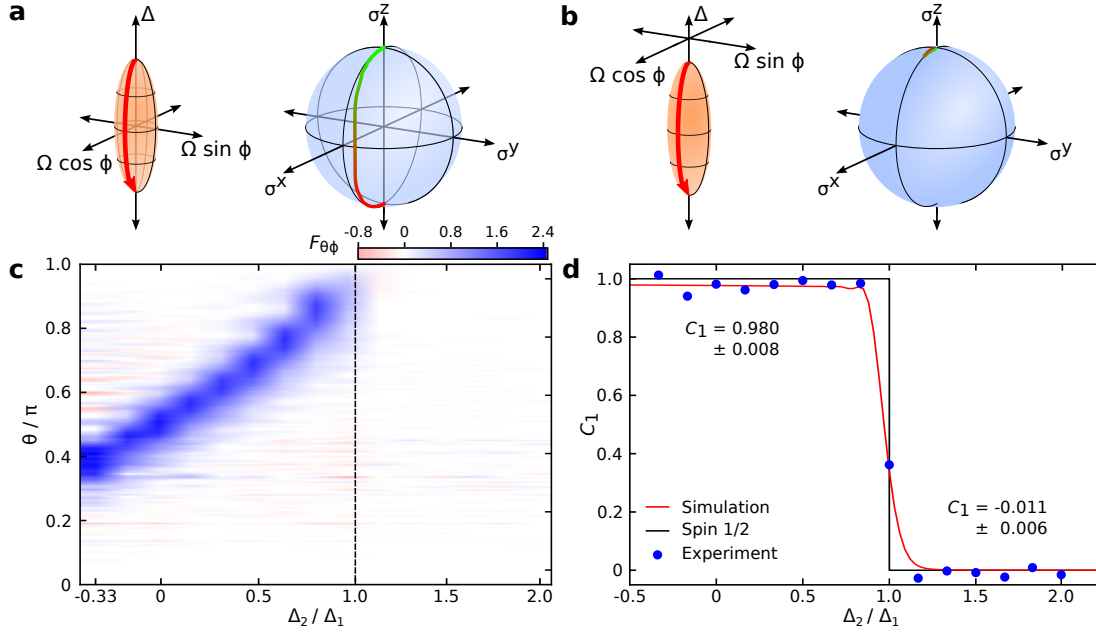


Figure 10. Adapted from Ref. [202]. (a) The parameter space and the implemented protocol for $\Delta_2 = 0$ in red (left). The corresponding calculated results for $\langle \vec{\sigma} \rangle$ represented in the Bloch sphere (right). (b) The same as for (a), with $\Delta_2 = 1.5\Delta_1$ (c) The Berry curvature measured as a function of Δ_2/Δ_1 , which is integrated in (d) to yield the Chern number C_1 .

jumps from 1 to 0, for $\Delta_2 = \Delta_1$. The parameters are chosen in order to initialize the qubit in its ground state at $\theta(t=0) = 0$ with fixed $\phi(t) = 0$ and a ramp with constant $\dot{\theta}$ is implemented. The evolution of the induced force $\mathcal{F}_\phi = -\partial H_{\text{qubit}}/\partial\phi$ is monitored and compared with the description of Eq. (66), with the Berry curvature given by Eq. (67). Experimentally, the latter is determined as the linear coefficient of $\langle \mathcal{F}_\phi \rangle$ as a function of $\dot{\theta}$. Given the curvature, the Chern number is calculated from Eq. (68). The comparison between theory and experiment is excellent. When the effect of the environment is considered by simulating the adiabatic evolution with Lindblad master equation small corrections are found which tend to soften the jump at the transition.

Results are summarized in Fig. 10. The upper panels show the protocols and the calculated results for $\langle \vec{\sigma} \rangle$, represented in the Bloch sphere for parameters in the topological phase (a) and outside it (b). It is clear that in the topological case the state wraps the Bloch sphere and $\langle \sigma_y \rangle \neq 0$. Instead, in the non-topological case there is no wrapping of the Bloch sphere and $\langle \sigma_y \rangle = 0$. The measured Berry curvature is shown in panel (c), while panel (d) shows the result for the Chern number. The plots with the label spin 1/2 correspond to the isolated system while "simulation" labels the results obtained by including the coupling to the environment modeled by a Lindbladian dynamics.

In Ref. [203] a similar protocol and measurement was performed in a cQED qubit with a different architecture and these results were verified. Furthermore, by mapping

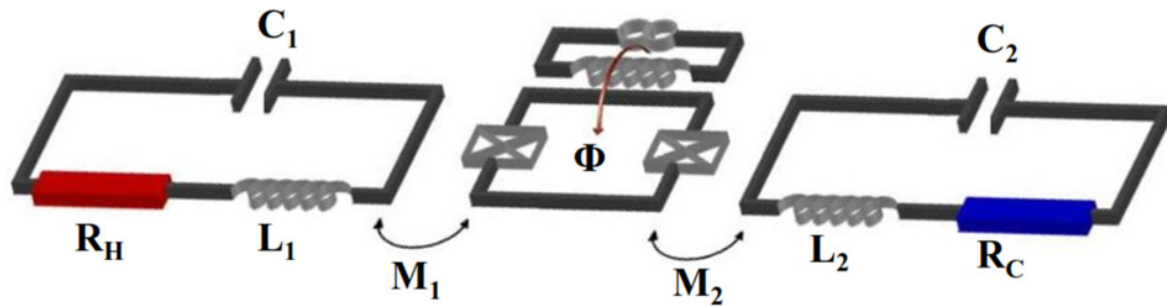


Figure 11. Sketch of the proposed experimental setup (Adapted from Ref. [380]).

states on the Bloch sphere to wave vectors in the first Brillouin zone of a lattice model, the topological transition of Haldane model [379] is simulated in a qubit.

11.4. Thermal machine and Otto cycle

An experimental setup to implement a non-equilibrium thermal machine on a superconducting qubit coupled to two resonators with a resistive element (LRC circuits) was proposed in Ref. [380] and further analyzed in Ref. [381]. The operation is argued to have a regime that corresponds to an Otto cycle.

The two resonators have different resonant frequencies, $\omega_{LC,1}$ and $\omega_{LC,2}$, and different temperatures. The qubit is described by the Hamiltonian of Eq. (41) with $\vec{B} = E_0(\Delta, 0, q(t))$, being q a time-dependent parameter modulated by changing the flux, which follows the protocol,

$$q(t) = \frac{1}{4} [1 + \cos(2\pi ft)]. \quad (145)$$

Hence, the level spacing of the qubit oscillates according to $\hbar\omega(t) = 2E_0\sqrt{\Delta^2 + q^2(t)}$. Each of the resonators has an associated noise spectral function of the form of Eq. (138) and it is coupled to the qubit operator σ^z through an inductive element. The degree of coupling depends on the degree of tuning between $\omega_{LC,j}$, $j = 1, 2$ and $\omega(t)$.

An ideal Otto cycle would consist in the following four steps: (a) For $q : 0 \rightarrow 1/2$: The qubit decouples from the resonators and evolves isolated from the reservoirs. Its population is determined by the cold resistor. (b) At $q = 1/2$ the qubit couples to the hot resonator and thermalizes with the hot resistor. The energy flows from the qubit to the resonator. (c) $q : 1/2 \rightarrow 0$: The qubit decouples from the resonators and evolves isolated from the reservoirs. (d) At $q = 0$ the qubit couples to the cold resonator and thermalized with the cold resistor. The energy flows from the resonator to the qubit. The full cycle operates as a refrigerator. Although the analogy to the Otto cycle is useful to understand the basics of the operation, the complete decoupling from the reservoirs does never occur in this setup and the device actually operates as a non-equilibrium thermal machine in permanent contact to the reservoirs, similar to the one discussed

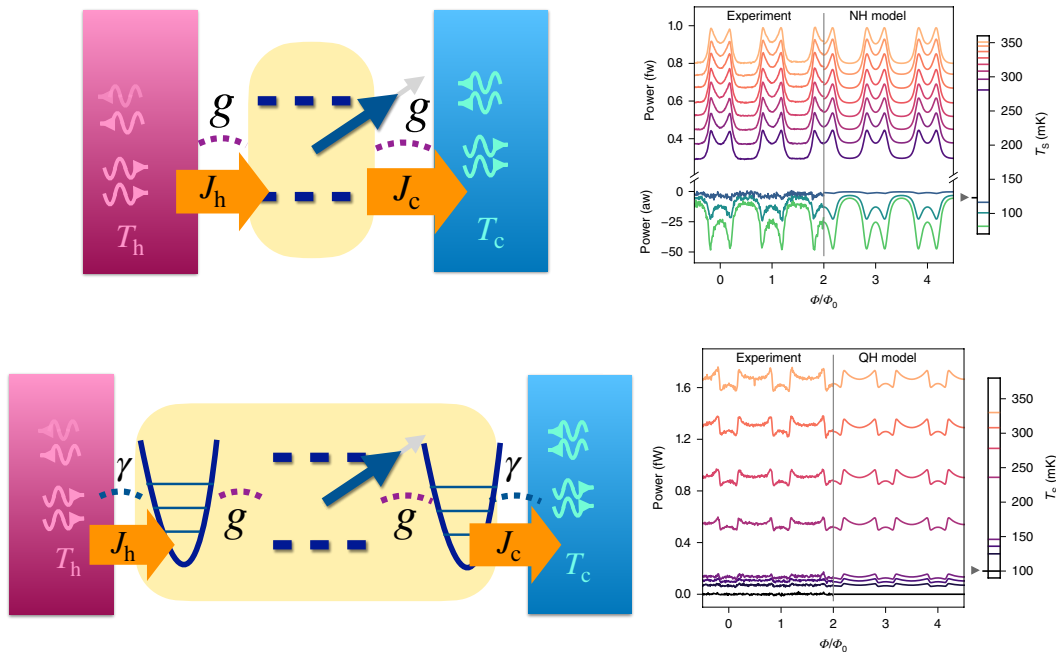


Figure 12. Left: Illustration of the thermal transport process when the qubit is contacted to reservoirs at different temperatures through resonators. Right: Experimental results for the total heat power absorbed by the cold reservoir for these two configurations (Adapted from Ref. [314]).

in Sec. 7.4. In both Refs. [380] and [381] the problem is solved by means of a non-equilibrium master equation. The description is extended to higher frequencies and the solution is argued to achieve a regime where the performance resembles the one of an Otto cycle. Estimates on the cooling power are presented in Ref. [380] and these are consistent with the present state of the art of the experimental detection possibilities. So far, the actual experiment has not been reported.

11.5. Thermal transport

As discussed in Sec. 9 when a few-level quantum system is coupled to two or more baths at different temperatures, there is typically a stationary heat flux from the hot to the cold bath through it.

In Ref. [314] a setup similar to the one described in that section was considered to experimentally study the thermal transport through a qubit. The configuration is similar to the one sketched in Fig. 6 (b). Instead of coupling the qubit to the reservoirs directly, the coupling is implemented to resonators with a resistive element, which are contacted to metallic reservoirs at different temperatures as sketched in Fig. 12. Hence, there are two couplings playing a role, which are, respectively, indicated in the Fig. with g (between the qubit and the resonators) and γ (between the resonators and the thermal baths). The proper separation into the quantum system and reservoirs in the description of the thermal transport through the device depends on where the thermal

bias effectively drops, as discussed in Sec. 9.3 and this depends on the ratio g/γ . For $g \ll \gamma$, each resonator is thermalized with its reservoir. In this regime, it is appropriate to define effective cold and hot baths to describe the combined systems of cold and hot reservoirs in contact to the corresponding resonator. This effective description is sketched in the upper part of Fig. 12 and implies a proper modeling of the spectral functions for the baths to represent the combined systems. In the opposite limit of $g \gg \gamma$, the temperature drop is more likely to take place in the contact between the resonator and the external reservoir. Therefore, in this case it is more appropriate to consider the quantum system consistent of the qubit hybridized with the resonators and this combined system coupled to the reservoirs, as sketched in the lower part of the figure. Both scenarios were successfully analyzed in Ref. [314] where the experimental data was properly modeled by means of master equations. In both configurations, the recorded power, corresponding to the heat current through the device through Eq. (141), is analyzed as a function of Φ , the magnetic flux through the qubit. Results are shown in the right-hand side of Fig. 12. An interesting feature there analyzed is the sensitivity of the heat transport to the magnetic flux. This is a signature of quantum coherence in the heat transport, which has been previously observed in the context of superconductors [341]. In the present case, we recall that this flux determines the effective level spacing of the qubit, and this is reflected in the transmission probability for the energy transport through the device.

A related experiment was reported in Ref. [315], basically in the same experimental device. Here, the focus was on the heat rectification properties of the system, implying a different amplitude in the heat current when the thermal bias is inverted. Heat rectification is known to be possible only in systems with many-body interactions as discussed in Sec. 9.4. In this experiment, a thermal rectification of 10 % was observed.

11.6. Steady-state heat engines and refrigerators

In Ref. [382] a device where two quantum LC resonators is proposed. The two resonators with natural frequencies $\Omega_c < \Omega_h$ are coupled via a transmission line to baths at temperatures $T_c < T_h$, respectively. They are connected through a Josephson junction, which is biased with a voltage $V = h(\Omega_h - \Omega_c)/2e$. If the occupation probability of the hot (h) cavity is larger than the cold (c) one, Cooper pairs tunnel against the bias by absorbing a photon in h and creating a photon in c. In this way, heat is converted into an electrical supercurrent that tunnels against the bias. The operation of this setup as a thermometer was analyzed in Ref. [383]. Interestingly, this device has been experimentally realized in Ref. [384], although no results on the heat transport or the mechanism of heat–work conversion have been reported so far.

A configuration of two resonators with a temperature bias, connected by a Josephson coupling was also considered in Ref. [385] to realize an autonomous refrigerator. In this case, in addition to the direct Josephson coupling, the two resonators are coupled through a third one with natural frequency Ω_r , forming a loop. The loop

is threaded by a flux ϕ , so that the Josephson Hamiltonian of the full device reads $E_J \cos(2\hat{\phi}_c + 2\hat{\phi}_h + 2\hat{\phi}_r + \phi)$, where $\hat{\phi}_\alpha = \sqrt{\pi e^2 Z_\alpha / \hbar}$ is the phase fluctuation in each resonator being Z_α the corresponding impedance. The non-linearity of this term and imposing the condition $\Omega_r = \Omega_c + \Omega_h$ favors the emission of photons from the cold resonator, with the consequent cooling.

12. Final remarks

The problem of the energetics and thermodynamic properties of new quantum devices is a topic of increasing interest, which motivates basic research while it is also paramount for the development of quantum technologies.

We have presented an overview of the main fundamental problems related to the energy dynamics of qubits, which are currently under active investigation. The rich variety of phenomena ranges from many-body strong correlations to the realization of thermal machines to convert heat into useful work and vice-versa. It also includes the fascinating topological properties which may help to provide a robust framework to control this dynamics.

We have intended to discuss theoretical results and to provide a brief description of the theoretical tools to address them in the different regimes along with their scope and limitations.

The main focus in connection with concrete realizations of these mechanisms has been put on superconducting devices. For this reason, we devoted some space to briefly explain the operation of these systems. We have also reviewed the main experimental advances in the study of quantum energy dynamics and thermodynamics in this qubit platforms. Nevertheless, many of the theoretical discussions are valid or can be simply translated to scenarios based on other qubit platforms, like quantum dots, NV centers and AMO systems.

We hope that this contribution may provide a motivating summary to stimulate more experimental research and help in triggering new theoretical ideas in this field.

13. Acknowledgements

LA thanks R. Fazio for many discussions and suggestions for this manuscript, as well as M. Perarnau-Llobet, L. Tosi, A. Jordan and A. Levy Yeyati for reading the manuscript and for their constructive comments and P. Terren Alonso for the help in checking equations. LA acknowledges support from CONICET-Argentina, FonCyT-Argentina through PICT-2017-2726, PICT-2018-04536, PICT-2020 and the Alexander von Humboldt Foundation (Germany). L.A. thanks KITP for the hospitality in the framework of the activity Energy and Information Transport in nonequilibrium Quantum Systems and the support by the National Science Foundation under Grant No. PHY-1748958, as well as the hospitality of ICTP-Trieste and the ICTP-Simons program.

Appendix A. Details on the calculation of the $\Lambda_{\ell,\ell'}^S$ for a driven qubit coupled to a single bath

We summarize some technical details to calculate Eq. (56) as reported in Ref. [?]. The procedure to calculate the matrix $\mathcal{M}(\vec{X})$ is based on the assumption that the master equation for the frozen density matrix is known and given by

$$\frac{d\rho^{(f)}}{dt} = \frac{\Gamma_g}{2}\mathcal{D}[\sigma^+]\rho^{(f)} + \frac{\Gamma_d}{2}\mathcal{D}[\sigma^-]\rho^{(f)}. \quad (\text{A.1})$$

$\Gamma_g(B)$ and Γ_d are gain and damping rates describing the effect of the coupling with the bosonic bath. These read $\Gamma_g(B) = [1 + n_B]\Gamma(B)$ and $\Gamma_d(B) = n_B\Gamma(B)$, being $n_B = (e^{2B\beta} - 1)^{-1}$ the Bose-Einstein distribution function depending on the temperature T of the bath ($\beta = 1/k_B T$). The function $\Gamma(B) = \gamma_0 B^s$ with $s = 1, > 1, < 1$ defines the spectral properties of the bosonic bath (Ohmic, super-Ohmic and sub-Ohmic, respectively). The other quantities in Eq. (A.1) are $\sigma^\pm = (\sigma^x \pm i\sigma^y)/2$ and the superoperators are $\mathcal{D}[O]\rho = O\rho O^\dagger - \{O^\dagger O, \rho\}$. In such a case, the quantities defined in Eq. (49) read

$$\mathcal{M} = \text{Diag}(-\Gamma^+(B)/2, -\Gamma^+(B)/2, -\Gamma^+(B)), \quad \vec{\gamma} = (0, 0, \Gamma^-(B)), \quad (\text{A.2})$$

being $\Gamma^\pm(B) = [\Gamma_d(B) \pm \Gamma_g(B)]/2$. The stationary solution of Eq. (A.1) in the vector notation introduced before is $\vec{\rho}^{(f)} = (0, 0, -\Gamma^-(B)/\Gamma^+(B))$, which leads to

$$\mathcal{M}^{-1}\frac{\partial\vec{\rho}^{(f)}}{\partial B} = \lambda_B \vec{z}, \quad \mathcal{M}^{-1}\frac{\partial\vec{\rho}^{(f)}}{\partial\theta} = \lambda_q \frac{\partial\vec{n}}{\partial\theta}, \quad \mathcal{M}^{-1}\frac{\partial\vec{\rho}^{(f)}}{\partial\varphi} = \lambda_q \frac{\partial\vec{n}}{\partial\varphi}, \quad (\text{A.3})$$

with

$$\lambda_B = \frac{1}{\Gamma(B)} \frac{\sinh(\beta B)}{\cosh^3(\beta B)}, \quad \lambda_q = \frac{1}{\Gamma(B)} \tanh^2(\beta B). \quad (\text{A.4})$$

To compute $\Lambda_{\ell,\ell'}^S$ from Eq. (53) we need to calculate the vectors defining the force operator introduced in Eq. (52). The result is

$$\vec{f}_B = \vec{n}, \quad \vec{f}_\theta = B \frac{\partial\vec{n}}{\partial\theta}, \quad \vec{f}_\varphi = B \frac{\partial\vec{n}}{\partial\varphi}. \quad (\text{A.5})$$

Appendix B. Master equation for a driven qubit asymmetrically coupled to two reservoirs

We present here the master equation derived as explained in Sec. 2.3 for a slowly driven qubit weakly coupled to thermal baths with Eqs. (79).

The instantaneous values of the parameters are $\vec{B} = (B_x, B_z)$. Hence, the matrix elements $\xi_{\alpha,jl}$ of the coupling are obtained by transforming Eqs. (79) to the instantaneous frame where the Hamiltonian of Eq. (41) is diagonal for these frozen parameters. The corresponding matrices are

$$\xi_l = \frac{1}{B} (B_z \sigma^z + B_x \sigma^x), \quad \xi_r = -\frac{1}{B} (B_x \sigma^z + B_z \sigma^x). \quad (\text{B.1})$$

Assuming an Ohmic bath, the rates of Eq. (15) are

$$\gamma_\alpha(\varepsilon) = \varepsilon \gamma_{\alpha,0} e^{-\varepsilon/\varepsilon_C}, \quad \varepsilon > 0, \quad (\text{B.2})$$

being ε_C and energy cutoff.

Introducing the notation of Eq. (47), the master equations for the frozen, Eqs. (14), and adiabatic, Eq (16), components read, respectively, for the present case

$$(\mathcal{E} + \mathcal{M}_l + \mathcal{M}_r) \vec{\rho}^{(f)} = \vec{\gamma}, \quad \sum_{\ell=x,z} \frac{\partial \vec{\rho}^{(f)}}{\partial B_\ell} \dot{B}_\ell = (\mathcal{M}_l + \mathcal{M}_r) \vec{\rho}^{(a)}, \quad (\text{B.3})$$

with

$$\mathcal{M}_\alpha = \begin{pmatrix} 0 & 0 & \bar{D}_\alpha \\ 0 & D_\alpha & 0 \\ 0 & 0 & D_\alpha \end{pmatrix}, \quad \mathcal{E} = \begin{pmatrix} 0 & -2B & 0 \\ 2B & 0 & 0 \\ 0 & 0 & 0 \end{pmatrix}, \quad (\text{B.4})$$

and

$$\vec{\gamma} = \frac{1}{B^2} (B_x B_z (\gamma_r - \gamma_l), 0, B_z^2 \gamma_l + B_x^2 \gamma_r), \quad (\text{B.5})$$

being $D_l = -B_x^2/B^2 \Gamma_l$, $\bar{D}_l = B_x B_z/B^2 \Gamma_l$ and $D_r = -B_z^2 \Gamma_r$, $\bar{D}_r = -B_x B_z/B^2 \Gamma_r$. $\Gamma_\alpha = \gamma_\alpha (e^{2B\beta_\alpha} - 1)^{-1}$, contains the information of the coupling with the baths with $\beta_\alpha = 1/(k_B T)$, and γ_α being the corresponding coupling strength.

References

- [1] de Leon NP, et al (2021) Science 372, 6539.
- [2] van der Wiel WG, et al (2002) Rev. Mod. Phys. 75, 1.
- [3] Burkard G, et al (2022) arXiv:2112.08863
- [4] Lahayeo MD, et al (2004) Science 304, 74.
- [5] Eichenfield M, et al (2009) Nature 462, 78
- [6] Carrega M, et al (2021) Nature Reviews Physics 3 698.
- [7] Arute F, Arya K and Martinis, JM (2019) Nature 574, 505
- [8] Wallraff A, et al (2004) Nature 431, 162
- [9] Friedenauer H, et al (2008) Nat. Phys. 4, 757
- [10] Blatt R and Roos C (2012) Nat. Phys. 8, 277
- [11] Childress, L, et al (2006) Science 314, 281
- [12] Schleich WP, et al (2016) Appl. Phys. B 122, 130.
- [13] Biamonte J, et al. (2017) Nature 549, 195.
- [14] Georgescu IM, Ashhab S and Nori F (2014) Rev. of Mod. Phys. 86, 153.
- [15] Auffèves A (2022) PRX Quantum 3, 020101
- [16] See "The quantum initiative manifesto", <https://quantum-energy-initiative.org/manifesto/>
- [17] Vinjanampathy S and Anders J (2016) Quantum thermodynamics, Contemporary Physics, 57, 545.
- [18] Goold J, et al (2016) J. Phys. A: Math. Theor. 49, 143001
- [19] Benenti G, et al (2017) Phys. Rep. 694, 1
- [20] Pekola JP and Karimi B (2021) Rev. Mod. Phys. 93, 041001
- [21] Landi GT and Paternostro M (2021) Rev. Mod. Phys. 93, 035008
- [22] Myers NM, Abah O, and Deffner S, arXiv:2201.0174
- [23] Rossnagel J, et al (2016) Science 352, 325.

- [24] Maslennikov G, et al (2019) Nat. Commun. 10, 1.
- [25] von Lindenfels D, (2019) Phys. Rev. Lett. 123, 080602.
- [26] Klatzow J, et al (2019) Phys. Rev. Lett. 122, 110601.
- [27] Peterson, JPS, et al (2019) Phys. Rev. Lett. 123, 240601.
- [28] Kastner MA (1992) Rev. Mod. Phys. 64, 849.
- [29] Koski JV, et al (2014) Proc. Natl. Acad. Sci. 111, 13786.
- [30] Pekola JP (2015) Nat. Phys. 11, 118.
- [31] Thierschmann H, et al. (2015) Nature nanotechnology 10, 854.
- [32] Josefsson M, et al (2018) Nature Nanotech 13, 920.
- [33] Dutta B, et al (2018) Nano letters 19, 506.
- [34] Dutta B., et al (2017) Phys. Rev. Lett. 119, 077701.
- [35] Sothmann B, Sánchez R, Jordan AN (2015) Nanotechnology 26, 032001.
- [36] Erdman PA, et al (2017) Phys. Rev. B 95, 245432.
- [37] Prete D, et al (2019) Nano Lett. 19, 5, 3033
- [38] Thierschmann H, et al (2015) Nature nanotechnology 10, 854.
- [39] Giazotto F and Martinez-Perez, M (2012) Nature 492, 401.
- [40] Ligato N, et al. (2022) Nature Physics 1.
- [41] Germanese G, et al (2022) Nature Nanotechnology 17, 1084.
- [42] Naik A, et al. (2006) Nature 443, 193.
- [43] Jezouin S, et al (2013) Science, 342 601.
- [44] Banerjee, et al (2018) Nature 559, 205.
- [45] Real M, et al (2020) Phys. Rev. App. 14, 034019.
- [46] Makhlin Y, Schön G, and Shnirman A (2001) Rev. Mod. Phys. 73, 357.
- [47] Clerk AA, et al (2010) Rev. Mod. Phys. 82, 1155.
- [48] Devoret MH and Schoelkopf RJ (2013) Science 339, 1169.
- [49] Wendin G (2017) Rep. Prog. Phys. 80, 106001.
- [50] Blais A, et al (2021) Rev. Mod. Phys. 93, 025005.
- [51] Walther H, et al (2006) Rep. Prog. Phys. 69, 1325.
- [52] Cottet A(2019), npj Quantum Inf 5, 21.
- [53] Loss D and DiVincenzo DP (1998) Phys. Rev. A 57, 120.
- [54] Balian R, "From Microphysics to Macrophysics" (SpringerVerlag,1992)
- [55] Landauer R (1987), IBM J. Res. Develop. 1957, 1, 223.
- [56] Landauer R (1987) Z. Phys. B 68, 217.
- [57] Büttiker M, et al (1985) Phys. Rev. B 31, 6207.
- [58] Büttiker M (1986) Phys. Rev. Lett. 57, 1761.
- [59] Fisher DS and Lee PA (1981) Phys. Rev. B 23, 6851.
- [60] Moskalets M and Büttiker M (2012) Phys. Rev. B 66, 205320
- [61] Arrachea L and Moskalets M (2006) Phys. Rev. B 74, 245322
- [62] Ludovico MF, et al (2014) Phys. Rev. B 89, 161306
- [63] Esposito, M, Ochoa MA, and Galperin M (2015) Phys. Rev. Lett. 114, 080602.
- [64] Rosselló G, López R, and Lim JS (2015) Phys. Rev. B 92, 115402.
- [65] Ludovico MF, et al (2016) Phys. Rev. B 94, 035436.
- [66] Bruch A, et al (2016) Phys. Rev. B 93, 115318.
- [67] Ludovico MF, et al (2018) Phys. Rev. B 97, 041416.
- [68] Haughian P, Esposito M, and Schmidt TL (2018) Phys. Rev. B 97, 085435.
- [69] Strasberg P, et al (2017) Phys. Rev. X 7, 021003.
- [70] Ridley M, et al arXiv:2201.02646.
- [71] Jacob SL, et al (2021) PRX Quantum 2, 020312.
- [72] Breuer HP, and Petruccione F (2002) "The theory of open quantum systems". Oxford University Press on Demand.
- [73] de Chiara, G, et al (2018) New J. of Phys. 20, 113024.

- [74] Purkayastha A, Dhar A, and Kulkarni M (2016) Phys. Rev. A 93, 062114.
- [75] Hewgill A, De Chiara G, and Imperato A (2020), arXiv:2008.04742.
- [76] Hofer, PP, et al (2017) New J. of Phys. 19, 123037.
- [77] Rivas A, et al (2010) New J. of Phys. 12, 113032.
- [78] Rivas A (2020) Phys. Rev. Lett. 124, 160601.
- [79] Levy A, and Kosloff R (2014) Europhys. Lett, 107, 20004.
- [80] Schoeller H and Schön G (1994) Phys. Rev. B 50, 18436.
- [81] König J, Schoeller H, and Schön G (1996) Phys. Rev. Lett. 76, 1715.
- [82] Splettstoesser J, et al (2006) Phys. Rev. B 74, 085305.
- [83] Brouwer PW (1998) Phys. Rev. B 58, R 10135.
- [84] Moskalets M, Büttiker M (2004) Phys. Rev. B 69, 20531.
- [85] Ludovico MF, et al (2016) Phys. Rev. B 93, 075136.
- [86] Bhandari B, et al (2020) Phys. Rev. B 102, 155407.
- [87] Bruus H and Flensberg K 2004 "Many-body quantum theory in condensed matter physics: an introduction". OUP Oxford.
- [88] Kolodrubetz M, Gritsev V and Polkovnikov A (2013) Phys. Rev. B 88, 064304.
- [89] Weinberg P, et al (2017) Phys. Rep 688.
- [90] Calvo HL, et al (2012) Phys. Rev. B 86, 245308.
- [91] Bhandari B, (2021) Phys. Rev. B 104, 035425
- [92] Rudner M and Lindner N (2020) Nat. Rev. Phys. 2, 229, and references therein.
- [93] Floquet G, On Linear Differential Equation with Periodic Coefficients, in Annales Scientifiques de l'Ecole Normale Supérieure (1883), Vol. 12, pp. 47-88.
- [94] Mi X, et al, arXiv preprint arXiv:2107.13571
- [95] Luttinger JM (1964) Phys. Rev. 135, A1505
- [96] Tataru G (2015) Phys. Rev. Lett. 114, 196601
- [97] Seifert U (2012) Rep. Prog. Phys. 75 126001.
- [98] Esposito M, Harbola U, Mukamel S (2009) Rev. of Mod. Phys. 81, 1665.
- [99] Jarzynski C (2011) Ann. Rev. Cond. Mat. Phys. 2, 329.
- [100] van den Broeck C(2010) J. Stat. Mech., page P10009.
- [101] Parrondo J, Horowitz J, and Sagawa T (2015) Nature Phys 11, 131.
- [102] Campisi M, Hänggi P and Talkner P(2011) Rev. Mod. Phys. 83, 771.
- [103] Strasberg P, "Quantum Stochastic Thermodynamics: Foundations and Selected Applications". Oxford University Press, (2021).
- [104] Wiseman HM (1996) Quantum Semiclass. Opt. 8, 205.
- [105] Brun T (2000) Phys. Rev. A 61, 042107.
- [106] Li Y, Chen X, and Fisher MPA (2019) Phys. Rev. B 100, 134306.
- [107] Bao Y, Choi S, and Altman E (2020) Phys. Rev. B 101, 104301.
- [108] Ippoliti M, et al (2021) Phys. Rev. X 11, 011030.
- [109] Elouard C, et al (2017) npj Quantum Information 3, 9.
- [110] Elouard C, et al (2017) NPJ Quantum Information 3, 9.
- [111] Jacobs K and Steck, DA (2006) Contemp. Phys. 47, 279.
- [112] Alonso JJ, Lutz E, and Romito A (2016) Phys. Rev. Lett. 116, 080403.
- [113] Bresque L, et al (2021) Phys. Rev. Lett. 126, 120605.
- [114] Manzano G, and Zambrini R (2022) AVS Quantum Sci. 4, 025302.
- [115] Deffner S, Paz JP, and Zurek WH (2016) Phys. Rev. E 94, 010103(R).
- [116] Brandner K, Bauer M, and Seifert U (2017) Phys. Rev. Lett. 119, 170602.
- [117] Di Stefano PG, et al (2020) Phys. Rev. Lett. 124, 110604.
- [118] Manzano G, Horowitz JM, and Parrondo JMR (2018) Phys. Rev. X 8, 031037.
- [119] Roncaglia AJ, Cerisola F, and Paz JP (2014) Phys. Rev. Lett. 113, 250601
- [120] Cerisola F, et al (2017) Nature Comm. 8, 1241.
- [121] Horowitz JM and J. M. R. Parrondo JMR (2013) New J. Phys. 15, 085028.

- [122] Leggio B, et al (2013) Phys. Rev. A 88, 042111.
- [123] Hekking FWJ and Pekola JP (2013) Phys. Rev. Lett. 111, 093602.
- [124] Gong Z, Ashida Y, and Ueda M (2016) Phys. Rev. A 94, 012107.
- [125] Di Stefano PG, et al (2018) Phys. Rev. B 98, 144514
- [126] Strasberg P (2019) Phys. Rev. Lett. 123, 180604.
- [127] Bhandari B and Jordan A, arXiv:2112.03971
- [128] Caldeira AO and Leggett AJ (1981) Phys. Rev. Lett. 46, 211.
- [129] Caldeira AO and Leggett AJ (1983) Annals of Physics 149, 374.
- [130] Leggett AJ, et al (1987) Rev. Mod. Phys. 59, 1.
- [131] Jaynes ET and Cummings FW (1963) Proc. IEEE. 51, 89.
- [132] Weiss U (1999) Quantum Dissipative Systems 4th edn (Singapore:WorldScientific)
- [133] Bray AJ and Moore MA (1982) Phys.Rev.Lett. 49, 1546.
- [134] Chakravarty S (1982) Phys.Rev.Lett. 49, 681.
- [135] Bulla R, Tong NH and Vojta M (2003) Phys.Rev.Lett. 91, 170601
- [136] Vojta M, Tong NH and Bulla R (2005) Phys.Rev.Lett. 94, 070604
- [137] Winter A, et al (2009) Phys.Rev.Lett. 102, 030601
- [138] Vojta M, Tong NH and Bulla R (2009) Phys.Rev.Lett. 102, 249904
- [139] Vojta M (2012) Phys. Rev. B 85, 115113
- [140] Chin AW, (2011) Phys.Rev.Lett. 107, 160601
- [141] Anderson PW and Yuval G (1971) J. Phys. C: Solid State Phys. 4, 607
- [142] Kosterlitz JM (1976) Phys.Rev.Lett. 37, 1577
- [143] Hewson AC (1997) The Kondo Problem to Heavy Fermions (Cambridge: Cambridge University Press)
- [144] Guinea F, Hakim V and Muramatsu A (1985) Phys.Rev.B 32, 4410
- [145] Guinea F (1985) Phys.Rev.B 32, 4486
- [146] Sundaresan NM et al (2015) Phys. Rev. X 5, 021035.
- [147] Forn-Díaz P et al (2017) Nat. Phys. 13, 39.
- [148] Magazzu L., et al (2018) Nat Commun 9, 1403.
- [149] Puertas-Martínez J. et al. (2019) npj. Quant. Inf. 5, 19.
- [150] Kuzmin R. et al. (2019) npj. Quant. Inf. 5, 20.
- [151] Houck AA, et al (2009) Quantum Inf Process 8, 105.
- [152] Weinhold F (1975) The J. of Chem. Phys. 63, 2479.
- [153] Ruppeiner G (1979) Phys. Rev. A 20, 1608
- [154] Salamon P, et al (1980) The Jour. of Chem. Phys. 73, 1001.
- [155] Salamon P and Berry RS (1983) Phys. Rev. Lett. 51, 1127.
- [156] Nulton J, et al (1985) The Jour. of Chem. Phys. 83, 334.
- [157] Schlögl F (1985) Z. für Physik B 59, 449.
- [158] Diosi L, et al (1996) The Jour. of Chem. Phys. 105, 11220.
- [159] Crooks GE (2007) Phys. Rev. Lett. 99, 100602.
- [160] Campisi M, Denisov, S and Hänggi P (2012) Phys. Rev. A 86, 032114.
- [161] Zulkowski PR, et al (2012) Phys. Rev. E 86, 041148.
- [162] Zulkowski PR, Sivak DA, and De Weese, MR (2013) PLoS ONE 8, e82754.
- [163] Sivak DA and Crooks GE (2012) Phys. Rev. Lett. 108, 190602.
- [164] Scandi M and Perarnau-Llobet M (2019) Quantum 3, 197.
- [165] Deffner S and Bonanca MVS (2020) Europhys. Lett. 131, 20001.
- [166] Abiuso P and Perarnau-Llobet M (2020) Phys. Rev. Lett. 124, 110606.
- [167] Brandner K and Saito K (2020) Phys. Rev. Lett. 124, 040602.
- [168] Miller HJD and Mehboudi M (2020) Phys. Rev. Lett. 125, 260602.
- [169] Miller HJD, et al (2021) Phys. Rev. Lett. 126, 210603.
- [170] Terren-Alonso P, (2022) Phys. Rev. X Quantum 3, 010326.
- [171] Eglinton J and Brandner K, arXiv: 2202.08759

- [172] Berry MV 2009 J. Phys. A: Math. Theor. 42 365303
- [173] Guery-Odelin D, et al Rev. Mod. Phys. 91, 045001 .
- [174] Sels D and Polkovnikov A (2017) Proc. of the Nat. Ac. of Sci. 114, E3909.
- [175] Passarelli G, Fazio R, Lucignano P (2022) Phys. Rev. A 105, 022618.
- [176] Acconcia T, Bonanca M, Deffner S (2015) Phys. Rev. E 92, 042148.
- [177] Martin I, Refael G, and Halperin B (2017) Phys. Rev. X 7, 041008.
- [178] Nathan F, Martin I, and Refael G (2019) Phys. Rev B 99, 094311.
- [179] Crowley PJD, Martin I and Chandran A (2020) Phys. Rev. Lett. 125, 100601.
- [180] Lü JT, Brandbyge M, and Hedegard P (2010) Nano Lett. 10, 1657.
- [181] Bode N, et al (2011) Phys. Rev. Lett. 107, 036804.
- [182] Thomas M, (2012) Phys. Rev. B 86, 195419.
- [183] Cangemi LM, et al (2020) Phys Rev B 102, 165418.
- [184] Cangemi LM, et al (2021) Phys Rev Res 3, 013237.
- [185] Berry MV (1984), Proc. R. Soc. London, Ser. A 392, 45. p. 7.
- [186] Berry MV (1989) in Geometric Phases in Physics, edited by A. Shapere and F. Wilczek (World Scientific, Singapore)
- [187] Berry M and Robbins J (1993) Proc. of The Royal Soc. A 442, 659.
- [188] Chruscinski D and Jamiolkowski A (2004) "Geometric Phases in Classical and Quantum Mechanics", Springer.
- [189] Thouless DJ, et al (1984) Phys. Rev. Lett. 49, 405.
- [190] Thouless DJ (1983) Phys. Rev. B 27, 6083.
- [191] Avron J , Osadchy D and Seiler R (2003) Physics Today 56, 38.
- [192] Xiao D, Chang M-C, and Niu Q (2010) Rev. Mod. Phys. 82, 1959.
- [193] Fradkin E (2013) "Field Theories of Condensed Matter Physics", Cambridge.
- [194] Bernevig BA and Hughes TL (2013) "Topological Insulators and Topological Superconductors", Princeton University Press.
- [195] Gritsev V and Polkovnikov A (2012) PNAS April 24, 109 6457.
- [196] Schroer MD, et al (2014) Phys. Rev. Lett. 113, 050402.
- [197] Qi X-L, Wu Y-S and Zhang S-C (2006) Phys. Rev. B 74, 085308.
- [198] Bernevig BA, Hughes TL and Zhang S-C (2006) Science 314, 1757.
- [199] Boyers E, et al (2020) Phys. Rev. Lett. 125, 160505.
- [200] Sundaram G and Niu Q (1999) Phys. Rev. B 59, 14915.
- [201] Long DM, et al arXiv:2109.11553
- [202] Kolodrubetz MH, et al (2018) Phys. Rev. Lett. 120, 150601.
- [203] Nathan F, et al (2021) Phys. Rev. Lett. 127, 166804.
- [204] Timms CI, Sieberer LM and Kolodrubetz MH (2022) Phys. Rev. Lett. 127, 270601.
- [205] Pothier H, et al Europhys. Lett. (1992) 17, 249.
- [206] Shutenko TA, Aleiner IL, and Altshuler BL (2000) Phys. Rev. B 61, 10366.
- [207] Avron JE, et al (2001) Phys. Rev. Lett. 87, 236601.
- [208] Arrachea L, Moskalets M, and Martin-Moreno L (2007) Phys. Rev. B 75, 245420.
- [209] Thingna J, et al (2014) Phys. Rev. B 90, 094517.
- [210] Hasegawa M and Kato T (2017) Jour of the Phys Soc of Japan 86, 024710.
- [211] Hasegawa M and Kato T (2018) J. of the Phys. Soc. of Japan 87, 044709.
- [212] Chamon C, et al (2011) Phys. Rev. Lett. 106, 135504.
- [213] Arrachea L, et al (2012) Phys. Rev. B 86, 125424.
- [214] Freitas N, and Paz JP (2017), Phys. Rev. E 95, 012146.
- [215] Gluza M, et.al.(2021) PRX Quantum 2, 030310.
- [216] Mucciolo ER, Chamon C, and Marcus CM (2002) Phys. Rev. Lett. 89, 146802.
- [217] Watson SK, et al (2003) Phys. Rev. Lett. 91, 258301.
- [218] Riwar RP, and Splettstoesser J (2010) Phys. Rev. B, 82, 205308.
- [219] Landauer R (1961) IBM Journal of Research and Development 5, 183.

- [220] Landauer R (1988) *Nature* 335, 779.
- [221] Bérut A, et al (2012) *Nature* 483, 187.
- [222] Jun Y, et al (2014) *Phys. Rev. Lett.* 113, 190601.
- [223] Gavrilov M and Bechhoefer J (2016), *Phys. Rev. Lett.* 117, 200601.
- [224] Hong J, et al (2016) *Sci. Adv.* 2, 10.1126/sciadv.1501492.
- [225] Martini L, et al (2016) *Nano Energy* 19, 108.
- [226] Gaudenzi R, et al (2018) *Nat. Phys.* 14, 565.
- [227] Saira O, et al (2021) *Phys. Rev. Res.* 2, 013249.
- [228] Dago S, et al (2021) *Phys. Rev. Lett.* 126, 170601.
- [229] Dago S and Bellon L (2022), *Phys. Rev. Lett.* 128, 070604.
- [230] Ciampini MA, et al (2021) arXiv:2107.04429
- [231] Scandi M, et al (2022) arXiv:2209.01852 (2022).
- [232] Segal D and Nitzan A (2006) *Phys. Rev. E* 73, 026109.
- [233] Ren J, Hänggi P, and Li B (2010) *Phys. Rev. Lett.* 104, 170601.
- [234] Leone R and Lévy L (2008) *Phys. Rev. B* 77, 064524.
- [235] Möttönen M, et al (2008) *Phys. Rev. Lett.* 100, 177201.
- [236] Beretta GP (2012) *Europhys. Lett.* 99, 20005.
- [237] Geva E and Kosloff R (1992) *J. Chem. Phys.* 96, 3054.
- [238] Feldmann T and Kosloff R (2003) *Phys. Rev. E* 68, 016101.
- [239] Brunner N, et al (2012) *Phys Rev E* 85, 051117.
- [240] Dann R, Kosloff R, and Salamon P (2020) *Entropy* 22, 1255.
- [241] Cavina V, Mari A, and Giovannetti V (2017) *Phys. Rev. Lett.* 119, 050601.
- [242] Kieu TD (2004) *Phys. Rev. Lett.* 93 140403.
- [243] Henrich MJ, Rempp F, and Mahler G (2007) *Eur. Phys. J. Spec. Top.* 151, 157.
- [244] Solfanelli A, Falsetti M, and Campisi M (2020) *Phys. Rev. B* 101, 054513.
- [245] Huang X-L, et al (2014) *Eur. Phys. J. D* 68, 32.
- [246] Bhattacharjee S and Dutta A (2021) *Eur Phys Jour B* 94, 239.
- [247] Lattune C, Sinayskiy and Petruccione F (2021) *Eur Phys Jour B* 230, 841.
- [248] Pancotti N, et al (2020) *Phys. Rev. X*, 10, 031015.
- [249] Yunger Halpern N (2019) *Phys. Rev. B* 99, 024203.
- [250] Das A and Mukherjee V (2020) *Phys. Rev. Research* 2, 033083.
- [251] Hartmann A, et al (2020) *Phys. Rev. Research* 2, 023145
- [252] Revathy BS, et al (2020) *Phys. Rev. Research* 2, 043247.
- [253] Erdman P, et al (2019) *New J. Phys.* 21 103049.
- [254] Cavina V, et al (2021) *Phys. Rev. A* 104, 032226
- [255] Erdman P and Noe F (2022) *npj Quantum Information* 8, 1.
- [256] Esposito M, et al (2010) *Phys. Rev. Lett.* 105, 150603.
- [257] Schmiedl T and Seifert U (2007) *Europhys. Lett.* 81, 20003.
- [258] Campisi M and Fazio R (2016) *Nat. Comm.* 7, 11895.
- [259] Yi J, Talkner P, and Kim YW (2017) *Phys. Rev. E* 96, 022108.
- [260] Campisi M, Pekola J, and Fazio R (2017) *New J. Phys.* 19, 053027.
- [261] Mohammady MH and Anders J (2017) *New J. Phys.* 19, 113026.
- [262] Buffoni L, et al (2019) *Phys. Rev. Lett.* 122, 070603.
- [263] Elouard C and Jordan AN (2018) *Phys. Rev. Lett.* 120, 260601.
- [264] Ding X, Yi, et al (2018) *Phys. Rev. E* 98, 042122.
- [265] Jordan AN, Elouard C, Auffeves A (2020) *Quantum Stud.: Math. Found.* 7, 203.
- [266] Bustos-Marún R, Refael G, and von Oppen F (2013) *Phys. Rev. Lett.* 111, 060802.
- [267] Fernández-Alcázar LJ, Bustos-Marún RA, and Pastawski HM (2015) *Phys. Rev. B* 92, 075406.
- [268] Calvo HL, Ribetto FD, and Bustos-Marún RA (2017) *Phys. Rev. B* 96, 165309.
- [269] Fernández-Alcázar LJ, Pastawski HM, and Bustos- Marún RA (2017) *Phys. Rev. B* 95, 155410.
- [270] Ludovico MF and Capone M (2018) *Phys. Rev. B* 98, 235409.

- [271] Arrachea L, von Oppen F (2015) *Physica E: Low-dimensional Systems and Nanostructures* 74, 596.
- [272] Potanina E, et al (2021) *Phys. Rev. X* 11, 021013.
- [273] Monsel J,
- [274] Ros A (2001) The isoperimetric problem, *Global Theory Minimal Surf.* 2, 175.
- [275] Parini E (2011) An introduction to the Cheeger problem, *Surv. Math. Appl.* 6, 9.
- [276] Leonardi GP (2015) in *New Trends in Shape Optimization*, vol. 166, p. 117 (Springer International Publishing, Cham).
- [277] Alicki R and Fannes M. (2013) *Phys. Rev. E* 87, 042123.
- [278] Binder F C, et al (2015) *New J. Phys.* 17 075015
- [279] Ferraro D, et al (2018) *Phys. Rev. Lett.* 120, 117702
- [280] Barra F (2019) *Phys. Rev. Lett.* 122, 210601
- [281] Rossini D, et al (2020) *Phys Rev Lett* 125, 236402
- [282] Mitchison MT, Goold J, Prior J (2020) arXiv preprint arXiv:2012.00350
- [283] Carrega M, et al (2020) *New J. Phys.* 22 083085
- [284] Monsel J, et al (2020) *Phys. Rev. Lett.* 124, 130601
- [285] Allahverdyan A, Balian R and Nieuwenhuizen T (2004) *Europhys. Lett.* 67 565
- [286] Hovhannisyanyan KV, et al (2013) *Phys. Rev. Lett.* 111, 240401.
- [287] Campaioli F, (2017) *Phys. Rev. Lett.* 118, 150601.
- [288] Gyhm J-Y, et al (2022) *Phys. Rev. Lett.* 128, 140501
- [289] Farina D, et al (2019) *Phys. Rev. B* 99, 035421.
- [290] Santos AC, et al (2019) *Phys. Rev. E* 100, 032107.
- [291] Quach, J Q and Munro W J (2020) *Phys. Rev. Applied* 14, 024092.
- [292] Andolina GM, (2019) *Phys. Rev. Lett.* 122, 047702
- [293] Dicke RH (1954) *Phys. Rev.* 93, 99
- [294] Cottet N, et al (2017) *Proc. of the Nat. Acad. of Sciences* 114, 29, 7561
- [295] Aleiner IL, Brouwer PW and Glazman LI (2002) *Phys. Rep.* 358, 309
- [296] Kouwenhoven L and Glazman L (2001) *Phys. World* 14, 33
- [297] Segal D, Millis AJ and Reichman DR (2010) *Phys.Rev.B* 82, 205323
- [298] Ruokola T and Ojanen T (2011) *Phys.Rev.B* 83, 045417
- [299] Chen T, Wang XB and Ren J (2013) *Phys.Rev.B* 87, 144303
- [300] Segal D (2014) *Phys.Rev.E* 90, 012148
- [301] Yang Y and Wu CQ, (2014) *Europhys.Lett.*107, 30003
- [302] Wang C, Ren J and Cao J (2015) *Sci.Rep.*5, 11787
- [303] Taylor E and Segal D (2015) *Phys.Rev.Lett.*114, 220401
- [304] Saito K, and Kato T (2013) *Phys.Rev.Lett.*111, 214301
- [305] Yamamoto T, et al (2018) *New J. Phys.* 20, 093014
- [306] Leggett A (1987) *Rev. Mod. Phys.* 59, 1.
- [307] Meir Y and Wingreen NS (1992) *Phys. Rev. Lett.* 68, 2512.
- [308] Haug H and Jauho AP, *Quantum Kinetics in Transport and Optics of Semiconductors* (Springer-Verlag, Berlin, 2008).
- [309] Pendry J (1983) *J. of Phys. A* 16, 2161.
- [310] Bekenstein JD, *Phys. Rev. Lett.* 1981, 46.
- [311] Bekenstein JD, *Phys. Rev. D* 1984, 30.
- [312] Datta S, *Lessons from Nanoscience: Lessons from Nanoelectronics: A New Perspective on Transport Part B: Quantum Transport*, World Scientific (2018)
- [313] Vadimov V, et al (2021) *Phys. Rev. B* 103, 214308
- [314] Ronzani A et al (2018) *Nature Physics* 14, 991
- [315] Senior J, et al (2020) *Comm. Physics* 3, 40
- [316] Magazzù L and Grifoni M (2019) *J. Stat. Mech* 2019, 104002.
- [317] Yamamoto T and Kato T (2021) *J. Phys.: Condens. Matter* 33, 395303

- [318] Xu M, Stockburger JT, and Ankerhold J (2021) Phys. Rev. B 103, 104304
- [319] Carrega M, et al (2022) PRX Quantum 3, 010323
- [320] Terraneo M, Peyrard M, and Casati G (2002) Phys. Rev. Lett. 88, 094302
- [321] Li B, Wang L, and Casati G(2004) Phys. Rev. Lett. 93, 184301
- [322] Segal D and Nitzan A (2005) Phys. Rev. Lett. 94, 034301
- [323] Hu B, Yang L, and Zhang Y (2006) Phys. Rev. Lett. 97, 124302
- [324] Casati G, Mejia-Monasterio C, and Prosen T (2007) Phys. Rev. Lett. 98, 104302
- [325] Yang N, et al (2007) Phys. Rev. B 76, 020301(R).
- [326] Zeng N and Wang J-S (2008) Phys. Rev. B 78, 024305.
- [327] Chang CW et al. (2006) Science 314, 1121.
- [328] Wu L-A, and Segal D (2009) Phys. Rev. Lett. 102, 095503
- [329] Arrachea L, Lozano GS, and Aligia AA (2009) Phys. Rev. B 80, 014425
- [330] Balachandran V, (2018) Phys. Rev. Lett. 120, 200603.
- [331] Balachandran V, (2019) Phys. Rev. E 99, 032136
- [332] Ruokola T and Ojanen T (2011) Phys. Rev. B 83, 241404(R).
- [333] Aligia AA, et al (2020) Phys. Rev. B 101, 075417
- [334] Palafox S, et al (2022) Phys. Rev. E 106, 054114
- [335] Mart'nez-Pérez M, Fornieri S, and Giazotto F (2015) F. Nature Nanotech 10, 303
- [336] Bours L, et al (2019) Phys. Rev. App. 11, 044073
- [337] Segal D and Nitzan A (2005) Phys. Rev. Lett 94, 034301
- [338] Díaz I and Sánchez R (2021) New J. Phys. 23, 125006
- [339] Portugal P , Flindt C, and Lo Gullo N (2021) Phys. Rev. B 104, 205420
- [340] Bhandari B, et al (2021) Phys. Rev. B 103, 155434.
- [341] Iorio A, et al (2021) Phys. Rev. Applied 15, 054050.
- [342] Ojanen T and Jauho AP (2008) Phys. Rev. Lett. 100, 155902.
- [343] Janvier C, et al (2015) Science 349, 1199.
- [344] Hays M, (2021) Science 373, 430
- [345] Mourik V, et al (2012) Science, 336, 1003.
- [346] Deng MT, et al (2016) Science, 354, 1557
- [347] Blais A, et al (2004) Phys. Rev. A 69, 062320
- [348] Koch J, et al (2007) Phys. Rev. A 76, 042319
- [349] Satrya CD, et al (2022) arXiv preprint arXiv:2207.12948.
- [350] Didier, N, et al (2015) Phys. Rev. Lett. 115, 203601.
- [351] Touzard S, et al (2019) Phys. Rev. Lett. 122, 080502.
- [352] Ikonen J, et al (2019) Phys. Rev. Lett. 122, 080503.
- [353] Dassonneville R, et al (2020) Phys. Rev. X 10, 011045.
- [354] Gambetta J, et al (2008) Phys Rev A 77, 012112
- [355] Naghiloo M (2019) arXiv preprint arXiv:1904.09291
- [356] Murch KW , et al (2013) Nature 502, 211.
- [357] Weber SJ, et al (2014) Nature 511, 570.
- [358] Ficheux Q, et al (2018) Nat Comm. 9, 1926
- [359] Naghiloo, M, et al (2020) Phys. Rev. Lett. 124, 110604
- [360] Bolund A and Molmer K (2014) Phys. Rev. A 89, 023827.
- [361] Alonso JJ, Lutz E, and Romito A (2016) Phys. Rev. Lett. 116, 080403
- [362] Di Stefano PG, (2018) Phys. Rev. B 98, 144514.
- [363] Rossi M, (2020) Phys Rev Lett 125, 080601
- [364] Campisi M, Fazio R, and Pekola JP (2015) New J. Phys. 17, 035012.
- [365] Feynman RP, "The Feynman Lectures on Physics", Vol. 1 (Chapter 46). Boston, MA: Addison-Wesley, 1963.
- [366] Elouard C, et al (2017) Phys. Rev. Lett. 118, 260603
- [367] Masuyama Y, et al (2018) Nature Comm. 9, 1291

- [368] Jarzynski C (1997) Phys. Rev. Lett. 78, 2690
- [369] Crooks GE (1999) Phys. Rev. E 60, 2721
- [370] Esposito M, Harbola U, and Mukamel S (2009) Rev. Mod. Phys. 81, 1665.
- [371] Campisi M, Hänggi MP, and Talkner P (2011) Rev. Mod. Phys. 83, 771.
- [372] Seifert U (2012) Rep. Progress Phys. 75, 126001.
- [373] Kawai R, Parrondo J, and Van den Broeck C (2007) Phys. Rev. Lett. 98, 080602
- [374] Funo K, Watanabe Y, and Ueda M (2013) Phys. Rev. E 88, 052121.
- [375] Lebedev AV, et al (2018) Phys. Rev. B 98, 214502.
- [376] Cottet N, Huard B (2018) arXiv:1805.01224.
- [377] Campisi M, Pekola J and Fazio R (2017), New J. Phys. 19 053027
- [378] Roushan P, (2014) Nature 515, 241.
- [379] Haldane FDM (1988) Phys. Rev. Lett. 61, 2015.
- [380] Karimi B and Pekola JP (2016) Phys. Rev. B 94, 184503.
- [381] Solfanelli A, Falsetti M and Campisi M (2020), Phys. Rev. B 101, 054513.
- [382] Hofer PP, Souquet J-R and Clerk AA (2016) Phys. Rev. B 93, 041418(R)
- [383] P. P. Hofer, et al (2017) Phys. Rev. Lett. 119, 090603
- [384] M. Westig, et al (2017) Phys. Rev. Lett. 119, 137001.
- [385] P. P. Hofer, et al (2016) Phys. Rev. B 94, 235420.